ISBN 978-82-471-1962-4 (printed ver.)
ISBN 978-82-471-1963-1 (electronic ver.)
ISSN 1503-8181

Doctoral theses at NTNU, 2009-12-03

Konrad Eichhorn Colombo

Mixed-Conducting Membrane-based Gas Turbine Power Plant for CO2 Capture

NTNU
Norwegian University of
Science and Technology

NTNU
Norwegian University of
Science and Technology

Thesis for the degree of
doctor philosophiae
Faculty of Engineering Science and Technology
Department of Energy and Process Engineering

Doctoral Thesis
Konrad Eichhorn Colombo
Doctoral theses at NTNU, 2009-12-03
NTNU

Konrad Eichhorn Colombo

Mixed-Conducting Membrane-based Gas Turbine Power Plant for CO_2 Capture

Thesis for the degree of doctor philosophiae

Trondheim, December 2009

Norwegian University of
Science and Technology
Faculty of Engineering Science and Technology
Department of Energy and Process Engineering

NTNU
Norwegian University of
Science and Technology

NTNU
Norwegian University of Science and Technology

Thesis for the degree of doctor philosophiae

Faculty of Engineering Science and Technology
Department of Energy and Process Engineering

ISBN 978-82-471-1962-4 (printed ver.)
ISBN 978-82-471-1963-1 (electronic ver.)
ISSN 1503-8181

Doctoral Theses at NTNU, 2009-12-03

Printed by Tapir Uttrykk

Preface

This thesis is submitted in partial fulfilment of the requirements for the degree Doctor of Philosophy at the Norwegian University of Science and Technology (NTNU).

The work was carried out at the Department of Energy and Process Engineering (NTNU) with Professor Olav Bolland as supervisor and Dr Vladislav V. Kharton as co-supervisor.

Abstract

At present, approximately 81% of the world's primary energy use relies on fossil fuels (natural gas, coal, and oil). As a result, emissions of the greenhouse gas CO_2 have increased dramatically, resulting in major effects on the climate of the globe. One option for reducing anthropogenic CO_2 emissions to the atmosphere is to capture the CO_2 produced by large, stationary point sources, such as power plants, and to store it in geological formations.

There are basically three technologies for CO_2 capture from power plants: post-combustion, pre-combustion, and oxy-combustion. The use of mixed-conducting membranes for integrated air separation in oxy-combustion power plants is often referred to as a promising technology with a relatively small efficiency penalty. However, this type of membrane adds several operational and material constraints that need to be considered to obtain sound process performance. The membrane-based gas turbine power plant analysed in this work includes a membrane reactor, where large amounts of CO_2 and H_2O are recycled to moderate the combustion temperature and to increase the driving force for oxygen permeation rates through the membranes. The membrane operates in a narrow range with respect to temperature, interactions with gaseous species such as CO_2, and temperature gradients. The use of mixed-conducting membranes for integrated air separation also creates a need for other critical process components that adds further constraints.

The membrane-based power plant was analysed with respect to design performance, steady-state and transient part-load (off-design) operation, transient response to failures, and performance deterioration due to degradation of individual process components as well as start-up and shut-down procedures. There was an emphasis on operational and material constraints that need to be considered to achieve a reasonable lifetime of critical process components.

A multi-scale modelling approach for the time and spatial domains was chosen for the detailed analysis of the membrane-based gas turbinef power plant. Key process components were based on spatially distributed conservation balances for energy, species, and mass. A stability diagram was incorporated into the membrane module model to investigate the risk of degradation. Performance maps were employed for proper off-design performance of the turbomachinery components.

For part-load operation, two load-control strategies were analysed for a mid merit gas turbine operating at constant rotational speed. In the first load-control strategy, variable guide vanes in the gas turbine compressor were used to manipulate the mass flow of air to the gas turbine compressor. This degree of freedom was used to control the turbine exit temperature. In the second load-control strategy, variable guide vanes were not used and the turbine exit temperature was allowed to vary. The mean solid-wall temperature of the membrane modules was maintained close to its design value, which leads to improved stability. Furthermore, the pressure in the recycle loop was controlled to minimize the mechanical load to the walls of the monolithic membrane modules and heat exchangers. Steam must be added to the membrane reactor to sustain sound process conditions.

It was found that the membrane-based gas turbine power plant had a narrow operating window due to operational and material constraints, when compared to a conventional gas turbine power plant. Moreover, the membrane-based power plant exhibits rather slow dynamics. Fast load-following is thus not recommended, nor is it even possible.

Two more general conclusions can be drawn from this work. First, the analysis of complex technical systems, such as the membrane-based power plant, should not be

subdivided into (i) design, (ii) off-design, and (iii) transient analysis. For instance, a process may have inherent dynamics that lead to constraining conditions for off-design operation. Secondly, operational and material constraints must be considered to arrive at a more realistic picture of the feasibility of novel processes.

Keywords

Gas Turbine Power Plant, Complex Technical System, Modelling, Simulation, Mixed-Conducting Membrane, Operational and Material Constraints, Oxy-Combustion, CO_2 Capture, Lanthanum Nickelate, Part-Load Operation, Off-Design Performance, Transient, Degradation, Stability and Failure Analysis, Start-Up and Shut-Down, Linear Model Reduction, Balanced Residualization

The work presented in this thesis is based on the following journal articles, referred to by their Roman numerals. The papers are appended at the end of the thesis.

I. Konrad Eichhorn Colombo, Lars Imsland, Olav Bolland, Svein Hovland; Dynamic modelling of an oxygen mixed-conducting membrane and model reduction for control; Journal of Membrane Science, Volume 336, Issues 1-2, 2009, Pages 50-60.

II. Konrad Eichhorn Colombo, Olav Bolland, Vladislav V. Kharton, Christoph Stiller; Simulation of an Oxygen Membrane-based Combined Cycle Power Plant: Part-Load Operation with Operational and Material Constraints; Energy & Environmental Science, Volume 2, Issue 11, 2009, 2, Pages 1310 – 1324.

III. Konrad Eichhorn Colombo, Vladislav V. Kharton, Olav Bolland; Simulation of an Oxygen Membrane-Based Gas Turbine Power Plant: Dynamic Regimes with Operational and Material Constraints; Energy & Fuels; DOI: 10.1021/ef9004253.

IV. Konrad Eichhorn Colombo, Vladislav V. Kharton, Alexandre P. Viskup, Andrei V. Kovalevsky, Aliaksandr L. Shaula, Olav Bolland; Simulation of an Oxygen Membrane-based Gas Turbine Power Plant: System Level Analysis of Operation Stability and Individual Process Unit Degradation; submitted to the Journal of Solid State Electrochemistry.

To my dear mother

"There is no substitute for hard work."

Thomas Alva Edison (1847-1931)

Thanks to those who have gone before me,

to reveal the Way.

Thanks to all who have stood by me,

to inspire me along the Way.

Thanks to those who have opposed me,

to let me go beyond the limits along the Way.

Acknowledgements

First of all, I wish to express my sincere gratitude to my supervisor, Professor Olav Bolland, for giving me the opportunity to pursue this very interesting PhD project. With a background in electrical engineering I certainly had many questions that a process engineer would not have asked. However, your patience and positive attitude let me fill the voids and your concept of guided anarchy has been invaluable to build up my own scientific identity. I also appreciate the time you gave me to develop my ideas without too much pressure. Thank you!

Last year, I contacted Dr Vladislav Kharton regarding a question on mixed-conducting membranes. From literature I already knew that he is one of the leading experts in this field. Our correspondence quickly intensified and a couple of months later he became my co-supervisor. Your extraordinary inspiring and professional guidance as well as passion for science, Dr Kharton, have been of incredible value to me and the quality of my work. Moreover, your illuminative way of answering all my questions is simply impressive. I truly enjoy working together with you and I hope that our collaboration will continue for many years!

In the autumn of 2007, I decided to take a break from my PhD to get some new input and inspiration for my work. Dr Mkhulu Mathe and Brian North from the Council for Scientific and Industrial Research (CSIR) invited me for a research visit to South Africa. This not only gave me the opportunity to be part of a highly talented research group but also to experience a beautiful country. Thank you so much for this fantastic opportunity!

I wish to thank Knut Ingvar Åsen, Jens Bragdø Smith and John Arild Svendsen at StatoilHydro for sharing insights as well as experimental and simulation results with me.

I wish to thank my colleagues at the Norwegian University of Science and Technology for friendship and fruitful discussions.

My warmest thanks go to Trevor Hadley and Jan van der Watt, my very special and wonderful friends from South Africa. I cannot express how thankful I am for all the moments we shared together. You had an incredibly positive impact on me, and when things became overwhelming you where there for me. I will always keep you in my heart!

The people I finally mention - my family - are those who mean the most to me. Thank you so much for all your love, support and encouragement and just for being the wonderful people you are!
My deepest thanks and respect go to my dear mom who, in a loving way, always encouraged me to prioritize my education and to work hard for my goals. You always believed in me and taught me that everything in life is possible. Thank you so much!

The financial support received from StatoilHydro, GE Global Research, Statkraft, Aker Clean Carbon, Shell, TOTAL, ConocoPhillips, ALSTOM, the Research Council of Norway (178004/I30 and 176059/I30), Gassnova (182070) is gratefully acknowledged.

Table of Contents

1 Introduction

1.1 Current Energy Situation

Modern industrial as well as developing countries depend heavily on energy[1]. Future increases in energy consumption will be difficult to stop, in view of the expected growth of the global economy combined with the need to compensate for declining soil fertility and fresh water availability. At the same time, society has access to high-quality reserves of fossil fuels and mineral ores [2]. Fully 81% of the globe's primary energy comes from fossil fuels, with 13% from renewable energy, and 6% from nuclear energy sources [2]. Fossil fuels, in particular for power generation, are expected to remain dominant with roughly an 80% [2] share of total primary energy through to 2050 [2-4]. In 2006, modern renewable energy sources produced approximately 17EJ, with the largest share of 11.1EJ from hydropower and 4.6EJ by biomass[2] [2]. Most of the renewable energy sources (45EJ) came from wood in developing countries. The average annual growth rate of modern renewable energy sources is about 3% [1]. The future potential of modern renewable energy sources is very sensitive to environmental changes, i.e. modern renewable energy sources can also have serious environmental impacts when used on a large scale [2-3].
At the end of 2007, more than 400 nuclear power plants were in operation with a total power generation capacity of 9.4EJ [2]. Recoverable conventional resources of uranium are estimated to 17.1 million tonnes, which would last for several hundred years at current rates of annual power generation [2]. During reactor operation, negligible amounts of CO_2 are emitted. But nuclear power faces considerable public opposition, based on the high risk to human and ecosystem health and safety[3,4].

The switch from fossil fuels to renewable, and possibly to nuclear energy sources, is further hampered by the fact that the current infrastructure is based on the use of fossil fuels [12]. To employ alternative energy sources on a large scale, extensive changes and construction would be necessary[5,6]. This would lead to hasten climate change in addition to faster depletion of fossil fuel sources [2].

---

[1] In 2007, the total world consumption of fossil fuels corresponded to an equivalent of 409,000,000,000,000,000,000J (409 exajoule) [1].
[2] Other forms of renewable energy sources are sunlight, wind, temperature difference in soil and sea, chemical difference between fresh water and sea water, tides, and differences in elevation [4-9].
[3] It should also be noted that in at least three countries (India, Iraq, and Israel) the use of research nuclear reactors has been aided to the development of nuclear weapons [10].
[4] Other nuclear sources for power generation, such as fusion, are not expected to be of practical relevance in the next few decades [11].
[5] Renewable technologies, such as wind power, could also produce greater risks of supply interruptions [12].
[6] This is a global viewpoint, i.e. the distribution of energy sources may be very different for individual countries. In Norway for instance, power generation in 2007 was composed of hydro power, with a total share of 98.26%, wind power, with a total share of 0.65%, and heat power, with a total share of 1.09% [13].

1.2 CO_2 Capture and Storage

Climate models predict that if anthropogenic greenhouse gases are not curbed, extreme climate events, such as droughts and intense storms, will occur more frequently, with significant consequences for the global ecosystem and human welfare[7] [3, 15-16, 25].

Carbon dioxide capture and storage (CCS) is one option in the portfolio of mitigation methods for the stabilization of anthropogenic greenhouse gases[8,9] [4, 8, 12, 32, 37-38]. In CCS, the CO_2 is captured at large point sources (for instance power plants), transported to a storage site, and injected into a geological formation, such as depleted oil and gas fields, unmineable coal seams, and saline formations, as shown in Figure 1[10,11]. At present CCS is operating on a trial basis, with 3 megatons of CO_2 per year captured from power plants or natural gas cleanup [12]. On a global scale, power generation is the largest contributor to anthropogenic CO_2 emissions[12,13] with over 7 gigatonnes every year [33, 35, 43-45]. Total anthropogenic emissions are 3.67 trillion tonnes of CO_2, about half of which has already been emitted since industrialization began [46].

---

[7] Of much concern is the fact that the Earth's climate represents a strongly nonlinear complex system [14-19] exhibiting feedbacks and emergent behavior, i.e. it is predisposed to unexpected outcomes [20-23]. Hence, certain phenomena may reinforce and prolong the multi-century-long recovery process until the climate has stabilized [15, 24]. Sea levels, for instance, may continue to rise even after land areas have begun to cool [15].

[8] The dominant anthropogenic global warming contribution is from CO_2 emissions because of its long lifetime in the atmosphere [26]. But other non-CO_2 'Kyoto gases', such as methane, nitrous oxide, hydrofluorocarbons, perfluorocarbons, and SF6, are expected to produce as much warming as 125 Gt of carbon in the form of CO_2 would [27], or one-third of total CO_2 equivalent [28]. Moreover, further complications arise as a result of specific properties of chemical species. Methane, for example, is chemically reactive leading to additional effects [29]. Consequently, a focus on CO_2 may prove insufficient in the near term if pollutants with shorter lifetimes do not gain comparable attention [26, 30-31].

[9] The concentration of CO_2 in the atmosphere has increased from a pre-industrial level of about 280ppm to the current concentration of 385ppm [4, 19, 32]. Proposals to limit atmospheric CO_2 to a concentration that would prevent most damaging climate change have focused on a goal of 500±50ppm [8, 33]. But leading environmental scientists suggest a limit of not more than 350ppm [27]. Ergo, CO_2 levels already exceed those that would provide long-term safety, and we need to do more than just stop, we need to reverse course [27]. In this respect photosynthesis is currently the only practical form of air capture [34]. Air capture has been ignored by the IPCC, but Canada, the United States and Switzerland have further developed this technology in form of prototypes [23, 35]. Geoengineering approaches have also been proposed to cope with global warming, such as by reducing the amount of energy entering the Earth by increasing the amount of sunlight that bounces back out into space without being absorbed [32, 36].

[10] On a global basis, the original static estimates of storage capacity are now being substantially downgraded to several decades rather than hundreds of years of emissions. It needs to be determined if CCS can provide a major contributor or a niche for CO_2 emissions mitigation [12]. Estimates of worldwide potential storage capacity range from 1700 to almost 11000 gigatonnes of CO_2 [39].

[11] First proposed in 1977 [40], ocean storage of CO_2 has also received considerable attention, but due to environmental, legal, and economic concerns, interest in ocean storage has declined [7, 34, 41].

[12] In 2007, there were 2211 power plants that emitted at least 1 megaton of CO_2: 1068 were in Asia with 559 in China alone; 567 in North America, with 520 in the United States; 375 in Europe, and 157 in Africa [42].

[13] The ocean is the largest carbon source with an outgassing of more than 90 gigatonnes per year. But it also absorbs over 92 gigatonnes per year [43].

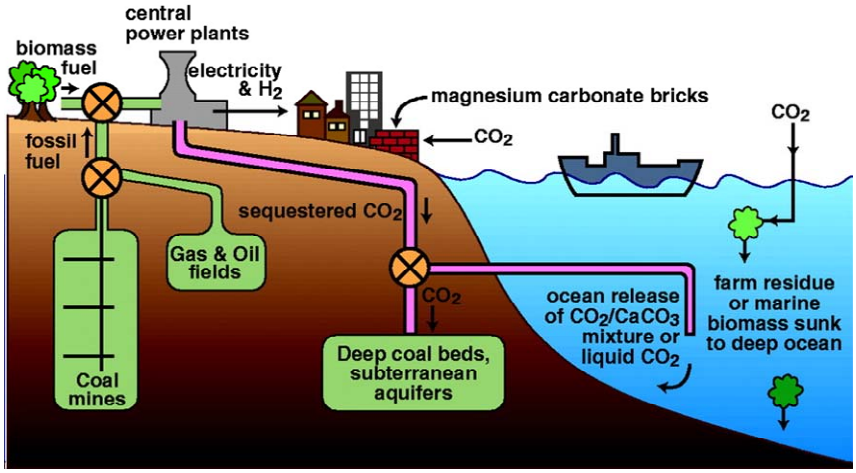

Figure 1: CO_2 capture and sequestration[32].

CCS assumes that small amounts of CO_2 will leak back from the storage sites to the atmosphere. In order to benefit from the use of CCS, the leakage rate and energy penalty must be lower than cases where CCS had not been implemented. In addition to major engineering challenges, decisions regarding the implementation of CCS also depend on political and economic considerations [47-48], since the capture process accounts for more than 70% of overall cost [7, 12, 49]. Implementation of CCS results in less efficient power plants in the sense that they produce more CO_2 for a given output of electricity. The additional energy requirement for CCS is in the range of 10-40% [4]. Available CO_2 capture technology is expected to capture about 85-95% of the CO_2 produced [4].

1.3 Power Cycles

There are three basic approaches for CO_2 capture from fossil fuel-based power generation processes: (i) post-combustion, (ii) pre-combustion, and (iii) oxy-combustion [4, 50-51], which will be briefly explained in the following subchapters.

1.3.1 Post-Combustion Processes

The post-combustion concept is shown schematically in Figure 2, where fuel is burned in air and the CO_2 is captured afterwards from the flue gas. The thermodynamic driving force for CO_2 separation is relatively small due to the high dilution with nitrogen in conjunction with a low total pressure. Chemical absorption is usually used with low CO_2 pressures. For high CO_2 pressures, physical absorption is used because it is less energy intensive than a chemical absorption process [52]. CO_2

capture from post-combustion power plants has the advantage that it can be applied to already constructed plants[14]. But major disadvantages include the large size of the equipment and the production of toxic by-products during the regeneration process of the solvent [12].

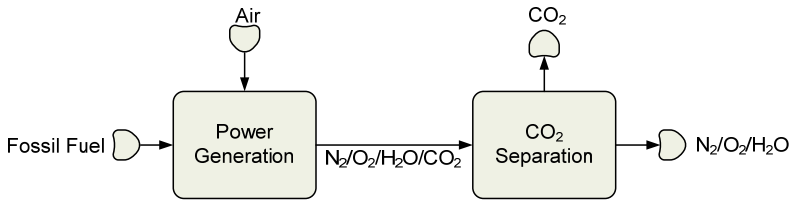

Figure 2: Post-combustion CO_2 capture from power plants [4].

1.3.2 Pre-Combustion Processes

In pre-combustion processes, shown in Figure 3, the fuel reacts with oxygen in an under-stoichiometric atmosphere to produce a synthetic gas (syngas) with high concentrations of carbon monoxide, hydrogen, water vapour, and CO_2. After CO shift conversion, the CO_2 is separated and the hydrogen is burned as fuel, for instance in an Integrated Gasification Combined Cycle plant (IGCC). Gasifiers can operate at pressures of 6.5MPa or higher. The thermodynamic driving force for the CO_2 separation is hence high, which allows for the use of cheaper capture processes [7]. On the other hand, pre-combustion capture is expected to have high construction costs and decreased short-term flexibility [12].

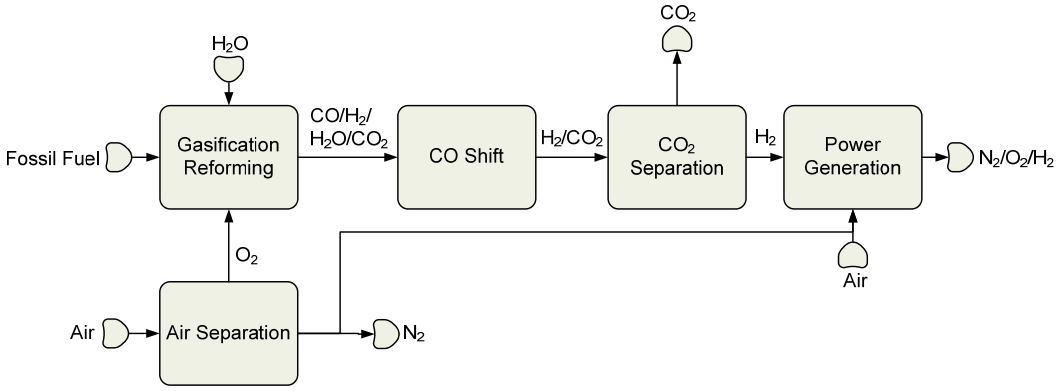

Figure 3: Pre-combustion CO_2 capture from power plants [4].

[14] It is expected that amine scrubbing will probably be the dominant technology for CO_2 capture from coal-fired power plants in 2030 [53].

1.3.3 Oxy-Combustion Processes

In oxy-combustion power plants, fuel is burned in a nearly stoichiometric atmosphere, i.e. oxygen purities are higher than 95%. The main products in the flue gas are then water vapour and CO_2. Oxygen can basically be produced either by external air separation or integrated air separation. Figure 4 shows the block diagram for oxy-combustion power plants with external air separation. The characteristic feature is the recycling of conversion products (mainly water vapour and CO_2) to moderate the combustion temperature. In this respect, different methods are possible: (i) recycling of water vapour and CO_2 in gas form, (ii) separation of water vapour and CO_2 with subsequent water vapour recycling, or (iii) liquid water recycling, or (iv) recycling of gaseous CO_2. Impurities such as water (vapour), oxygen, and nitrogen[15] are removed before end storage. The principle of integrated air separation is shown in Figure 5.

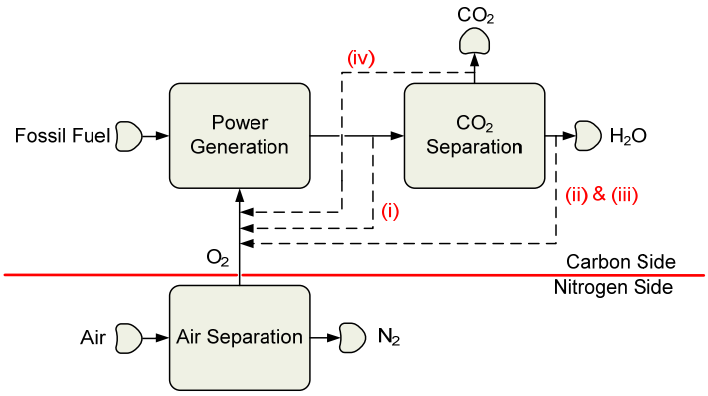

Figure 4: Oxy-combustion CO_2 capture from power plants with separate air separation [4, 54].

[15] Entering the carbon side through the fuel.

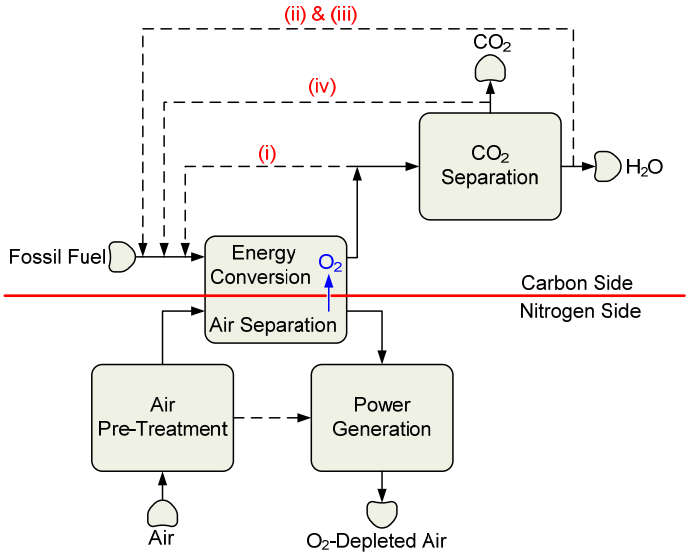

Figure 5: Oxy-combustion CO_2 capture from power plants with integrated air separation [4, 54].

1.4 Importance of Membrane-based Power Plants with CO_2 Capture

As stated above, one option for power plants with CO_2 capture is the oxy-combustion concept, where dilution of CO_2 with nitrogen is avoided. Cryogenic air separation, usually applied in the large-scale production of oxygen, is very energy-intensive [55] and does not offer many possibilities for system improvements. The membrane-based combined cycle power plant analysed in this work[16] was introduced as a highly efficient and cost-effective process for CO_2 capture [50, 56-57] with an efficiency penalty of only four percentage points, including the compression of the CO_2 to 100 bar [56] (6.2 percentage points were found in this work, including compression of the CO_2 to 110 bar). In addition to the relatively low efficiency penalty, the membrane-based power plant concept relies on standard air-based gas turbine technology [56]. As a result, large modifications of the turbomachinery are not required when compared to other oxy-combustion power plants, which use CO_2 and/or water (vapour) as working fluid [58-59]. The basic process of the membrane-based gas turbine power plant was originally invented by StatoilHydro (formerly Norsk Hydro, Norway) [56].

For the analysis of (power) processes (with CO_2 capture), modelling and simulation plays a vital role. Despite the plethora of publications dealing with novel processes, there is a lack in our current understanding of the interplay of process components in off-design or transient operation, and even more, in the quantitative analysis of (long-term) stability, failure response, and operability in general. Furthermore, even for the analysis of off-design and transient process behaviour, highly simplified (zero-dimensional) models are often used. It is just not possible to make quantified

[16] In the literature, this is usually referred to as the so-called Advanced Zero Emission (gas turbine power) Plant (AZEP) [56].

statements of internal phenomena. The design, off-design, and transient analysis of processes must be carried out together. For instance, conclusions drawn from an off-design analysis may not be true for the process during transients.

The overall aim of this work was to obtain fundamental insights into gas turbine power plants with mixed-conducting membranes for integrated air separation by means of mathematical modelling and numerical simulation. Several material-specific properties of the oxygen mixed-conducting membrane[17], obtained experimentally [56, 60-72], were incorporated into a detailed gas turbine power plant model. The main modelling and simulation tool used in this work was gPROMS [73-74], a state-of-the-art equation-oriented software tool.

1.5 Applied Methods for the Analysis of a Membrane-Based Gas Turbine Power Plant

1.5.1 Multi-Disciplinary Analysis

This work underlines the strong interaction between process engineering, applied mathematics, material science, and cybernetics, as shown in Figure 6, to provide high-quality information about the feasibility of a membrane-based power plant.

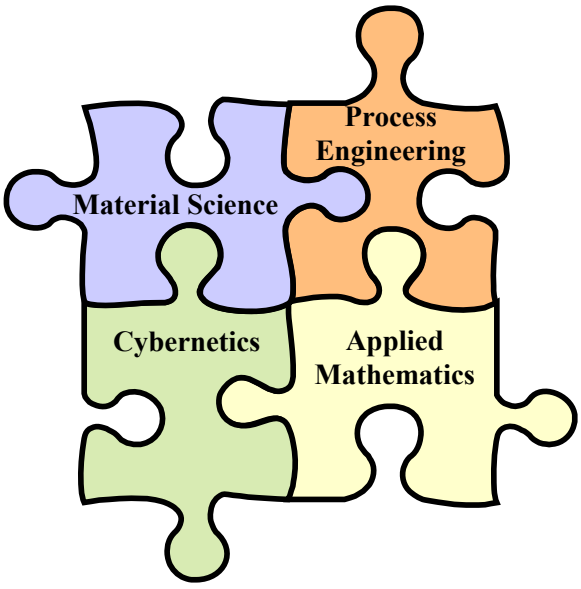

Figure 6: Multi-disciplinary approach for the analysis of a membrane-based power plant.

[17] Mixed-conducting membranes for oxygen separation are also referred to with acronyms such as OMCMs (Oxygen Mixed-Conducting Membranes) ITMs (Ion Transport Membranes), OTMs (Oxygen Transport Membranes), and MIEC (Mixed Ionic Electronic Conducting) membranes.

1.5.2 Multi-Scale Modelling

The membrane-based gas turbine power plant, and related complex (technical) systems in general, are characterized by phenomena that span a large range of spatial and time scales. These phenomena are in many cases a result of the compounding role between individual sub-systems in these two domains. The multi-scale modelling approach[18] has found its way into many fundamental as well as applied scientific disciplines, such as mathematics, medicine, and chemical engineering [76-87]. At present, it is dominantly used by the material science community [85, 87].
In this work, a multi-scale modelling approach was applied to incorporate knowledge from different disciplines. The essential step for successful multi-scale modelling is to focus on the right level of description [88] and the most important phenomena in the system. There is a delicate balance between the inclusion of sufficient details to account for individual process component behaviour, and the limitations on the most essential phenomena to make it possible to solve the model with current state-of-the-art simulation tools[19]. The most detailed process component in the membrane-based gas turbine power plant model is the membrane module itself. Apart from the solid phase for the insulation, which was modelled in two dimensions, species and energy conservation balances were formulated in one dimension. A two- or even a three-dimensional model would lead to a considerably larger model size without gaining more insight into the physics of the system. Furthermore, it is expected that gPROMS would not sustain the numerical robustness that was obtained in this work[20].
The step from steady-state to transient models leads to a much larger impact in terms of system complexity than the consideration of an additional spatial coordinate. This is because the resulting dynamics of a complex system may be very different from those of individual process components. For instance, whereas thermal inertia of the stand-alone membrane module was found to be rather fast (paper I), when the module is included in the power plant, much longer transients were found for the whole system (paper III). Conclusions drawn from the behaviour of individual process unit could not be transferred a priori to the highly integrated process.

1.5.3 Simulation Tools

[18] The expressions ‘scales’ and ‘level’ are used interchangeably in the literature by several authors. Here, we follow the approach used by Li et al. [75], where a level can include several scales in the system's hierarchy.
[19] It can also be stated as follows: "A good theoretical model of a complex system should be like a good caricature: It should emphasize those features which are most important and should downplay the inessential details" [83].
[20] One monolithic membrane module and heat exchanger, respectively, consists of approximately 6600 gas channels. The membrane reactor assumed in this work is connected to a mid merit gas turbine with a power output of approximately 20MW and includes 576 monoliths of each type (membrane module, high-temperature heat exchanger, low-temperature heat exchanger, and bleed-gas heat exchanger). Modelling of all gas channels in the membrane reactor would lead to a set of several million energy balances for the gas phase alone. An even more dramatic increase would arise when considering all chemical species in the system. In comparison, the power plant model used in this work consists of approximately 14000 equations.

The main simulation tool for the analysis of the membrane-based power plant was gPROMS [73-74], a commercially available state-of-the-art equation-oriented modelling and simulation software package. gPROMS is able to solve a mixed set of time-dependent partial differential, integral, and algebraic equations of nearly arbitrary complexity. The equations are solved simultaneously rather than sequentially, which is one of the main advantages of gPROMS[21]. The current version of gPROMS (3.2.0) offers only one solver (DASOLV solver) for the solution of mixed differential and algebraic equations. The DASOLV solver applies the implicit, variable time step/variable order backward differentiation formulae[22] [74]. The time step is automatically adjusted. Physical gas phase properties were taken from Multiflash [74].
The membrane-based gas turbine power plant model included a number of parameters that were based on experimental data and tentative diagrams. To generate a continuous function of the set of specific values, non-linear least squares regression was applied using DataFit[23] [91]. Regression was used for:

- Transport parameters for the membrane, including temperature-dependent oxygen ion concentration (c_0), oxygen self-diffusion coefficient (D_0), and fitting parameter for the oxygen partial pressure dependency of oxygen flux (n) used in the calculation of the oxygen permeation (Papers I-IV)

- Approximate stability limits with respect to temperature, CO_2 as well as oxygen pressure, specifying unstable regimes due to carbonate formation and oxidation (Papers II-IV)

- compressor off-design performance maps with respect to mass flow, pressure ratio, isentropic efficiency, and surge line (Papers II-IV)

- gas turbine turbine off-design performance maps with respect to isentropic efficiency (Papers II-IV)

- cooling flow requirements for the gas turbine turbine (Papers II-IV)

- part-load performance maps of the membrane-based gas turbine power plant, with and without afterburners, and the two load-control strategies, with and without variable guide vanes, with respect to mass flow of air, steam, fuel to the catalytic combustors as well as afterburners, and total pressure in the recycle loop as a function of the power output (Papers II-IV).

The steam cycle and heat recovery steam generator in design and part-load (off-design) was executed in GTPRO/GTMASTER [92] (Paper II).

[21] In fact, for a sparse, square set of equations there can be found irreducible subsets of equations that can be solved themselves without involving all unknowns of the problem [89].
[22] The second solver (SRADAU) is based on a variable time step, fully-implicit Runge-Kutta method [74]. The solution of the models developed in this work using the SRADAU solver of previous gPROMS versions showed that both solvers give similar performance in terms of accuracy, numerical stability, and required CPU time.
[23] DataFit utilizes the Levenberg-Marquardt method, which represents an optimal compromise between steepest descent (only efficient far from the minimum) and the Gauss-Newton method (only efficient when close to the minimum) [90].

It was found that Multiflash gives rather poor fluid properties at low temperatures. Therefore, the heat exchanger for steam production and cooling before flash condensation were executed in Aspen HYSYS [93] (Paper II).
Matlab[94] was used for system analyses of the membrane module as well as conventional and membrane-based gas turbine power plants after linearization in gPROMS. More specifically, it was used for:

- Model reduction of the membrane module model (Paper I)
- Calculation of the eigenvalues for the membrane module model (Paper I)
- Calculation of the relative gain arrays for the conventional and membrane-based power plant with and without afterburners and the two load control strategies at different load points and frequencies (Papers II-IV).

1.6 Project Description

1.6.1 Thesis Structure

The following chapters in this part of the thesis provide a brief overview of natural gas-fired power plants with CO_2 capture using mixed-conducting membranes. A separate chapter was dedicated to a more general overview of mixed-conducting membranes, including materials, crystal structure, mechanisms of oxygen transport, stability and module designs, with an emphasis on $La_2NiO_{4+\delta}$, which was the prototype membrane material assumed in this work. The first part closes with some recommendations for further work.
The second part of the thesis deals with the detailed modelling of a monolithic membrane module for integrated air separation in oxy-combustion power plants. Steady state as well as transient analyses were performed with the membrane module model. Moreover, linear model reduction was used to generate models with a lower number of system states while preserving their main dynamic characteristics. This reduced-order model can be used for control purposes (Paper I).
In the third part of the thesis, the membrane module model was extended by adopting a tentative stability diagram to analyse the risk of degradation. The membrane module model was included in a detailed gas turbine power plant model for integrated air separation. Operational and material-specific constraints were included to provide more realistic conditions for the power plant analysis. For part-load operation, two different load control strategies were investigated for the turbomachinery operating at constant rotational speed. The gas turbine power plant was linked to a bottoming steam cycle and CO_2 conditioning system to analyse the overall effect of CO_2 capture in comparison to a conventional combined cycle power plant (Paper II).
The fourth part of the thesis deals with the transient analysis of the membrane-based gas turbine power plant for the two load-control strategies. The operational and material-specific constraints were emphasized to obtain suitable load-decrease as well as load-increase rates of the power plant. Possible start-up and shut-down procedures were presented on a qualitative basis (Paper III).

The fifth part of the thesis analyses the effect of the degradation of individual gas turbine power plant components on its overall performance. Based on experimental and literature data, global degradation rates were included in the power plant model. Degradation of the membranes was emphasized. But performance deterioration of turbomachinery components was also included (Paper IV).

1.6.2 Author's Scientific Contributions with Respect to Findings

- Combining academic analysis methods with highly practical issues
- Emphasizing the importance of incorporating substantial knowledge from material science and control engineering into process engineering by means of a multi-scale modelling approach (spatial and time domain)
- Development of a detailed transient model of a monolithic mixed-conducting membrane module
- Adoption of material-specific properties into the membrane module model to define its operating window
- Development of transient membrane-based gas turbine power plant models (with and without afterburners) using the models mentioned above
- Collection of material and operational constraints for individual membrane reactor components and the gas turbine power plant to define the operating window for the safe operation of gas turbine power plants
- Determination of design specifications for the gas turbine power plants where material and operational constraints were not violated
- Determination of part-load operating windows for the gas turbine power plants for two load-control strategies where material and operational constraints were not violated
- Determination of suitable load change rates (decreases and increases) for the gas turbine power plants using the two load control strategies where material and operational constraints were not violated
- Implementation of degradation effects of individual process components to analyse the long-term stability of the power plants
- Development of start-up and shut-down procedures for the gas turbine power plants that lead to minimized stresses for the membrane modules and other critical membrane reactor components

It is important to mention that the entire gas turbine power plant models with all physical properties (thermodynamic properties, performance maps, and material-specific properties) were implemented in one simulation tool only, namely gPROMS.

1.6.3 Author's Research Contributions with Respect to Papers I-IV

Paper I

The author conceived of the paper concept, performed the main simulation work as well as the interpretation of results, and wrote the paper.

Paper II

The author conceived of the paper concept, performed the main simulation work as well as the interpretation of results, and wrote the paper.

Paper III

The author conceived of the paper concept, performed the simulation work as well as the interpretation of results, and wrote the paper.

Paper IV

The author conceived of the paper concept, performed the simulation work as well as the interpretation of results, and wrote major parts of the paper. The experimental data used for the selection of some model parameters and validation of selected results, were provided by Dr Vladislav Kharton (University of Aveiro, Portugal) and his colleagues from the University of Aveiro and from the Belarus State University, Minsk. The author participated in the analysis of the experimental data, and performed the interpretation necessary for the model formulation.

2 Natural Gas-Fired Power Plants with Mixed-Conducting Membranes

2.1 Conventional Combined Cycle Power Plant without CO_2 Capture

2.1.1 Gas Turbine Power Plant (Brayton Cycle)

A conventional gas turbine power plant is shown in the upper part of Figure 7. The corresponding pressure-volume and temperature-entropy slopes for the ideal process are shown in Figure 8. The working fluid (air) is compressed isentropically (1→2), mixed with the fuel and burnt under isobaric conditions (2→3). The hot exhaust gas is afterwards expanded isentropically through the turbine (3→4) [95-96] and fed to the steam cycle.

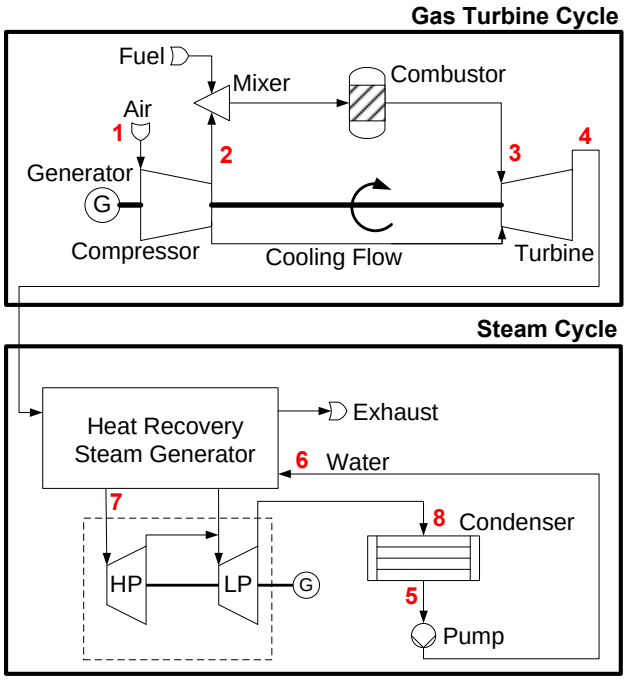

Figure 7: Conventional combined cycle power plant [97-98].

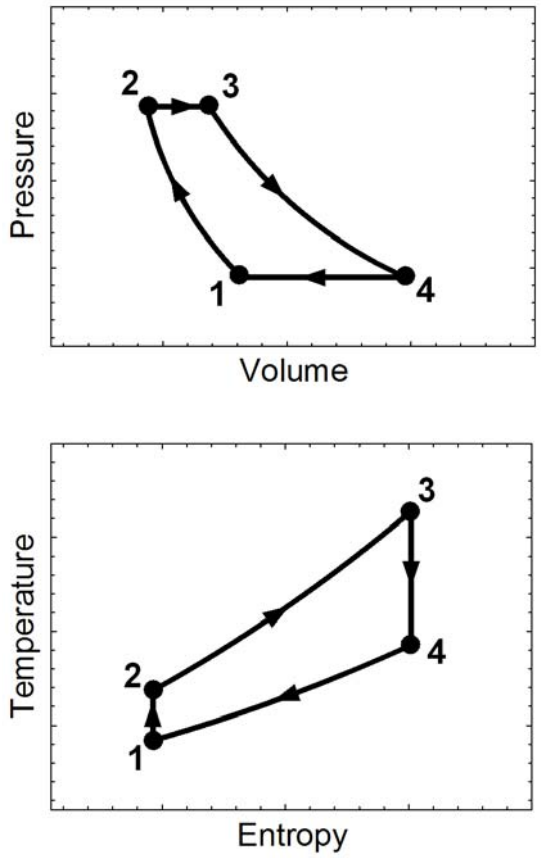

Figure 8: Pressure-volume and temperature-entropy slope for the ideal Brayton cycle shown in the upper part of Figure 7 [95-96].

2.1.2 Steam Cycle (Rankine Cycle)

The steam cycle of a combined cycle power plant is shown in the lower part of Figure 7, with the corresponding temperature-entropy diagram in Figure 9. The feed pump raises the pressure of the water isentropically (5→6), and supplies it to the heat recovery steam generator, where it is first heated to the boiling point isobarically (6→6'). The steam is then further heated isothermally (6'→6'') and finally superheated isobarically to raise the temperature to the desired operating value[24] (6''→7). The superheated steam is expanded isentropically through the steam turbine to generate power (7→8). The steam emerges from the turbine outlet both cooled and wet. The remaining moisture is condensed out isothermally and returned to the feed pump (8→5) to start the cycle again [95-96]. Combined cycle power plants achieve high efficiencies in the range of 50-60% and are used for base-load power generation [97-99].

[24] Supplementary firing could also be applied [99].

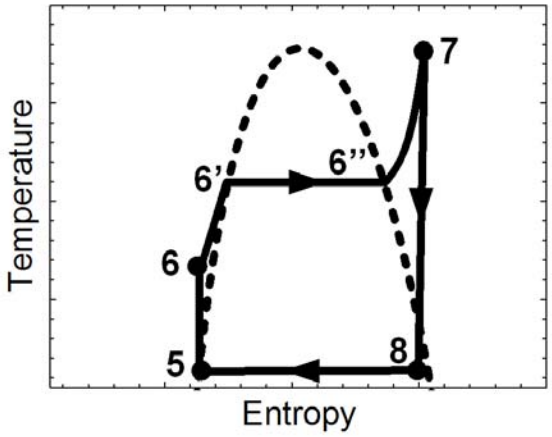

Figure 9: Pressure-volume and temperature-entropy slopes in the ideal Rankine cycle shown in the lower part of Figure 7 [95-96].

2.2 Mechanism of Air Separation by Membranes

In general terms, a membrane is regarded as a barrier between two enclosures that preferentially allows one molecule to permeate owing to the presence of a driving force. Figure 10A-D gives a brief overview of air separation mechanisms using membranes [100-106].

2.2.1 Porous Membrane

Figure 10A shows the principle of air separation using a porous membrane where the diffusivity of oxygen is higher than that of nitrogen. However, the small difference between the kinetic diameter of nitrogen (3.64Å) and oxygen (3.46Å) molecules makes air separation very difficult by a size separation mechanism [107-108].

2.2.2 Solid Electrolytes

Figure 10B shows a solid oxide electrolyte that is sandwiched between two gas-permeable electron-conductive electrodes. The oxygen ion conductor is dense and gas tight. The direct passage of oxygen molecules is hence blocked, but oxygen ions can migrate through the membrane. Electric charge neutrality is maintained by a simultaneous flux of electrons in the opposite direction using an external circuit.

2.2.3 Mixed-Conducting Membranes

Compared to solid electrolytes, mixed-conducting materials have the ability to conduct both ions and electrons. External circuitry is therefore not required. The principle is schematically shown in Figure 10C. Mixed-conducting membranes will be further discussed in Chapter 3.

2.2.4 Dual-Phase Membranes

Figure 10D shows a dual-phase membrane that can be visualized as a dispersed metallic phase in an oxygen ion conductor.

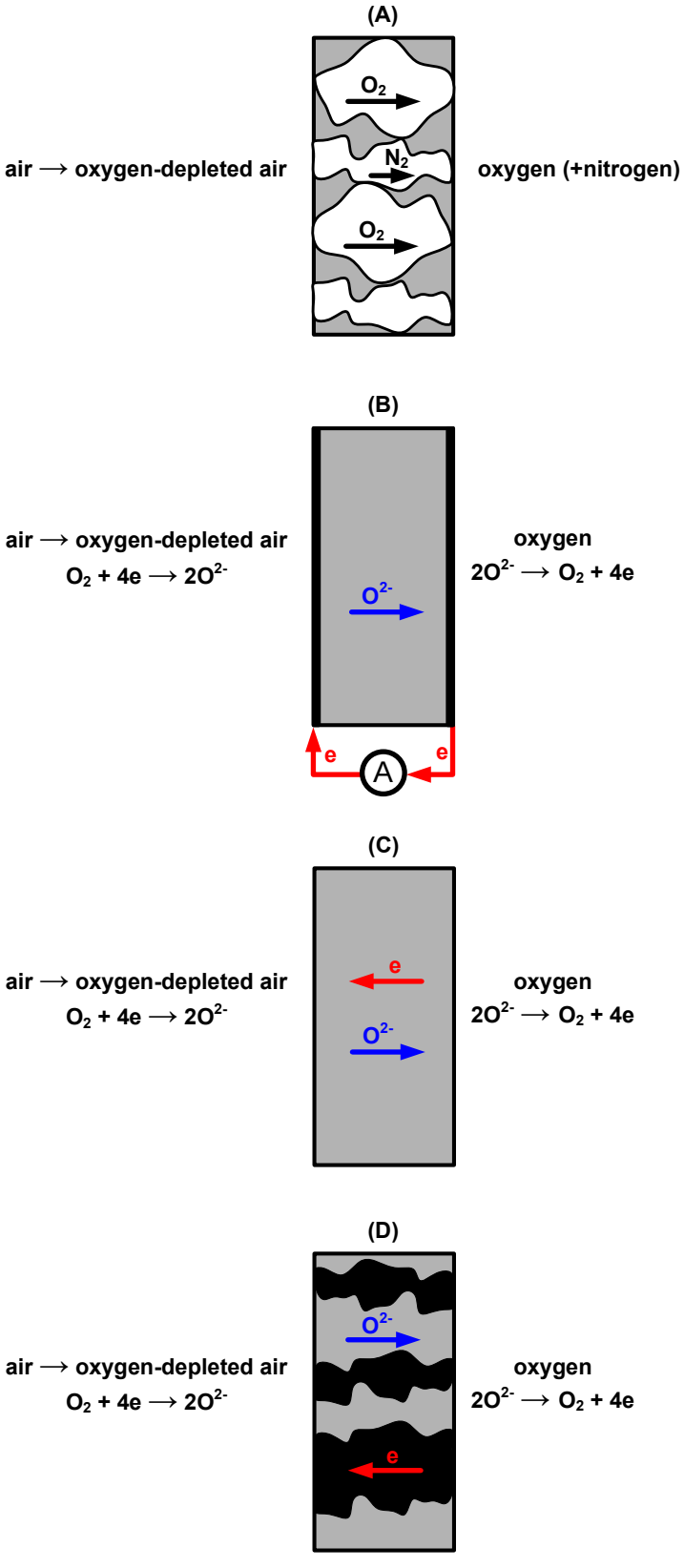

Figure 10: Oxygen transport mechanisms in membranes: (A) Porous membrane, (B) Solid electrolyte cell, (C) mixed-conducting oxide, and (D) dual-phase membrane [100-106].

2.3 Mixed-Conducting Membrane-based Combined Cycle Power Plant for Oxygen Production

2.3.1 Gas Turbine Power Plant (Brayton Cycle)

Mixed-conducting membranes can be integrated into conventional gas turbine power plants for the separation of oxygen from air, as shown in Figure 11 [54, 109-111]. The temperature of the compressed air from the gas turbine compressor is too low for sufficient oxygen transport through the membranes. They must thus be located after a combustor. However, there is a trade-off between the temperature increase and the oxygen that is available for separation. The oxygen permeation rate increases with both temperature and the oxygen pressure gradient. Furthermore, there is a higher temperature limit for the membrane that should not be exceeded to maintain stability. The higher temperature limit of the membrane is well below the temperature limit of modern gas turbines. Afterburners can be applied to raise the temperature of the gas to the turbomachinery limit, resulting in higher power output and increased efficiency. In order to increase the driving force for the oxygen transport through the membranes, different techniques can be applied, depending on the membrane module design: (i) pressurizing the oxygen-rich gas stream, (ii) producing a vacuum on the permeate side of the membranes, and (iii) use of a sweep gas that can easily be separated from the oxygen product by condensation, such as steam[25].

2.3.2 Steam Cycle (Rankine Cycle)

Steam can be supplied from the steam cycle when it is used as a sweep gas in the membrane modules, as shown in Figure 11.

[25] Direct conversion of the oxygen at the permeate side (e.g. oxidation of methane) to increase the oxygen chemical potential gradient is possible as well [54, 112-113]. However, problems related to stability of the membrane are then more pronounced and many high-permeability materials, such as La_2NiO_4, cannot be used [54, 114].

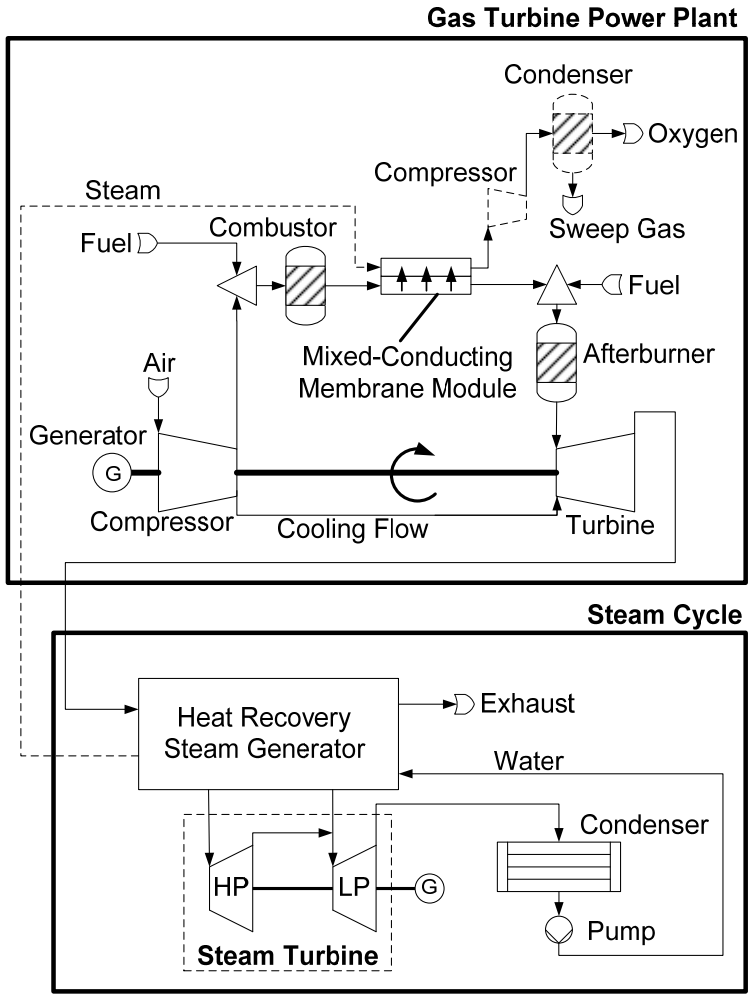

Figure 11: Membrane-based combined cycle power plant for oxygen production [54, 109].

2.4 Mixed-Conducting Membrane-based Combined Cycle Power Plant with Integrated Air Separation

2.4.1 Gas Turbine Power Plant (Brayton Cycle)

External Reactor Concept

The concept of an external combustor in gas turbine power plants has been put into use previously, for instance by ABB[26] (single silo-type combustor) and Siemens (two silo-type combustors) [115-116]. The important characteristics of this design are the relatively low fluid velocity, resulting in reduced pressure drops, and improved burn-

[26] One example is the ABB GT13E machine.

out of fuel[27] due to longer residence time[28] of the fluid in the combustors. Moreover, with the higher turbine inlet temperature, this arrangement requires large amounts of cooling air, i.e. the negative effect of the large areas of cool surface on the burn-out becomes more pronounced at off-design in addition to being less resistive in terms of damage due to transient forces. For these and other structural reasons, manufacturers have moved away from silo-type arrangements and turned towards the annular combustors design[29]. Part-load can then be achieved by burner group staging [98, 116, 118]. In the membrane-based power plant shown in Figure 12, an external reactor system is used.

[27] In particular for lower quality fuels.
[28] But longer residence times lead to increased formation of NOx [98].
[29] In the annular design, burners are arranged in rings around the annulus [117].

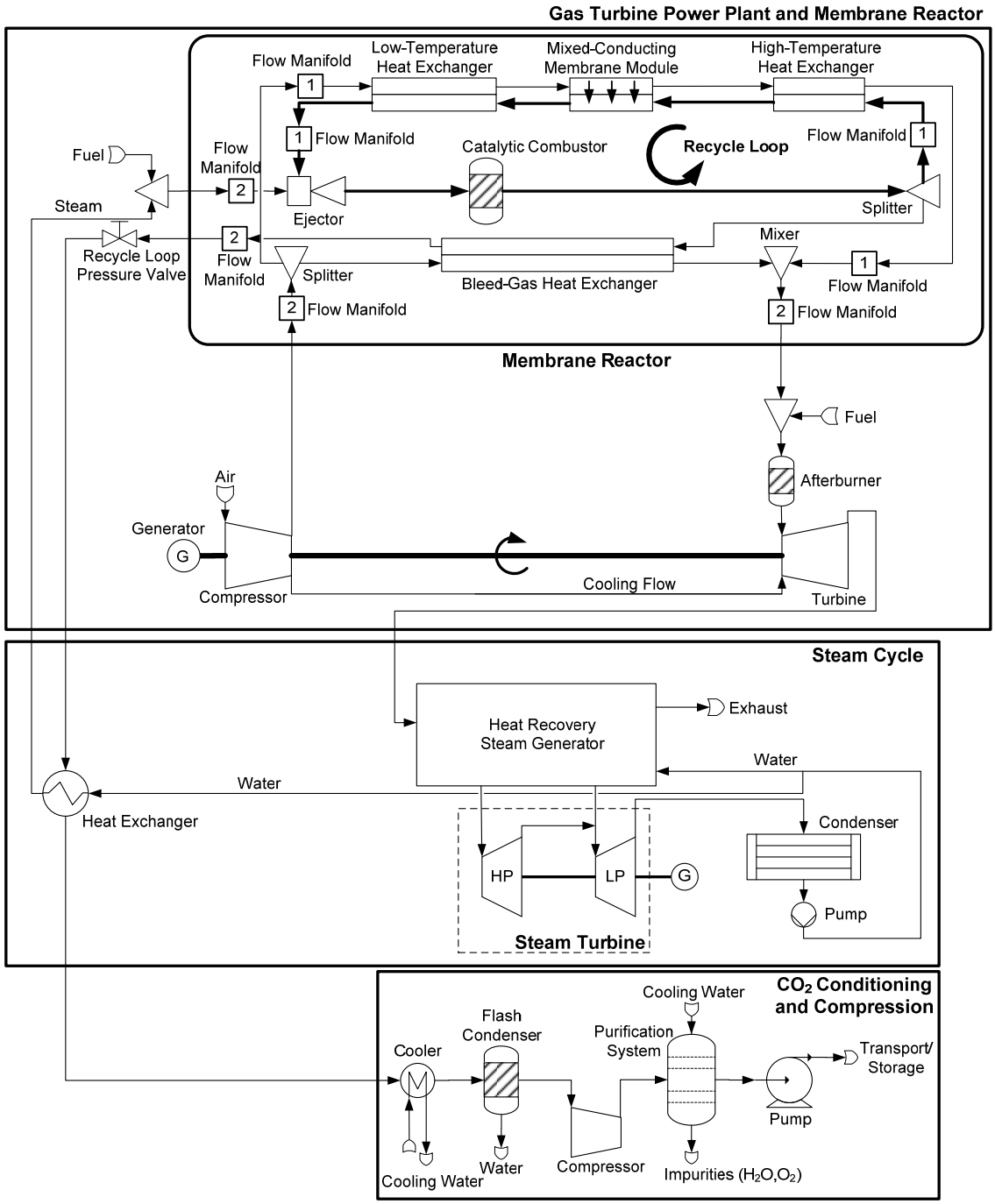

Figure 12: Membrane-based combined cycle power plant for integrated air separation [54, 56, 119].

Oxygen Mixed-Conducting Membrane Reactor

In the membrane reactor, the compressed air coming from the gas turbine compressor is split, where the majority is led to the low-temperature heat exchangers to raise the temperature of the air. Afterwards, the compressed air enters the membrane modules where oxygen is transported from the air to the sweep gas side. The temperature of the oxygen-depleted air is further raised before it is fed into the high-temperature heat exchangers. The minor part of the compressed air from the gas turbine compressor is led to the bleed-gas heat exchanger branch where the temperature of air is further increased by the combustion products of the catalytic combustors[30]. Fuel is induced to the membrane reactor by ejectors. Steam is added to the fuel to ensure proper ejector performance. In the catalytic combustors, the highly diluted oxygen in the sweep gas is burnt at nearly stoichiometric conditions. Excess oxygen is, however, required for stable combustor operation and to avoid the formation of unfavourable species, such as carbon monoxide.

Standard combustor technology cannot be applied due to the low oxygen concentrations and high dilution with water vapour and CO_2 [120-122]. The bulk of the combustion products are fed into the branch comprising the high-temperature heat exchanger, membrane modules, and low-temperature heat exchangers. In conjunction with the ejectors and catalytic combustors, this branch represents a recycle loop, as indicated in Figure 12. The heated oxygen-depleted gas from the high-temperature heat exchanger as well as the air coming from the bleed-gas heat exchanger are mixed before being fed into the afterburners where the temperature is further raised.

A certain amount of CO_2 is emitted when using afterburners[31]. A technological realization of the membrane reactor is shown in Figure 13 [56], where the membrane modules and heat exchanger are fabricated as two-fluid monoliths in counter-current flow mode [119], indicated in Figure 14. The use of monolith-type modules leads to a high packing density with a quite homogeneous temperature distribution [111, 123-124]. However, the two-fluid monolith technology results in a complex manifold system [111].

[30] In fact, all the compressed air could be directly fed to the low-temperature heat exchanger, but the use of the bleed-gas heat exchanger has the advantage that the temperatures of the low-temperature heat exchanger, membrane module, and high-temperature heat exchanger are higher, which leads to improved operation in terms of material constraints. Nevertheless, cooling of the sweep gas before entering the heat recovery steam generator is necessary in any case.

[31] This power plant is also known as the AZEP85. The CO_2 capture rate is approximately 85% [51, 57]. In this work, a capture rate of approximately 71% was found for the design case of the power plant with afterburners (Paper II). The power plant configuration without afterburners (AZEP100) would in theory lead to 100% CO_2 capture rates.

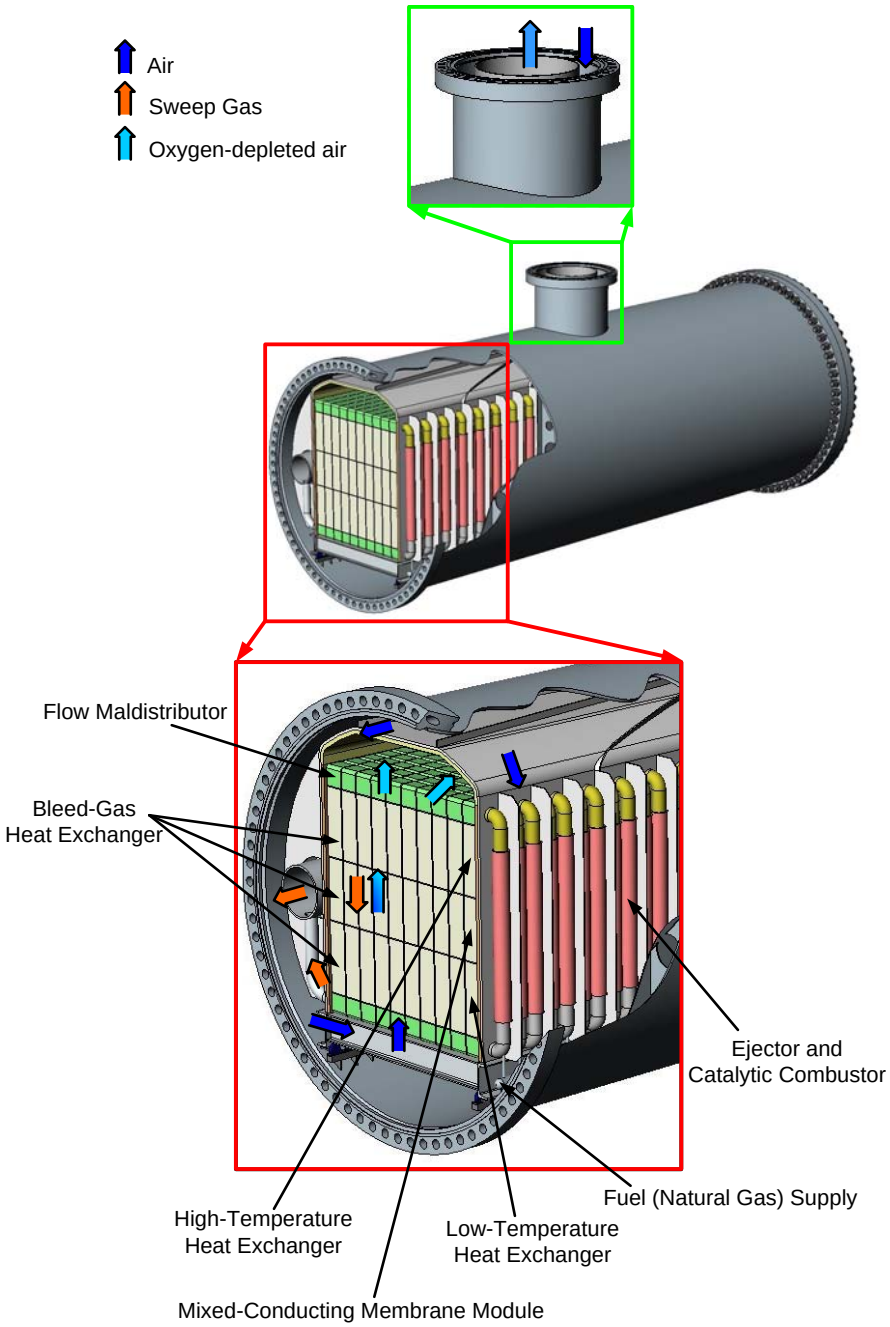

Figure 13: Membrane reactor [56].

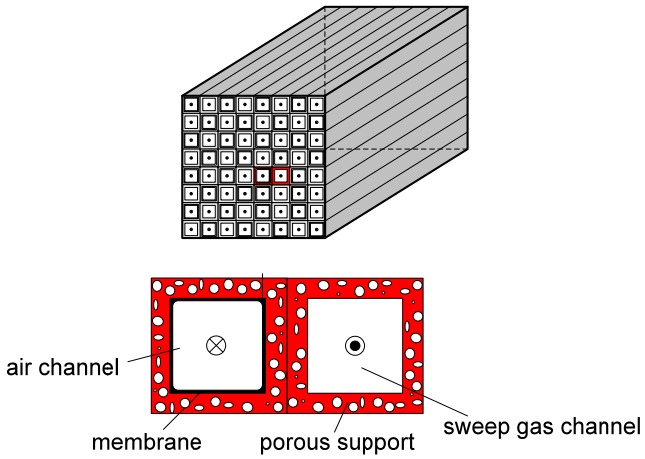

Figure 14: Mixed-conducting membrane module: Two-fluid monolith (top), modelling manifold (bottom) [119].

2.4.2 Steam Cycle (Rankine Cycle)

The membrane reactor requires external steam for proper ejector performance. Water can be extracted from the steam cycle, which is then heated by a heat exchanger using the heat from the combustion products prior to CO_2-compression, see Figure 12. Excess steam can be sent back to the steam cycle for additional power generation (Figure 2 in paper II).

2.4.3 CO_2 Conditioning and Compression

The product fluid from the catalytic combustors mainly consists of water vapour and CO_2 and can easily be separated by condensation. However, the excess oxygen that is required for stable operation of the catalytic combustors in the membrane reactor leads to undesirable dilution of the CO_2-rich gas stream with oxygen. After passing the steam-producing heat exchanger, the CO_2-rich gas is further cooled before entering the flash condenser, where most of the water leaves the line. The CO_2-rich gas is then compressed and inter-cooled before being fed to the purification system, which produces a highly concentrated CO_2 stream. The remaining impurities like water vapour and oxygen are among those compounds that need to be removed due to specifications set by the industry [125]. When leaving the purification system, the CO_2-rich fluid is in liquid form and then compressed to the end pressure for transport and storage.

3 Air Separation with Mixed-Conducting Membranes

3.1 Air Separation

Oxygen constitutes approximately 20.9% of the dry atmosphere[32] and represents the third largest volume of chemicals produced worldwide [54], with major consumption areas in the primary metal production, chemicals, and gasification industry [127].

3.2 Oxygen Mixed-Conducting Membranes

Mixed-conducting membranes have the potential to be a clean, efficient, and economical method for oxygen production as well as integrated air separation in oxy-combustion power plants. In the absence of leaks and cracks, mixed-conducting membranes show an infinite permselectivity for oxygen. However, elevated operation temperatures are required, typically higher than 950K [100-101, 110, 128-131], so some integration is necessary. Furthermore, the operating window of mixed-conducting membranes is relatively narrow because of several counteractive material properties. These include a desired high oxygen permeation rate, but at the same time low thermal and chemical expansion rates, mechanical strength, resistance in atmospheres containing large amounts of CO_2 and water vapour, sufficient resistance to CO and sulphur, compatibility with other materials, and low cost.

3.2.1 Materials for Oxygen Mixed-Conducting Membranes

Most of the materials that are suitable for mixed-conducting membranes belong to the families with perovskite (ABO_3), Ruddlesden-Popper type ($A_{n+1}B_nO_{3n+1}$), fluorite (AO_2), pyrochlore ($A_2B_2O_7$) and brownmillerite ($A_2B_2O_5$) crystal structures, and their derivatives [54, 101, 103, 132-133]. The ideal perovskite structure is shown in Figure 15. The A-site cation is ideally coordinated to 12 oxygen ions and the B-site cation is coordinated to six oxygen ions. Normally, the A site cation is larger than the B site cation[33,34]. Within the family of perovskite-related materials, the Ruddlesden-Popper compounds $A_{n+1}B_nO_{3n+1}$ have attracted particular attention due to specific properties

[32] Other main components of the dry atmosphere are N_2 with 78.12% and Ar with 0.93% [126].

[33] The radius of the cations, which can be incorporated into the A and B sites of the perovskite lattice, can be specified by the Goldschmidt tolerance factor, defined by

$t_s = \frac{r_a + r_0}{\sqrt{r_A + r_0}}$ [102, 134-135]. Per definition, an ideal cubic perovskite has a tolerance factor of one.

A perovskite structure is usually formed in an approximate range of $0.75<t_s<1$ [134-135].

[34] The ideal perovskite is not able to conduct oxide ions, so a certain number of oxygen vacancies must therefore be available. When variable-valence cations are present in the B sublattice, the oxides are then likely to become oxygen deficient under reducing conditions and at elevated temperatures [136]. In the mixed-conductor, electro-neutrality must be fulfilled, i.e. the sum of charges of the A and B cations must be equal to the total charge of oxygen anions [134].

originating from their layered structures, built of alternating ABO_3 perovskite-like layers and rock-salt AO sheets [54, 103]. Since the early studies by Teraoka et al. [137-139], a wide range of materials belonging to the class of acceptor-doped perovskites have been investigated [104, 140-141]. These materials show a high degree of oxygen deficiency, that is, generation of oxygen vacancies in the crystal lattice, enabling the oxygen anions to have relatively high mobility. The high electronic conductivity stems from the electronic structure of the transition metal cations, in particular their capability to exist in variable valence states under the membrane operation conditions [141]. The properties of the $(Ln,AE)TMO_3$ perovskite materials where Ln, AE, and TM are lanthanide, alkaline-earth, and transition metal cations, respectively, depend strongly on the dopant type and concentration. Due to their precursor cost and cation size, the most common trivalent A-site cation is lanthanum [102]. The alkaline earth elements[35] introduced in the A-sublattice are calcium, strontium, and barium [102-103]. The choice of the A-site element has a definite influence on the perovskite properties, but there is a stronger impact created by the ratio of tri- and divalent cations.

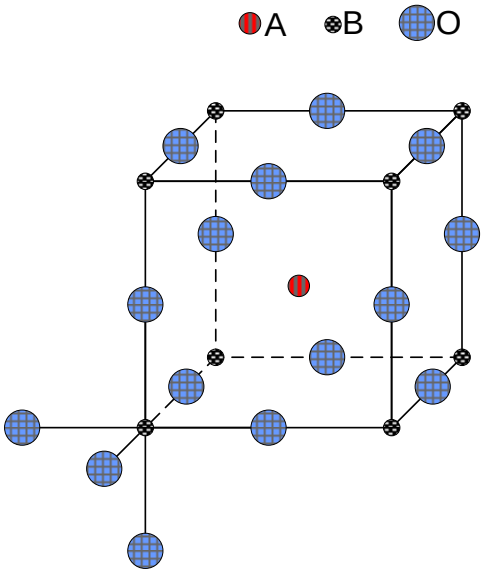

Figure 15: Ideal perovskite structure [142].

3.2.2 Ruddlesden-Popper Phase $La_2NiO_{4+\delta}$

In $La_2NiO_{4+\delta}$, consecutive perovskite layers ($LaNiO_3$) alternate with rock-salt layers (LaO), according to the general formula of Ruddlesden-Popper nickelates $(LaO)(LaNiO_3)_n$[36,37] with n=1. This structure belongs to the K_2NiF_4 type and is shown

[35] Alkaline-earth elements comprise Be, Mg, Ca, Sr, Ba, and Ra.

[36] The oxygen non-stoichiometry 'δ' (a number of extra oxygen anions or vacancies charge-compensated by the formation of electronic defects, per formula unit) in $La_2NiO_{4+\delta}$ can vary widely and can reach values up to 0.25 [143-147].

in Figure 16. The advantages of this material are a relatively high oxygen-ionic and p-type electronic conductivity, moderate thermal expansion coefficients, and moderate dimensional change on varying partial pressure of oxygen [71, 147-151]. Moderate acceptor doping of $La_2NiO_{4+\delta}$ with alkaline earth elements increases the electrical conductivity and decreases the oxygen content [147]. On the other hand, alkaline-earth and rare-earth elements[38] tend to react with CO_2 [133].

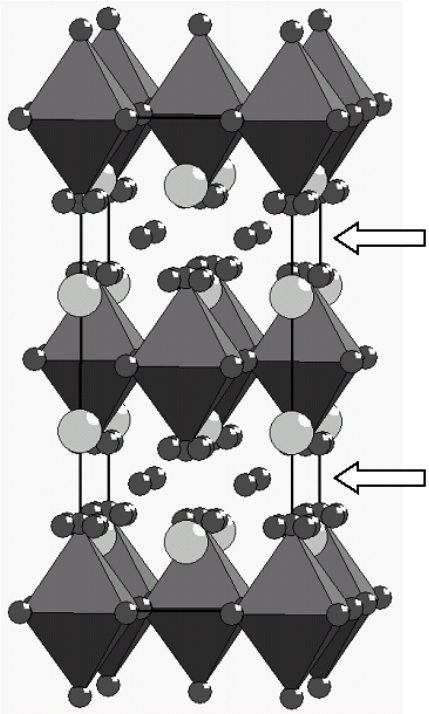

Figure 16: Crystal structure of $La_2NiO_{4+\delta}$ on the basis of neutron diffraction data taken from [144]. Figure taken from [149].

Other materials, such as A-site deficient perovskites and fluorites, are more stable in relation to CO_2 than $La_2NiO_{4+\delta}$. Examples of relatively stable perovskites reported in the literature include $La_{0.5}Sr_{0.5}FeO_{3-\delta}$, $La_{0.2}Sr_{0.8}Co_{0.41}Fe_{0.41}Cu_{0.21}O_{3-\delta}$, and $La_{0.85}Ce_{0.1}Ga_{0.3}Fe_{0.65}Al_{0.05}O_{3-\delta}$ [152-153]. On the other hand, thermal and chemical expansion rates are also among the factors that cause the most deterioration, leading to mechanical stresses. As a general rule, the perovskite structure is characterized by higher expansivity when compared to the layered structures. There are several groups of perovskite-type mixed conductors, which show higher oxygen permeation rates than $La_2NiO_{4+\delta}$, such as $(AE,Ln)(Co,Fe)O_{3-\delta}$ (AE=Sr, Ba). However, these also have an extremely high thermal expansion and high reactivity with CO_2 [128].
Coating a thin membrane layer onto a porous substrate of the same or similar composition, instead of using a relatively thick self-supported membrane, resulted in a

[37] This material shows several different structures, depending on the temperature as well as small changes in the stoichiometry [148].
[38] Rare-earth elements comprise Sc, Y, La, Ce, Pr, Nd, Pm, Sm, Eu, Gd, Tb, Dy, Ho, Er, Tm, Yb, and Lu.

breakthrough. In addition to providing sufficient mechanical strength, the support layer increases the specific membrane-surface area and, in a partly reduced state, may act as catalyst for oxygen exchange. For most known mixed-conductors, a catalytically active layer is necessary to provide sufficient performance, including all $SrCoO_3$- and $SrFeO_3$-based phases [154]. The porous support layer for $La_2NiO_{4+\delta}$ will increase its stability in the presence of CO_2 due to increasing oxygen fluxes and, therefore, the oxygen chemical potential at the membrane permeate-side surface, and to the diffusion limitations for CO_2 transfer towards the dense membrane surface in the pores.

A reasonable compromise between oxygen permeation rates as well as thermo-mechanical and thermodynamic stability in atmospheres with CO_2 and water vapour can be achieved by using composite membranes [54, 100, 102, 155]. For instance, mixed-conductors with high electronic and ionic conductivities such as $La_{0.7}Sr_{0.3}MnO_{3-\delta}$, can be combined with suitable oxide solid electrolytes, such as $Ce_{0.8}Gd_{0.2}O_{2-\delta}$ [155]. But long-term stability may be again a problem due to the formation of blocking layers between the constituent phases at elevated temperatures [155].

Membrane performance can be further improved by a proper choice of the module design, thermodynamic conditions during heating/cooling, and operating conditions. On the other hand, changes in these parameters may lead to a non-negligible increase in manufacturing and operation costs.

Moreover, the use of mixed-conducting membranes for integrated air separation in gas turbine power plants results in substantially higher process complexity. Operation at critical process conditions may be beneficial from a material point of view, but may also raise the need for unconventional (and expensive) control systems.

3.2.3 Oxygen Transport

In mixed-conducting membranes in an oxygen chemical potential gradient, oxygen ions and electrons migrate simultaneously through the membrane bulk but in opposite directions[39]. This simultaneous transport of both charge carriers is the key difference between mixed-conducting membranes and fuel cells, such as solid-oxide fuel cells[40]. In a general case, the overall oxygen permeation through a nonporous ceramic membrane is controlled by bulk ambipolar diffusion, governed by the ionic and electronic conductivities, and surface exchange kinetics [71, 106]. Surface exchange reactions may involve many sub-steps, including adsorption from the gas phase, charge transfer reactions between the adsorbed species and the bulk, and their reverse reactions [101, 147, 156-159]. Each of these surface reactions can be rate-controlling [100]. The oxygen transport through thick membranes, meaning membranes with a thickness greater than the characteristic length[41], is controlled by bulk diffusion.

[39] The oxygen ions and electrons can either be transported in the same phase (single-phase membrane) or in different phases (dual-phase membrane), as shown in Figure 10D.

[40] The solid electrolyte in fuel cells is a pure ionic conductor. Electrons are transported via an external conduction pathway from the anode (oxidation) to the cathode (reduction), as shown in Figure 10B.

[41] The characteristic length is given by $L_c = \frac{D_s}{k_s}$, with D_s and k_s as the self-diffusion and surface-exchange coefficient, respectively [100].

Reducing the membrane thickness results in enhanced oxygen permeation as long as bulk diffusion prevails, but eventually the surface reactions become rate-limiting [71, 100].
A membrane exposed to an oxygen partial pressure gradient can be visualized by dividing it into three zones: an interfacial zone on the high oxygen partial pressure (air) side, a central bulk zone, and an interfacial zone on the low oxygen partial pressure (sweep gas) side, as shown in Figure 17.

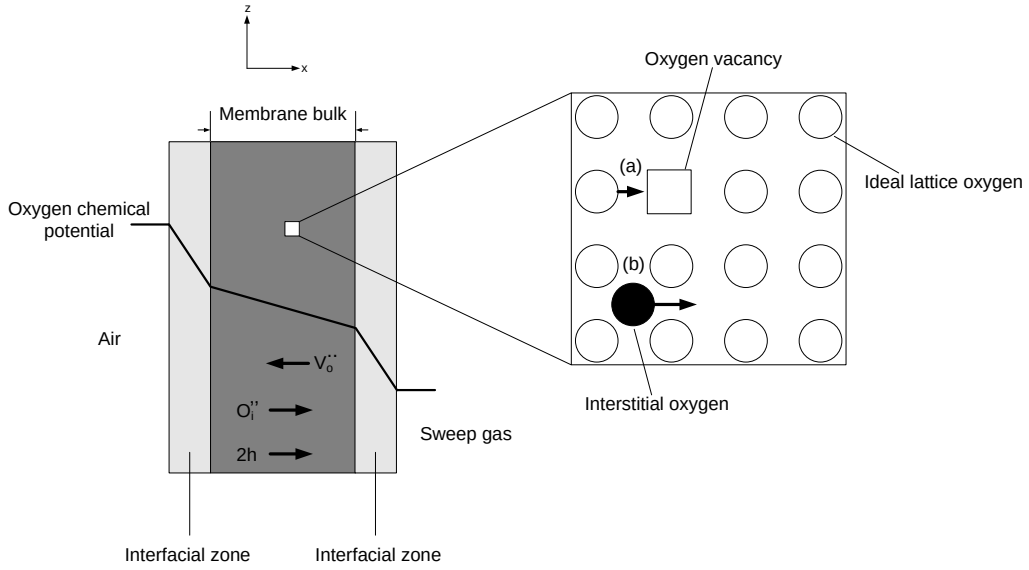

Figure 17: Oxygen permeation through the oxygen mixed-conducting membrane and lattice diffusion mechanism (a) via vacancy, (b) via interstitial positions.

In contrast to oxygen transport through perovskite compounds, oxygen transport through the $La_2NiO_{4+\delta}$-bulk is anisotropic [104] and proceeds via a combination of interstitial oxygen ion ($O_i^{"}$) migration through the rock-salt layers and anion migration through oxygen vacancies ($V_o^{\cdot\cdot}$) in the perovskite layers, formed according to [100-101, 159-160]

Equation 1 $$\frac{1}{2}O_2 \rightleftharpoons O_i^{"} + 2h$$

Equation 2 $$\frac{1}{2}O_2 + V_o^{\cdot\cdot} \rightleftharpoons O_o^x + 2h$$

where O_2 represents the oxygen molecule, O_o^x a regular oxygen anion having an effective neutral change in the lattice, and h a p-type electronic charge carrier (electron hole).

3.2.4 Stability

The operating conditions for mixed-conducting membranes (in energy applications) are very demanding, often combining elevated temperature, large gradients in partial pressures, and the presence of reactive species. The stability of these devices is therefore of particular interest and will be briefly discussed in the following subchapters.

Kinetic Stability

When exposing an oxide material to various gradients (chemical, thermal, electrical, mechanical) the mobile component fluxes can result in different degradation phenomena of kinetic origin. That means if the applied thermodynamic gradient is removed, the direct fluxes will disappear, but the material can be irreversibly degraded [55].

Kinetic demixing refers to the change of state of a multi-component material from originally homogeneous to chemically inhomogeneous, within the phase stability domain [55, 161]. In a ternary oxide like $La_2NiO_{4+\delta}$, demixing of the different cations will occur because the A- and B-site cations have different mobilities. Kinetic demixing can occur even if the ternary compound is in equilibrium [161]. In general, the degree of demixing increases with larger differences in mobility between the cations as well as decreasing thickness of the material. The result is a concentration gradient with an enrichment of the more mobile cation species on the high oxygen potential side while the slower component is left behind and becomes enriched on the low oxygen potential side [55, 161-163], as shown in Figure 18. However, this simple mechanism may be influenced by microstructural factors, because the cation diffusion processes in the major phase, in pores, in formed secondary phases, and along grain boundaries are different. Degradation by demixing of thin membrane layers coated onto a porous support to enhance the driving force may thus be more pronounced when compared to thicker self-supported (bulk-controlled) membranes. In an ideal case, demixing is a purely kinetic effect and is not directly related to the thermodynamics of the system [55, 162]. For oxygen-deficient perovskite materials containing no alkaline metal cations, the cation diffusion is usually several orders of magnitude lower than the oxygen diffusion and the cation contribution to the electrical conductivity can be neglected [55, 164]. However, the effect of kinetic demixing is of paramount importance in the long-term stability of the membrane [55, 164].

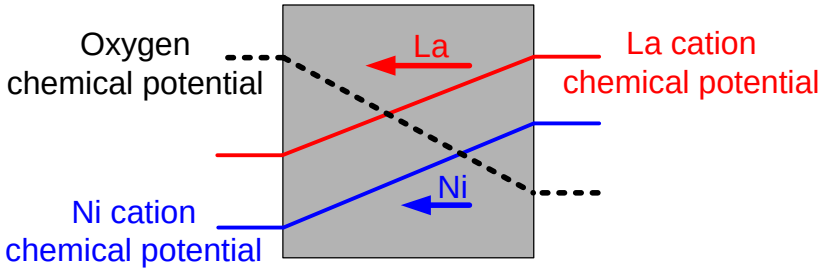

Figure 18: Cation chemical potential and transport in $La_2NiO_{4+\delta}$ [55].

Kinetic decomposition refers to the decomposition of the material and formation of secondary phases [55, 163-164]. The origin of this phenomenon is again the difference in cation mobility, but now demixing is driven to the point where the stability field of the oxide is left [163].

Thermodynamic Stability

The thermodynamic stability domain describes equilibrium conditions when a given phase exists. For the processes under consideration, the reactions leading to membrane decomposition include reduction (low-p(O_2) stability boundary), oxidation (high-p(O_2) stability boundary), and the formation of carbonates and hydroxides expressed by the corresponding partial pressures of CO_2 and water vapour. An extended discussion on the thermodynamic stability of $La_2NiO_{4+\delta}$-based membranes can be found in Papers II and IV.

3.2.5 Membrane Module Technology

The membrane module design has a strong influence on the oxygen permeation rate and its long-term stability [102, 104]. Different module designs have been developed, such as two-fluid monoliths, hollow-fibres, single tube, and tube-and-plate configurations [54, 102, 165]. Each of them has its advantages and drawbacks in terms of area-to-volume ratio, size, cost of production, up-scaling, ease of sealing and use of a sweep gas, and resistance to thermo-mechanical, mechanical, and chemical stresses [54, 102, 104]. Some of the advantages of monoliths are low axial dispersion, uniform distribution of flow, and up-scale capability[123]. In a membrane-based power plant for integrated air separation (Figure 12), the use of a sweep gas is the only viable method to increase the driving force for oxygen transport. Large mechanical stresses in the monolithic membrane modules and heat exchangers would occur if large pressure differences between the two fluids were applied.

3.2.6 Generality of Modelling Results using Membrane Materials other than $La_2NiO_{4+\delta}$

The brief discussion presented above on mixed-conducting materials is far from exhaustive. But it should be clear that so far, there is no composition that satisfies all requirements in terms of high oxygen permeation rates, stability, and cost.
The membrane material selected for this work was $La_2NiO_{4+\delta}$. Physical properties were kindly provided by partners [166-167]. It should be emphasized that the assumption of this particular membrane material (and also the assumption of a monolithic module design) does not result in a substantial loss of generality. As far as the overall performance of the power plant is concerned, the steady-state and transient behaviour can be understood as rather generic (Papers II-III). However, degradation rates of the membrane material (Paper IV) refer to $La_2NiO_{4+\delta}$.

3.3 Further Methods for Air Separation

3.3.1 Cryogenics

Cryogenic distillation is currently the technology that is the most developed for the large-scale production of oxygen. Purities higher than 99% can be achieved [54, 168]. In addition, cryogenics can produce separate streams of oxygen, nitrogen, and argon. The major drawback of cryogenic air separation is its energy requirements [55], caused by the need for air compression to provide the required cooling.

3.3.2 Adsorption

Pressure swing adsorption and vacuum swing adsorption are based on the increased amount of adsorbate at elevated pressure that can be deposited on the adsorbent. Adsorption takes place at high pressure, desorption at low pressure. Oxygen production is performed predominantly on zeolites, where nitrogen is bound more strongly on the surface than oxygen [126, 168] with typical purities of 93-95% [168]. Bed size represents the controlling factor with regard to capital cost, which stems from the cyclic nature of the adsorption process [168].

3.3.3 Polymeric Membranes

Polymeric membranes are used for oxygen enrichment[42] with an oxygen mole fraction in the range of 25-50% [107, 168-169]. The mechanism for separation is based on the preferred dissolution and diffusion of oxygen over nitrogen in these materials [54,

[42] Or oxygen depletion of air.

170], see Figure 10A. The operation temperature is limited due to the thermal stability of the polymers [54].

4 Conclusions

This work presents an investigation of a membrane-based gas turbine power plant for CO_2 capture in terms of design, off-design (part-load, degradation), and transient operation (part-load, failure incidents, changes in ambient conditions and fuel composition, and start-up and shut-down). The original process design was proposed by StatoilHydro (the former Norsk Hydro).

The emphasis was on operational and material constraints to maintain sound performance of the gas turbine power plant for its entire operating range. For the mixed-conducting membrane modules, material-specific properties were incorporated, inter alia, by means of a tentative stability diagram, which showed regions where degradation can be expected to occur. For the membrane module and heat exchanger models, one-dimensional conservation balances were applied for energy, species, and mass. Turbomachinery components were based on off-design performance map models.

4.1 Steady-State and Transient Operation of the Mixed-Conducting Membrane

The membrane modules were assumed to be fabricated as two-fluid monoliths with a checkerboard counter-current flow distribution. Furthermore, it was assumed that the thin membrane layer was coated onto a thermo-mechanical and chemical compatible porous substrate to provide mechanical strength and also to increase the oxygen permeation, as discussed above. The membrane layer was coated onto the air side, whereas the porous substrate was exposed to the sweep gas. This configuration leads to improved stability due to reduced interaction between the membrane layer and gaseous species, such as CO_2 and water vapour. Oxygen transport through the mixed-conducting membrane was strongly dependent on the operation temperature (which should be higher than 1170K to achieve both high performance and sufficient stability in CO_2-containing atmospheres) and the oxygen pressure gradient between the feed and permeate stream. The thermal response of the monolithic membrane module model was relatively fast because of the thin solid walls (membrane layer and porous support) of 0.33mm. Assuming constant inlet conditions for both fluids, a steady-state can be reached after approximately five minutes when starting from ambient temperature to operating conditions.
A literature survey showed that the Ruddlesden-Popper compound $La_2NiO_{4+\delta}$ can be regarded as a promising material for this application because of its relatively good properties for oxygen transport, moderate thermal and chemical expansion, stability in terms of interaction with gaseous species such as CO_2, and relatively easy processing.

4.2 Design Operation of the Membrane-based Gas Turbine Power Plant with Afterburners and Combined Cycle Power Plant Analyses with CO_2 Conditioning and Compression

Assuming a combustion temperature of 1473K in the catalytic combustors and a turbine inlet temperature of approximately 1530K, the gas turbine power plant reaches a net electric efficiency of 33.4%, compared to 35.8% for a conventional gas turbine power plant with the same key specifications, i.e. the mass flow of air entering the gas turbine compressor and the turbine inlet temperature. The combined cycle net electric efficiency of the membrane-based power plant with CO_2 capture was 47.1%, the power output was 30.4MW, whilst the conventional combined cycle power plant without CO_2 capture had a net electric efficiency of 53.3% and a power output of 36.2MW. Hence, CO_2 capture leads to a power output penalty of 16% and an efficiency reduction of 6.2 percentage points. The CO_2 capture rate was found to be approximately 71%[43]. It should also be mentioned that the CO_2 conditioning system for the membrane-based combined cycle power plant required large amounts of cooling water of approximately 235kg/s, which can be a limiting factor with respect to location of this CO_2 capture power plant.

4.3 Part-Load Operation of the Membrane-based Gas Turbine Power Plant with Afterburners and Combined Cycle Power Plant Analyses with CO_2 Conditioning and Compression

The mid merit gas turbine assumed in this work was operated at constant rotational speed. In this respect, two load-control strategies were analysed. In the first load-control strategy, variable guide vanes were used to manipulate the mass flow of air to the gas turbine compressor. This degree of freedom was used to control the turbine exit temperature. In the second load-control strategy, variable guide vanes were not used and the turbine exit temperature was allowed to vary. For both load-control strategies, the mean solid-wall temperature[44] of the membrane modules was maintained close to its design value, which led to improved stability. Moreover, the pressure in the recycle loop was controlled to minimize the mechanical load on the walls of the monolithic membrane modules and heat exchangers. Simulations revealed that the load-control strategy with variable guide vanes in the gas turbine compressor was superior due to improved combined cycle efficiencies and a larger part-load operating window. For this load-control strategy the variable guide vanes were the limiting constraint with a maximum air mass flow reduction of 30%. The load can be reduced to approximately 62% of the design value. Further load reduction by reducing

[43] The CO_2 capture rate is thus substantially lower than the figure of 85% reported in the literature [51, 57].

[44] The mean solid-wall temperature is defined as: $\overline{T}_{solid} = \frac{1}{L}\int_0^L T_{\text{solid}}\, dl$

the mass flow of fuel would lead to stability problems of the membrane modules due to carbonate formation. During part-load operation, the performance of the catalytic combustors in the membrane reactor improved because of higher oxygen mole fractions. For the load-control strategy without variable guide vanes, the catalytic combustors were the constraining process components. The limit of the excess oxygen mole fraction of 0.5% had already been reached at approximately 82% of the design value.

4.4 Design and Part-Load Operation of the Membrane-based Gas Turbine Power Plant without Afterburners

Comparison of the membrane-based gas turbine power plant with and without afterburners reveals that design changes were required with respect to membrane reactor and turbomachinery components when assuming the same turbine outlet temperature and excess oxygen concentration in the catalytic combustors. It should be emphasized that the latter design had one less degree of freedom. Variable guide vanes can thus not be applied to control the turbine exit temperature. Load-control without variable guide vanes is not feasible due to the material constraints of the membrane modules. It was shown that there were substantial cuts in part-load capability, which means the load can only be reduced to approximately 73% compared to 58% for the design with afterburners. For both power plants, the variable guide vanes were the limiting process component for part-load operation.

4.5 Start-Up and Shut-Down of the Mixed-Conducting Membrane-based Gas Turbine Power Plant with Afterburners

To ensure safe start-up and shut-down procedures, the membrane-based gas turbine power plant requires several critical auxiliary process components so that detrimental process conditions can be avoided. Moreover, a complex time schedule for the membrane reactor and turbomachinery is needed. Technical gases such as nitrogen must be available, presumably in the range of tonnes. Furthermore, small amounts of the evaporating components of the membrane and porous support layer must be injected to prevent degradation. However, these additives should be recollected afterwards to avoid clogging the process units located downstream of the membrane modules. This requires additional process equipment (e.g. valves), which are regarded as highly critical. Start-up times of several hours will be required for the membrane-based power plant, which are much longer compared to those for conventional mid merit gas turbine power plants.

4.6 Transient Operation of the Mixed-Conducting Membrane-based Gas Turbine Power Plant with Afterburners

It was shown that the membrane-based gas turbine power plant exhibits rather slow dynamics when compared to conventional gas turbine power plants. For the two load-control strategies presented in 4.3, relatively slow load-decrease rates must be applied to reach the part-load limit determined by steady-state simulations. For the load-control strategies with variable guide vanes, the ejectors were the limiting process components when relatively high load-reduction rates were applied (variable guide vanes were the limiting process components at steady-state). However, transition times could be reduced when stepped load-reduction procedures were applied, i.e. relatively high load-reduction rates followed by relaxation times at constant power output. The minimum load of approximately 58%, found by steady-state simulations, could then be reached in less than 32 minutes (compared to 36 minutes for continuous load reduction). For the load-control strategy without variable guide vanes in the gas turbine compressor, load-reduction capability was not much affected by the load-rates. The excess oxygen in the catalytic combustors remained the limiting constraint, as in the steady-state case. However, simulations revealed that load-reduction rates must be sufficiently long to avoid instability of the catalytic combustors when operated at the limit of excess oxygen. The minimum load of approximately 82%, found for steady-state operation, can be reached within 40 minutes.
For both load-control strategies, much longer load-increase rates must be applied (approximately 132 minutes for the load-control strategy with variable guide vanes and 67 minutes without variable guide vanes) because of thermodynamic stability regions, which would be passed through if relatively high load increase rates were applied, i.e. already in the range of the load-decrease rates. In order to substantiate this hypothesis, the power plant design was modified so that the membrane modules were operated at higher as well as lower mean solid-wall temperatures. In this respect, higher mean solid-wall temperatures were beneficial from a load-change point of view. On the other hand, there is a higher temperature limit for the mean solid-wall of the membranes that should not be exceeded to maintain stability. Ergo, the range within which the temperature can be raised is limited.

4.7 Long-Term Stability of the Mixed-Conducting Membrane-based Gas Turbine Power Plant with and without Afterburners

The membrane-based gas turbine power plant was analyzed with respect to long-term stability, considering the first 1000 operating hours. Based on experiments, a global degradation rate of 3.3%/1000 operation hours was assumed for the $La_2NiO_{4+\delta}$ membranes. Degradation rates for individual turbomachinery components were also incorporated.
Simulations revealed that the ideal operating line (assuming perfect control and no performance deterioration over time) was substantially shifted due to individual

process component deterioration. The excess oxygen concentration in the catalytic combustors was in this respect one of the most critical factors.
Changes in ambient temperature and fuel composition were found to have a substantial impact on the operation and stability of the membrane-based power plant. Consequently, even though the power plant may be located in an area where the climate is benign, controllers must not only account for a shift from ideal process conditions in the operating line due to degradation, but also for already relatively small external changes.
Standard measures to suppress performance deterioration in conventional gas turbine power plants, such as solvent-based online washing, are likely to be detrimental to the membrane-based gas turbine power plant due to interaction between the solvent and the membranes. The power plant needs to be shut down and cooled so that direct contact is avoided. However, the start-up and shut-down procedure for the membrane-based power plant were regarded as highly complex and error prone. Frequent start-ups and shut-downs are assumed to accelerate degradation.

4.8 Response of the Mixed-Conducting Membrane-based Gas Turbine Power Plant with Afterburners to Operating Incidences

The transient behaviour of the membrane-based power plant in the case of failures was found to be poor.
A sudden total breakdown of the fuel supply to the afterburners led to a drop of the excess oxygen mole fraction well below the limit where stable combustion can be maintained. Moreover, the mechanical stability limit (total pressure difference) of the monolithic membrane modules and heat exchangers was also exceeded.
A malfunction of the recycle loop valve, resulting in a sudden drop of pressure in the recycle loop (-5 bar), was found to have a detrimental effect on the mechanical stability of the monolithic membrane modules and heat exchangers.
The response of the membrane-based power plant to a failure of the variable guide vanes was detrimental because of the temperature increase that results if the fuel supply is not adjusted. Some parts of the membrane modules exceeded the higher temperature limit where high temperature creep is likely to occur.

4.9 Some General Conclusions

The membrane-based power plant shares some similarities with fuel cell gas turbine hybrid cycles, in particular solid oxide fuel cells. Very intensive research on stand-alone fuel cells [78, 171-188] as well as hybrid cycles [189-205] has been conducted in the past two decades. Within the fuel cell community, long-term stability has been recognized as one of the essential issues that must be explicitly addressed if these devices are to be commercialized. On a system level, fuel cell durability of more than 70000 hours has been reported with a degradation rate of 0.3%/1000 hours [186]. Mixed-conducting membranes have not yet been able to obtain durability values like these. Compared to solid oxide fuel cell systems, mixed-conducting membrane

systems for energy applications are at a rather early stage of development. Considering the continuing development of solid oxide fuel cell systems and the knowledge gained in this work, it can be expected that mixed-conducting membranes for integrated air separation will not be commercialized on a large-scale within the next years. However, designing a membrane-based power plant with a lower degree of integration, and most likely allowing for higher CO_2 emissions, could make this type of power plant competitive with other power plant concepts that incorporate CO_2 capture. Furthermore, if the stability of mixed-conducting membranes can be improved, considerably less complex process designs (e.g. the process design in Figure 11) will become very attractive for a potential method for oxygen production.

5 Suggestions for Further Work

5.1 Modelling

- The oxygen transport was assumed to be controlled by both bulk diffusion as well as surface kinetics, implemented by means of an approximate of Wagner equations and empirical coefficients to incorporate surface kinetics. The membrane module model could be further improved by applying (simple) global reaction schemes for the description of surface kinetics. However, the first attempts showed a drastic loss in numerical stability when (fast) kinetics are incorporated.

- The membrane module model could be improved by incorporating the mass transfer resistance caused by the porous support[45].

- Another module design (e.g. tube-and-shell) could be assumed and analysed with respect to key parameters such as mechanical stability, area-to-volume ratio, and ease of sealing.

- $La_2NiO_{4+\delta}$ was assumed as the prototype material in this work. Other material could be studied in view of oxygen permeation, stability and other membrane specific properties.

- A procedure similar to that used for the membrane-based power plant with integrated air separation could also be used for a membrane-based power plant for oxygen production, shown in Figure 11. Different materials could be tested in view of the optimal module design, stability, and overall power plant performance.

- The ejector model used in this work was assumed to operate in the critical mode, i.e. at high actuating fluid pressures. For the simulation of start-up and shut-down procedures, the ejector model should be improved so that operation in the sub-critical and even back flow regime is covered [206-207].

- The membrane-based power plant could be investigated in terms of possible instabilities, such as state multiplicity, using bifurcation analysis methods [208-209]. Numerical bifurcation analysis is a powerful tool for the analysis of stability limits of nonlinear dynamic systems [210-214]. One such tool for bifurcation analysis is DIVA, which can cope with high-order DAE systems of chemical processes [213-214]. Furthermore, gPROMS and DIVA can communicate via the CAPE-OPEN interface[46] [214].

[45] Its neglect is valid for this work since a relatively thin support was assumed allowing for only small total pressure differences across the solid phase of the monolithic membrane modules (and heat exchangers). Furthermore, the porous support is also assumed to be catalytically active. Improved operability by relaxing the total pressure constraint is paid by the use of a thicker support layer, which in turn would lead to a reduced average oxygen flux due to the mass transport resistance.

[46] Both gPROMS and DIVA can solve systems of differential index one [74, 211].

- The control of the membrane-based gas turbine power plant, based on standard PID control methods, is subject of the current investigation. Improved handling of constraints could be achieved by model predictive control. In this respect, improved model reduction techniques such as the Karhunen-Loève-Galerkin method, could be applied for the design of controller [215-216].

5.2 Experiments

- So far, little experimental work has been conducted on seals when compared to material properties of mixed-conducting membranes [217-218]. The seals must also withstand extreme conditions with regard to elevated temperature and pressure as well as high concentrations of CO_2 and H_2O. Further experimental work is needed here as well.

- Material properties with regard to coke formation, catalyst deactivation and others could be incorporated into the combustor model to improve the range of operating conditions.

- The membrane module model could be extended by incorporating properties for chemical and thermo-mechanical stability [184-185, 219].

References

1. Statistical review of world energy, www.bp.com, 2008.
2. Moriarty, P., Honnery, D., *What energy levels can the Earth sustain?* Energy Policy, 2009. **37**(7): p. 2469-2474.
3. Chow, J., Kopp, R.J, Portney, P.R., *Energy Resources and Global Development.* Science, 2003. **28**(302): p. 1528-1531.
4. Metz, B., Davidson, O., de Coninck, H., Loos, M., Meyer, L., *IPCC Special Report, Carbon Dioxide Capture and Storage, Summary for Policymakers*. 2005.
5. Callaway, E., *Energy: To catch a wave.* Nature, 2007. **450**: p. 156-159.
6. Franklin M. Orr, J., *CO2 capture and storage: are we ready?* Energy & Environmental Science, 2009.
7. Plasynski, S.I., Litynski, J. T., McIlvried, H. G., Srivastava, R. D., *Progress and New Developments in Carbon Capture and Storage.* Critical Reviews in Plant Sciences, 2009: p. 123-138.
8. Pacala, S., Socolow, R., *Stabilization Wedges: Solving the Climate Problem for the Next 50 Years with Current Technologies* Science, 13 August 2004. **305**: p. 968-972.
9. Forsberg, C.W., *Sustainability by combining nuclear, fossil, and renewable energy sources.* Progress in Nuclear Energy, 2009. **51**(1): p. 192-200.
10. Sailor, W.C., Bodansky, D., Braun, C., Fetter, S., van der Zwaan, B., *NUCLEAR POWER: A Nuclear Solution to Climate Change?* Science, 2000. **288**: p. 1177-1178.
11. Parkins, W.E., *Fusion Power: Will It Ever Come?* Science, 2006. **311**: p. 1380.
12. Haszeldine, R.S., *Carbon Capture and Storage: How Green Can Black Be?* Science, 2009. **325**(5948): p. 1647-1652.
13. Norwegian Water Resources and Energy Directorate, www.nve.no, 2009.
14. Rind, D., *Complexity and Climate.* Science, 1999. **284**(105): p. 105-107.
15. Parry, M., Lowe, J., Hanson, C., *Overshoot, adapt and recover.* Nature, 2009. **458**(7242): p. 1102-1103.
16. Schneider, S., *The worst-case scenario.* Nature, 2009. **458**(7242): p. 1104-1105.
17. Wigley, T.M.L., Roecker, W.S., *CO2 Emissions: A Piece of the Pie.* Science, 2007. **316**(5826): p. 829 - 830.
18. Arneth, A., Unger, N., Kulmala, M., Andreae, M.O., *Clean the Air, Heat the Planet?* Science, 2009. **326**(5952): p. 672-673.
19. Hansen, J., Johnson, D., Lacis, A., Lebedeff, S., Lee, P., Rind, D., Russell, G., *Climate Impact of Increasing Atmospheric Carbon Dioxide.* Science, 1981. **213**(4511): p. 957-966.
20. Balazs, A.C., Epstein, I.R., *Emergent or Just Complex?* Science, 2009. **325**: p. 1632-1634.
21. Foote, R., *Mathematics and Complex Systems.* Science, 2007. **318**(410): p. 410-412.
22. Cho, A., *Ourselves and Our Interactions: The Ultimate Physics Problem?* Science, 2009. **325**: p. 406-408.
23. Keith, D.W., *Why Capture CO2 from the Atmosphere?* Science, 2009. **325**(5948): p. 1654-1655.

24. Hansen, J., Nazarenko, L., Ruedy, R., Sato, M., Willis, J., Del Genio, A., Koch, D., Lacis, A., Lo, K., Menon, S., Novakov, T., Perlwitz, J., Russell, G., Schmidt, G.A., Tausnev, N., *Earth's Energy Imbalance: Confirmation and Implications.* Science, 2005. **308**(5727): p. 1431 - 1435.
25. Kerr, R.A., *Amid Worrisome Signs of Warming, 'Climate Fatigue' Sets In.* Science. **326**(5953): p. 926-928.
26. Jackson, S.C., *Parallel Pursuit of Near-Term and Long-Term Climate Mitigation.* Science, 2009. **326**(5952): p. 526-527.
27. Monastersky, R., *A burden beyond bearing.* Nature, 2009. **458**(7242): p. 1091-1094.
28. Meinshausen, M., Meinshausen, N., Hare, W., Raper, S.C.B., Frieler, K., Knutti, R., Frame, D.J., Allen, M.R., *Greenhouse-gas emission targets for limiting global warming to 2 °C.* Nature, 2009. **458**(7242): p. 1158-1162.
29. Shine, K.P., Sturges, W.T., *CO2 is not the only gas.* Science, 2007. **315**: p. 1804-1805.
30. Cohen, J., Rau, A., Brüning, K., *Bridging the Montreal-Kyoto Gap.* Science, 2009. **326**(5953): p. 940-941.
31. Shindell, D.T., Faluvegi, G., Koch, D.M., Schmidt, G.A., Unger, N., Bauer, S.E., *Improved Attribution of Climate Forcing to Emissions.* science, 2009. **326**(5952): p. 716-718.
32. Hoffert, M.I., Caldeira, K., Benford, G., Criswell, D.R., Green, C., Herzog, H., Jain, A.K., Kheshgi, H.S., Lackner, K.S., Lewis, J.L., Lightfoot, H.D., Manheimer, W., Mankins, J.C., Mauel, M.E., Perkins, L.J., Schlesinger, M.E., Volk, T., Wigley, T.M.L., *Advanced Technology Paths to Global Climate Stability: Energy for a Greenhouse Planet.* Science, 2002. **298**(981): p. 981-987.
33. Schmidt, G., Archer, D., *Too much of a bad thing.* Nature, 2009. **458**(7242): p. 1117-1118.
34. Lackner, K.L., *A Guide to CO2 Sequestration.* Science, 2003. **300**(5626): p. 1677-1678.
35. Jones, N., *Sucking it up.* Nature, 2009. **458**(7242): p. 1094-1097.
36. Morton, O., *Great white hope.* Nature, 2009. **458**(7242): p. 1097-1100.
37. Schrag, D.P., *Preparing to Capture Carbon.* Science, 2007. **315**(812).
38. Ansolabehere, S., Beer, J., Deutch, J., Ellerman, D., Friedmann, J., Herzog, H., Jacoby, H.D., Joskow, P.L., McRae, G., Lester, R., Moniz, E.J., Steinfeld, E., *The Future of Coal*, Massachusetts Institute of Technology, Cambridge, http://web.mit.edu/coal/, 2007
39. Orr Jr., F.M., *Onshore Geologic Storage of CO2.* Science, 2009. **325**(5948): p. 1656-1658.
40. Marchetti, C., *On geoengineering and the CO2 problem* Climatic Change, 1977. **1**(1): p. 59-68.
41. Seibel, B.A., Walsh, P.J., *Potential Impacts of CO2 Injection on Deep-Sea Biota.* Science, 2001. **294**(5541): p. 319 - 320.
42. Schrag, D.P., *Storage of Carbon Dioxide in Offshore Sediments.* Science, 2009. **325**(5948): p. 1656-1658.
43. Normile, D., *Round and Round: A Guide to the Carbon Cycle.* Science, 2009. **325**(5948): p. 1642-1643.
44. Schiermeier, Q., Tollefson, J., Scully, T., Witze, A., Morton, O., *Electricity without carbon.* Nature, 2008. **5**: p. 24-29.
45. Broecker, W.S., *CO2 Arithmetic.* Science, 2007. **315**: p. 1371.

46. Allen, M.R.F., D.J., Huntingford, C., Jones, C.D., Lowe, J.A., Meinshausen, M., Meinshausen, N., *Warming caused by cumulative carbon emissions towards the trillionth tonne.* Nature, 2009. **458**(7242): p. 1163-1166.
47. Herzog, H., Caldeira, K., Reilly, J., *An Issue of Permanence: Assessing the Effectiveness of Temporary Carbon Storage* Climate Change, 2003. **59**(3): p. 293-310.
48. Stone, E.J., Lowe, J.A., Shine, K.P., *The impact of carbon capture and storage on climate.* Energy & Environmental Science, 2009. **2**: p. 81-91.
49. Feron, P.H.M., Hendriks, C.A., *CO_2 Capture Process Principles and Costs. Oil & Gas Science and Technology - Rev. IFP*, 2005. **60**(3): p. 451-459.
50. Steeneveldt, R., Berger, B., Torp, T. A., *Co2 capture and storage: Closing the knowing-doing gap.* Chemical Engineering Research and Design, 2006. **84**(9 A): p. 739-763.
51. Kvamsdal, H.M., Jordal, K., Bolland, O., *A quantitative comparison of gas turbine cycles with CO2 capture.* Energy, 2007. **32**(1): p. 10-24.
52. Damen, K., van Troost, M., Faaij, A., Turkenburg, W., *A comparison of electricity and hydrogen production systems with CO2 capture and storage. Part A: Review and selection of promising conversion and capture technologies.* Progress in Energy and Combustion Science, 2006. **32**(2): p. 215-246.
53. Rochelle, G.T., *Amine Scrubbing for CO2 Capture.* Science, 2009. **325**(5948): p. 1652-1654.
54. Bose, A.C., *Inorganic Membranes for Energy and Fuel Applications*. 2009.
55. Fontaine, M.L., Larring, Y., Norby, T., Grande, T., Bredesen, R., *Dense ceramic membranes based on ion conducting oxides.* Annales de Chimie (Science des Materiaux), 2007. **32**(2): p. 197-212.
56. Griffin, T., Sundkvist, S. G., Åsen, K., Bruun, T., *Advanced zero emissions gas turbine power plant.* Journal of Engineering for Gas Turbines and Power, 2005. **127**(1): p. 81-85.
57. Moller, B.F., Torisson, T., Assadi, M., Sundkvist, S.G., Sjodin, M., Klang, A., Åsen, K.I., Wilhelmsen, K., *AZEP gas turbine combined cycle power plants - Thermo-economic analysis.* International Journal of Thermodynamics, 2006. **9**(1): p. 21-28.
58. Sanz, W., Jericha, H., Bauer, B., Gottlich, E., *Qualitative and quantitative comparison of two promising oxy-fuel power cycles for CO2 capture.* Journal of Engineering for Gas Turbines and Power, 2008. **130**(3).
59. Imsland, L., Snarheim, D., Foss, B.A., Ulfsnes, R., Bolland, O., *Control issues in the design of a gas turbine cycle for CO2 capture.* International Journal of Green Energy, 2005. **2**(2): p. 303-315.
60. Kharton, V.V., Yaremchenko, A. A., Tsipis, E. V., Valente, A. A., Patrakeev, M. V., Shaula, A. L., Frade, J. R., Rocha, J., *Characterization of mixed-conducting La2Ni0.9Co 0.1O4+ membranes for dry methane oxidation.* Applied Catalysis A: General, 2004. **261**(1): p. 25-35.
61. Kovalevsky, A.V., Kharton, V. V., Yaremchenko, A. A., Pivak, Y. V., Naumovich, E. N., Frade, J. R., *Stability and oxygen transport properties of Pr2NiO4+ ceramics.* Journal of the European Ceramic Society, 2007. **27**(13-15): p. 4269-4272.
62. Shaula, A.L., Naumovich, E.N., Viskup, A.P., Pankov, V.V., Kovalevsky, A.V., Kharton, V.V., *Oxygen transport in La2NiO4 + : Assessment of surface*

limitations and multilayer membrane architectures. Solid State Ionics, 2009. **180**(11-13): p. 812-816.
63. Tsipis, E.V., Naumovich, E.N., Shaula, A.L., Patrakeev, M.V., Waerenborgh, J.C., Kharton, V.V., *Oxygen nonstoichiometry and ionic transport in La2Ni(Fe)O4 +*. Solid State Ionics, 2008. **179**(1-6): p. 57-60.
64. Yaremchenko, A.A., Kharton, V.V., Patrakeev, M.V., Frade, J.R., *P-type electronic conductivity, oxygen permeability and stability of La2Ni0.9Co0.1O4+*. Journal of Materials Chemistry, 2003. **13**(5): p. 1136-1144.
65. Kharton, V.V., Viskup, A.P., Kovalevsky, A.V., Naumovich, E.N., Marques, F.M.B., *Ionic transport in oxygen-hyperstoichiometric phases with K2NiF4-type structure.* Solid State Ionics, 2001. **143**(3-4): p. 337-353.
66. Kharton, V.V., Kovalevsky, A. V., Yaremchenko, A. A., Snijkers, F. M. M., Cooymans, J. F. C., Luyten, J. J., Markov, A. A., Frade, J. R., Marques, F. M. B., *Oxygen transport and thermomechanical properties of SrFe(Al)O 3- - SrAl2O4 composites: Microstructural effects.* Journal of Solid State Electrochemistry, 2006. **10**(8): p. 663-673.
67. Shaula, A.L., Kharton, V.V., Marques, F.M.B., Kovalevsky, A.V., Viskup, A.P., Naumovich, E.N., *Oxygen permeability of mixed-conducting composite membranes: Effects of phase interaction.* Journal of Solid State Electrochemistry, 2006. **10**(1): p. 28-40.
68. Yaremchenko, A.A., Kharton, V. V., Valente, A. A., Snijkers, F. M. M., Cooymans, J. F. C., Luyten, J. J., Marques, F. M. B., *Performance of tubular SrFe(Al)O3-SrAl2O4 composite membranes in CO2- and CH4-containing atmospheres.* Journal of Membrane Science, 2008. **319**(1-2): p. 141-148.
69. Linder, U., Eriksen, E.H., Åsen, K.I., *A method of operating a combustion plant, and a combustion plant using separated oxygen to enrich combustion air, PCT Int. Appl. (2001), WO 2001092703 A1 20011206*. 2001.
70. Linder, U., Eriksen, E., Åsen, K., *Method of operating a combustion plant and a combustion plant*. 2004, 20040011048: United States.
71. Smith, J.B., Norby, T., *On the steady-state oxygen permeation through La2NiO4+delta membranes.* Journal of the Electrochemical Society, 2006. **153**(2): p. 233-8.
72. Vigeland, B., Glenne, R., Breivik, T., Julsrud, S., *Membrane and use thereof*. 2003: United States Norsk, Hydro Asa (Oslo, NO).
73. Barton, P.I., Pantelides, C. C., *Modeling of combined discrete/continuous processes.* AIChE Journal, 1994. **40**(6): p. 966-979.
74. Process Systems Enterprise, www.psenterprise.com, 2009.
75. Li, J., Ge, W., Zhang, J., Kwauk, M., *Multi-scale compromise and multi-level correlation in complex systems.* Chemical Engineering Research and Design, 2005. **83**(6 A): p. 574-582.
76. Maroudas, D., *Multiscale modeling of hard materials: Challenges and opportunities for chemical engineering.* AIChE journal 2000.
77. Pfafferodt, M., Heidebrecht, P., Sundmacher, K., Wurtenberger, U., Bednarz, M., *Multiscale simulation of the indirect internal reforming unit (IIR) in a molten carbonate fuel cell (MCFC).* Industrial and Engineering Chemistry Research, 2008. **47**(13): p. 4332-4341.
78. Bessler, W.G., *Electrochemistry and transport in solid oxide fuel cells*, Habilitation thesis, Universität Heidelberg, 2007.

79. Franco, A.A., Tembely, M., *Transient multiscale modeling of aging mechanisms in a PEFC cathode.* Journal of the Electrochemical Society, 2007. **154**(7): p. B712-B723.
80. Franco, A.A., Schott, P., Jallut, C., Maschke, B., *A Multi-Scale Dynamic Mechanistic Model for the Transient Analysis of PEFCs.* Fuel Cells, 2007. **7**(2): p. 99-117.
81. Franco, A.A., Gerard, M., *Multiscale model of carbon corrosion in a PEFC: Coupling with electrocatalysis and impact on performance degradation.* Journal of the Electrochemical Society, 2008. **155**(4): p. B367-B384.
82. Franco, A.A., Passot, S., Fugier, P., Anglade, C., Billy, E., Gutaz, L., Guillet, N., De Vito, E., Mailley, S., *PtxCoy catalysts degradation in PEFC environments: Mechanistic insights: I. multiscale modeling.* Journal of the Electrochemical Society, 2009. **156**(3): p. B410-B424.
83. Herz, A.V.M., Gollisch, T., Machens, C.K., Jaeger, D., *Modeling Single-Neuron Dynamics and Computations: A Balance of Detail and Abstraction* Science, 2006. **314**: p. 80-85.
84. Kulkarni, K., Moon, J., Zhang, L., Lucia, A., Linninger, A.A., *Multiscale modeling and solution multiplicity in catalytic pellet reactors.* Industrial and Engineering Chemistry Research, 2008. **47**(22): p. 8572-8581.
85. Li, J., Kwauk, M., *Exploring complex systems in chemical engineering - The multi-scale methodology.* Chemical Engineering Science, 2003. **58**(3-6): p. 521-535.
86. Vlachos, D.G., Mhadeshwar, A. B., Kaisare, N. S., *Hierarchical multiscale model-based design of experiments, catalysts, and reactors for fuel processing.* Computers and Chemical Engineering, 2006. **30**(10-12): p. 1712-1724.
87. Raimondeau, S. and D.G. Vlachos, *Recent developments on multiscale, hierarchical modeling of chemical reactors.* Chemical Engineering Journal, 2002. **90**(1-2): p. 3-23.
88. Goldenfeld, N., Kadanoff, L.P., *Simple lessons from complexity.* Science, 1999. **284**(2).
89. Lang, Y.D. and L.T. Biegler, *Large-scale nonlinear programming with a CAPE-OPEN compliant interface.* Chemical Engineering Research and Design, 2005. **83**(6 A): p. 718-723.
90. Dhir, S., Uppaluri, R., Purkait, M. K., *Oxidative desulfurization: Kinetic modelling.* Journal of Hazardous Materials, 2009. **161**(2-3): p. 1360-1368.
91. Oakdale Engineering, w.c.c., *DataFit*: Oakdale, PA 15071, USA.
92. Thermoflow, *Inc. GT PRO & GT MASTER*. 2008: Sudbury, MA 01776, USA.
93. Aspen Technology, I., *Aspen HYSYS*. 2006: Cambridge, Massachusetts U.S.A. p. HYSYS Aspentech.
94. Mathworks, *Matlab*, www.mathworks.com, 2008.
95. Çengel, Y.A., Boles, M.A., *Thermodynamics: an engineering approach*. 2007, Boston: McGraw-Hill. XXXI, 976 s.
96. Smith, J.M., Abbott, M.M., Van Ness, H.C., *Introduction to chemical engineering thermodynamics* seventh edition ed. McGraw-Hill chemical engineering series. 2005, Boston: McGraw-Hill.
97. Horlock, J.H., *Advanced gas turbine cycles*. 2007, Malabar, Fla.: Krieger. xx, 203 s.
98. Saravanamuttoo, H.I.H., Rogers, G.F.C., Cohen, H., Straznicky, P.V., *Gas turbine theory*. 6th ed. ed. 2009: Harlow : Prentice Hall.

99. Kehlhofer, R., Warner, J., Nielsen, H., Bachmann, R., *Combined-cycle gas & steam turbine power plants* second edition ed. 1999.
100. Gellings, P.J., Bouwmeester, H.J.M., *The CRC handbook of solid state electrochemistry*. 1997: Boca Raton, Fla. : CRC Press.
101. Sunarso, J.B., S., Serra, J. M., Meulenberg, W. A., Liu, S., Lin, Y. S., Diniz da Costa, J. C., *Mixed ionic-electronic conducting (MIEC) ceramic-based membranes for oxygen separation.* Journal of Membrane Science, 2008. **320**(1-2): p. 13-41.
102. Sammells, A.F., Mundschau, M.V., *Nonporous Inorganic Membranes for Chemical Processing*. first edition ed. 2006, Weinheim: Wiley-VCH.
103. Leo, A., Liu, S., Costa, J.C.D. da, *Development of mixed conducting membranes for clean coal energy delivery.* International Journal of Greenhouse Gas Control, 2009. **3**(4): p. 357-367.
104. Julbe, A., Farrusseng, D., Guizard, C. *Limitations and potentials of oxygen transport dense and porous ceramic membranes for oxidation reactions*. 2005: Elsevier.
105. Bredesen, R., Jordal, K., Bolland, O., *High-temperature membranes in power generation with CO2 capture.* Chemical Engineering and Processing, 2004. **43**(9): p. 1129-58.
106. Liu, Y., X. Tan, and K. Li, *Mixed conducting ceramics for catalytic membrane processing.* Catalysis Reviews - Science and Engineering, 2006. **48**(2): p. 145-198.
107. Bernardo, P., E. Drioli, and G. Golemme, *Membrane Gas Separation: A Review/State of the Art.* Industrial & Engineering Chemistry Research, 2009. **48**(10): p. 4638-4663.
108. Mulder, M., *Basic principles of membrane technology*. 1996, Dordrecht: Kluwer. 564 s.
109. Drioli, E., Romano, M., *Progress and new perspectives on integrated membrane operations for sustainable industrial growth.* Industrial and Engineering Chemistry Research, 2001. **40**(5): p. 1277-1300.
110. Dyer, P.N., Richards, R. E., Russek, S. L., Taylor, D. M., *Ion transport membrane technology for oxygen separation and syngas production.* Solid State Ionics, Diffusion &amp, Reactions, 2000. **134**(1-2): p. 21-33.
111. Drioli, E., Giorno, L., *Membrane operations: innovative separations and transformations*. 2009, Weinheim: Wiley-VCH. XXV, 551 s.
112. Tan, X., Li, K., *Design of mixed conducting ceramic membranes/reactors for the partial oxidation of methane to syngas.* AIChE Journal, 2009. **55**(10): p. 2675-2685.
113. Kondratenko, E.V., Wang, H., Kondratenko, V.A., Caro, J., *Selective oxidation of CH4 and C2H6 over a mixed oxygen ion and electron conducting perovskite--A TAP and membrane reactors study.* Journal of Molecular Catalysis A: Chemical, 2009. **297**(2): p. 142-149.
114. Zhu, D.C., Xu, X. Y., Feng, S. J., Liu, W., Chen, C. S., *La2NiO4 tubular membrane reactor for conversion of methane to syngas.* Catalysis Today, 2003. **82**(1-4): p. 151-156.
115. Becker, B., Schetter, B. *Use of LHV gas in a gas turbine*. 1993. Espoo, Finl: Publ by Elsevier Science Publ Ltd.
116. Moore, J.M. *NO_x emission control in gas turbines for combined cycle gas turbine plant*. in *Proceedings of the Institution of Mechanical Engineers. Part*

A. Journal of power and energy. 1997: Professionnal Engineering Publishing, Bury St Edmunds.
117. Perry, R.H., Green, D.W., *Perry's chemical engineers' handbook*. 2008, New York: McGraw-Hill.
118. Davis, L.B., Black, S.H. , *Dry Low NOx Combustion Systems for GE Heavy-Duty Gas Turbines*, G.P. Systems, Editor. 2000.
119. Bruun, T., Werswick, B., Åsen, K. I., Fuglerud, T., *Reactor for Mixing and Reacting Two or More Fluids As Well As Transferring Heat Between Said Fluids and a Method for Operating Said Reactor*. 2008, Norsk Hydro.
120. Griffin, T., Winkler, D., Wolf, M., Appel, C., Mantzaras, J. *Staged catalytic combustion method for the advanced zero emissions gas turbine power plant*. 2004. Vienna, Austria: American Society of Mechanical Engineers.
121. Eriksson, S., Boutonnet, M., Jaras, S., *Catalytic combustion of methane in steam and carbon dioxide-diluted reaction mixtures.* Applied Catalysis A: General, 2006. **312**(1-2): p. 95-101.
122. Eriksson, S., Wolf, M., Schneider, A., Mantzaras, J., Raimondi, F., Boutonnet, M., Jaras, S., *Fuel-rich catalytic combustion of methane in zero emissions power generation processes.* Catalysis Today, 2006. **117**(4): p. 447-453.
123. Chen, J., Yang, H., Wang, N., Ring, Z., Dabros, T., *Mathematical modeling of monolith catalysts and reactors for gas phase reactions.* Applied Catalysis A: General, 2008. **345**(1): p. 1-11.
124. Sundkvist, S.G., Julsrud, S., Vigeland, B., Naas, T., Budd, M., Leistner, H., Winkler, D., *Development and testing of AZEP reactor components.* International Journal of Greenhouse Gas Control, 2007. **1**(2): p. 180-187.
125. Pipitone, G., Bolland, O., *Power generation with CO2 capture: Technology for CO2 purification.* International Journal of Greenhouse Gas Control, 2009. **3**(5): p. 528-534.
126. Häring, H.-W., *Industrial gases processing*. 2008, Weinheim: Wiley-VCH. XIV, 296 s.
127. Air products & Chemicals, www.airproducts.com, 2009.
128. Kharton, V.V., Kovalevsky, A. V., Viskup, A. P., Shaula, A. L., Figueiredo, F. M., Naumovich, E. N., Marques, F. M. B., *Oxygen transport in Ce0.8Gd0.2O2-delta-based composite membranes.* Solid State Ionics, 2003. **160**(3-4): p. 247-58.
129. Marques, F.M.B., Kharton, V. V., Naumovich, E. N., Shaula, A. L., Kovalevsky, A. V., Yaremchenko, A. A., *Oxygen ion conductors for fuel cells and membranes: selected developments.* Solid State Ionics, 2006. **177**(19-25 SPEC. ISS.): p. 1697-1703.
130. Tan, X., Li, K., *Oxygen production using dense ceramic hollow fiber membrane modules with different operating modes.* AIChE Journal, 2007. **53**(4): p. 838-845.
131. Ten, E.J.E., Bouwmeester, H.J.M., Verweij, H., *Oxidative coupling of methane in a mixed-conducting perovskite membrane reactor.* Applied Catalysis A:General, 1995. **130**(2): p. 195-195.
132. Balachandran, U., Dusek, J. T., Mieville, R. L., Poeppel, R. B., Kleefisch, M. S., Pei, S., Kobylinski, T. P., Udovich, C. A., Bose, A. C., *Dense ceramic membranes for partial oxidation of methane to syngas.* Applied Catalysis A: General, 1995. **133**(1): p. 19-29.

133. Zeng, Q., Zuo, Y., Fan, C., Chen, C., *CO2-tolerant oxygen separation membranes targeting CO2 capture application.* Journal of Membrane Science, 2009. **335**(1-2): p. 140-144.
134. Pena, M.A., Fierro, J. L. G., *Chemical structures and performance of perovskite oxides.* Chemical Reviews, 2001. **101**(7): p. 1981-2017.
135. Bard, A.J., Inzelt, G., Scholz, F., *Electrochemical dictionary*. 2008, Berlin: Springer. XIV, 723 s.
136. Atkinson, A., Ramos, T.M.G.M., *Chemically-induced stresses in ceramic oxygen ion-conducting membranes.* Solid State Ionics, 2000. **129**(1-4): p. 259-69.
137. Teraoka, Y., Zhang, H.-M., Furukawa, S., Yamazoe, N., *Oxygen permeation through perovskite-type oxides.* Chemistry Letters, 1985. **14**(11): p. 1743-1746.
138. Teraoka, Y., Nobunaga, T., Yamazoe, N., *Effect of Cation Substitution on the Oxygen Semipermeability of Perovskite-type Oxides.* Chemistry Letters, 1988. **17**(3): p. 503-506.
139. Teraoka, Y., Nobunaga, T., Okamoto, K., Miura, N., Yamazoe, N., *Influence of constituent metal cations in substituted LaCoO3 on mixed conductivity and oxygen permeability.* Solid State Ionics, 1991. **48**(3-4): p. 207-212.
140. Caro, J., *Membranreaktoren für die katalytische Oxidation.* Chemie Ingenieur Technik, 2006. **78**(7): p. 899-912.
141. Hendriksen, P.V., Larsen, P.H., Mogensen, M., Poulsen, F.W., Wiik, K., *Prospects and problems of dense oxygen permeable membranes.* Catalysis Today, 2000. **56**(1-3): p. 283-295.
142. West, A.R., *Solid state chemistry and its applications*. 1984, Chichester: Wiley. vii, 734 s.
143. Zinkevich, M., Aldinger, F., *Thermodynamic analysis of the ternary La-Ni-O system.* Journal of Alloys and Compounds, 2004. **375**(1-2): p. 147-161.
144. Paulus, W., Cousson, A., Dhalenne, G., Berthon, J., Revcolevschi, A., Hosoya, S., Treutmann, W., Heger, G., Le Toquin, R., *Neutron diffraction studies of stoichiometric and oxygen intercalated La2NiO4 single crystals.* Solid State Sciences, 2002. **4**(5): p. 565-573.
145. Bannikov, D.O., Cherepanov, V. A., *Thermodynamic properties of complex oxides in the La-Ni-O system.* Journal of Solid State Chemistry, 2006. **179**(8): p. 2721-2727.
146. Bannikov, D.O., Safronov, A.P., Cherepanov, V.A., *Thermochemical characteristics of Lan+1NinO3n+1 oxides.* Thermochimica Acta, 2006. **451**(1-2): p. 22-26.
147. Schroeder, M., Dragan, M.A., *Oxygen transport in La2-xSrx NiO4+: Membrane permeation and defect chemical modelling.* Journal of Materials Science, 2007. **42**(6): p. 1972-1983.
148. Minervini, L., Grimes R.W., Kilner J.A., Sickafus, K.E., *Oxygen migration in $La_2NiO_{4+\delta}$.* Journal of material chemistry, 2000. **10**(10): p. 2349-2354
149. Kharton, V.V., Kovalevsky, A. V., Avdeev, M., Tsipis, E. V., Patrakeev, M. V., Yaremchenko, A. A., Naumovich, E. N., Frade, J. R., *Chemically induced expansion of La2NiO4+-based materials.* Chemistry of Materials, 2007. **19**(8): p. 2027-33.
150. Tsipis, E.V., Naumovich, E.N., Shaula, A.L., Patrakeev, M.V., Waerenborgh, J.C., Kharton, V.V., *Oxygen nonstoichiometry and ionic transport in La2Ni(Fe)O4 + [delta].* Solid State Ionics, 2008. **179**(1-6): p. 57-60.

151. Tsipis, E.V., Naumovich, E.N., Patrakeev, M.V., Waerenborgh, J.C., Pivak, Y.V., Gaczynski, P., Kharton, V.V., *Oxygen non-stoichiometry and defect thermodynamics in La2Ni0.9Fe0.1O4+[delta]*. Journal of Physics and Chemistry of Solids, 2007. **68**(7): p. 1443-1455.
152. Dong, X., Zhang, G., Liu, Z., Zhong, Z., Jin, W., Xu, N., *CO2-tolerant mixed conducting oxide for catalytic membrane reactor.* Journal of Membrane Science, 2009. **340**(1-2): p. 141-147.
153. Carolan, M.F., Motika, S. A., Dyer, P. N., Alba, P. B., *Novel compositions capable of operating under high carbon dioxide partial pressures for use in solid-state oxygen producing devices*, EP0732306, 2005.
154. Yaremchenko, A.A., Kharton, V.V., Avdeev, M., Shaula, A.L., Marques, F.M.B., *Oxygen permeability, thermal expansion and stability of SrCo0.8Fe0.2O3-[delta]-SrAl2O4 composites.* Solid State Ionics, 2007. **178**(19-20): p. 1205-1217.
155. Kharton, V.V., Kovalevsky, A.V., Viskup, A.P., Figueiredo, F.M., Yaremchenko, A.A., Naumovich, E.N., Marques, F.M.B., *Oxygen permeability and Faradaic efficiency of Ce0.8Gd0.2O2-[delta]-La0.7Sr0.3MnO3-[delta] composites.* Journal of the European Ceramic Society, 2001. **21**(10-11): p. 1763-1767.
156. Boukamp, B.A., van Hassel, B.A., Vinke, I.C., de Vries, K.J., Burggraaf, A. J., *Oxygen transfer process on solid oxide/noble metal electrodes; studied with impedance spectroscopy, dc polarization and isotope exchange.* Electrochimica Acta, 1993. **38**(14): p. 1817-1825.
157. Lee, S., Yu, J.H., Seo, D.W., Woo, S.K., *Thick-film type oxygen transport membrane: Preparation, oxygen permeation and characterization.* Journal of Electroceramics, 2006. **17**(2-4): p. 719-722.
158. Raj, E.S., Kilner, J.A., Irvine, J.T.S., *Oxygen diffusion and surface exchange studies on (La0.75Sr0.25)0.95Cr0.5Mn0.5O3.* Solid State Ionics, 2006. **177**(19-25 SPEC. ISS.): p. 1747-1752.
159. Xu, S.J., Thomson, W.J., *Oxygen permeation rates through ion-conducting perovskite membranes.* Chemical Engineering Science, 1999. **54**(17): p. 3839-3850.
160. Zhang, W., Smit, J., van Sint Annaland, M., Kuipers, J. A. M., *Feasibility study of a novel membrane reactor for syngas production. Part 1: Experimental study of O2 permeation through perovskite membranes under reducing and non-reducing atmospheres.* Journal of Membrane Science, 2007. **291**(1-2): p. 19-32.
161. Schmalzried, H., Laqua, W., Multicomponent oxides in oxygen potential gradients, Oxidation of Metals, 1981. **15**(3-4): p. 339-353.
162. Stølen, S., Grande, T., Allan, N.L., *Chemical thermodynamics of materials: macroscopic and microscopic aspects*. 2004, Chichester: Wiley. XII, 395 s.
163. Martin, M., *Materials in thermodynamic potential gradients.* The Journal of Chemical Thermodynamics, 2003. **35**(8): p. 1291-1308.
164. Lein, H.L., Wiik, K., Grande, T., *Kinetic demixing and decomposition of oxygen permeable membranes.* Solid State Ionics, 2006. **177**(19-25): p. 1587-1590.
165. Vente, J.F.H., Wim G., Ijpelaan, R., Rusting, F. T., *On the full-scale module design of an air separation unit using mixed ionic electronic conducting membranes.* Journal of Membrane Science, 2006. **278**(1-2): p. 66-71.

166. Åsen, K.I., personal communication, *Gas Processing and CO2, StatoilHydro*; 2008, Porsgrunn, Norway.
167. Kharton, V.V., personal communication, *Department of Ceramics and Glass Engineering, CICECO*. 2009: Aveiro, Portugal.
168. Smith, A.R., Klosek, J., *A review of air separation technologies and their integration with energy conversion processes.* Fuel Processing Technology, 2001. **70**(2): p. 115-135.
169. Baker, R.W., *Future Directions of Membrane Gas Separation Technology.* Industrial & Engineering Chemistry Research, 2002. **41**(6): p. 1393-1411.
170. Freeman, B.D., Pinnau, I., *Polymeric Materials for Gas Separations*, in *Polymer Membranes for Gas and Vapor Separation*. 2009, American Chemical Society: Washington, DC. p. 1-27.
171. Kee, R.J., Zhu, H., Sukeshini, A.M., Jackson, G.S., *Solid oxide fuel cells: Operating principles, current challenges, and the role of syngas.* Combustion Science and Technology, 2008. **180**(6): p. 1207-1244.
172. Zhu, H., Kee, R.J., *Thermodynamics of SOFC efficiency and fuel utilization as functions of fuel mixtures and operating conditions.* Journal of Power Sources, 2006. **161**(2): p. 957-964.
173. Chaisantikulwat, A., Diaz-Goano, C., Meadows, E. S., *Dynamic modelling and control of planar anode-supported solid oxide fuel cell.* Computers and Chemical Engineering, 2008. **32**(10): p. 2365-2381.
174. Qi, Y., Huang, B., Luo, J., *1-D dynamic modeling of SOFC with analytical solution for reacting gas-flow problem.* AIChE Journal, 2008. **54**(6): p. 1537-1553.
175. Achenbach, E., *Three-dimensional and time-dependent simulation of a planar solid oxide fuel cell stack.* Journal of Power Sources, 1994. **49**(1-3): p. 333-348.
176. Achenbach, E., *Response of a solid oxide fuel cell to load change.* Journal of Power Sources, 1995. **57**(1-2): p. 105-109.
177. Riensche, E., Achenbach, E., Froning, D., Haines, M. R., Heidug, W. K., Lokurlu, A., von Andrian, S., *Clean combined-cycle SOFC power plant - cell modelling and process analysis.* Journal of Power Sources, 2000. **86**(1): p. 404-410.
178. Qi, Y., Huang, B., Luo, J., *Dynamic modeling of a finite volume of solid oxide fuel cell: The effect of transport dynamics.* Chemical Engineering Science, 2006. **61**(18): p. 6057-6076.
179. Shimada, T., Kato, T., Tanaka, Y., *Numerical analysis of thermal behavior of small solid oxide fuel cell systems.* Journal of Fuel Cell Science and Technology, 2007. **4**(3): p. 299-307.
180. Mueller, F., Jabbari, F., Gaynor, R., Brouwer, J., *Novel solid oxide fuel cell system controller for rapid load following.* Journal of Power Sources, 2007. **172**(1): p. 308-323.
181. Gaynor, R., Mueller, F., Jabbari, F., Brouwer, J., *On control concepts to prevent fuel starvation in solid oxide fuel cells.* Journal of Power Sources, 2008. **180**(1): p. 330-342.
182. Selimovic, A., Kemm, M., Torisson, T., Assadi, M., *Steady state and transient thermal stress analysis in planar solid oxide fuel cells.* Journal of Power Sources, 2005. **145**(2): p. 463-9.

183. Nakajo, A., Stiller, C., Harkegard, G., Bolland, O., *Modeling of thermal stresses and probability of survival of tubular SOFC.* Journal of Power Sources, 2006. **158**(1): p. 287-294.
184. Nakajo, A., Wuillemin, Z., Van Herle, J., Favrat, D., *Simulation of thermal stresses in anode-supported solid oxide fuel cell stacks. Part I: Probability of failure of the cells.* Journal of Power Sources, 2009. **193**(1): p. 203-215.
185. Nakajo, A., Wuillemin, Z., Van Herle, J., Favrat, D., *Simulation of thermal stresses in anode-supported solid oxide fuel cell stacks. Part II: Loss of gas-tightness, electrical contact and thermal buckling.* Journal of Power Sources, 2009. **193**(1): p. 216-226.
186. Vielstich, W., Gasteiger, H. A., Lamm, A., *Handbook of fuel cells: fundamentals, technology and applications; Volume 5*. Vol. 5. 2009, Chichester: Wiley. b.
187. Vielstich, W., Gasteiger, H.A., Lamm, A., *Handbook of fuel cells: fundamentals, technology and applications; Volume 6*. Vol. 6. 2009, Chichester: Wiley. b.
188. Bhattacharyya, D., Rengaswamy, R., *A Review of Solid Oxide Fuel Cell (SOFC) Dynamic Models.* Industrial & Engineering Chemistry Research. **0**(0).
189. Mueller, F., Jabbari, F., Brouwer, J., Roberts, R., Junker, T., Ghezel-Ayagh, H., *Control design for a bottoming solid oxide fuel cell gas turbine hybrid system.* Journal of Fuel Cell Science and Technology, 2007. **4**(3): p. 221-230.
190. Roberts, R.A. and J. Brouwer, *Dynamic simulation of a pressurized 220 kW solid oxide fuel-cell-gas-turbine hybrid system: Modeled performance compared to measured results.* Journal of Fuel Cell Science and Technology, 2006. **3**(1): p. 18-25.
191. Campanari, S., *Full Load and Part-Load Performance Prediction for Integrated SOFC and Microturbine Systems.* Journal of Engineering for Gas Turbines and Power, 2000. **122**(2): p. 239-246.
192. Lin, P.-H. and C.-W. Hong, *On the start-up transient simulation of a turbo fuel cell system.* Journal of Power Sources, 2006. **160**(2 SPEC. ISS.): p. 1230-1241.
193. Chan, S.H., Ho, H. K., Tian, Y., *Modelling for part-load operation of solid oxide fuel cell-gas turbine hybrid power plant.* Journal of Power Sources, 2003. **114**(2): p. 213-27.
194. Milewski, J., Miller, A., Saacinski, J., *Off-design analysis of SOFC hybrid system.* International Journal of Hydrogen Energy, 2007. **32**(6): p. 687-698.
195. Costamagna, P., Magistri, L., Massardo, A. F., *Design and part-load performance of a hybrid system based on a solid oxide fuel cell reactor and a micro gas turbine.* Journal of Power Sources, 2001. **96**(2): p. 352-368.
196. Mueller, F., Gaynor, R., Auld, A.E., Brouwer, J., Jabbari, F., Samuelsen, G.S., *Synergistic integration of a gas turbine and solid oxide fuel cell for improved transient capability.* Journal of Power Sources, 2008. **176**(1): p. 229-239.
197. Onda, K., Iwanari, T., Miyauchi, N., Ito, K., Ohba, T., Sakaki, Y., Nagata, S., *Cycle analysis of combined power generation by planar SOFC and gas turbine considering cell temperature and current density distributions.* Journal of the Electrochemical Society, 2003. **150**(12): p. A1569-A1576.
198. Song, T.W., Sohn, J.L., Kim, T.S., Ro, S.T., *Performance characteristics of a MW-class SOFC/GT hybrid system based on a commercially available gas turbine.* Journal of Power Sources, 2006. **158**(1): p. 361-367.

199. Yang, J.S., J.L. Sohn, and S.T. Ro, *Performance characteristics of part-load operations of a solid oxide fuel cell/gas turbine hybrid system using air-bypass valves.* Journal of Power Sources, 2008. **175**(1): p. 296-302.
200. Yang, J.S., J.L. Sohn, and S.T. Ro, *Performance characteristics of a solid oxide fuel cell/gas turbine hybrid system with various part-load control modes.* Journal of Power Sources, 2007. **166**(1): p. 155-164.
201. Magistri, L., Traversa, A., Cerutti, F., Bozzolo, M., Costamagna, P., Massardo, A. F., *Modelling of pressurised hybrid systems based on integrated planar solid oxide fuel cell (IP-SOFC) technology.* Fuel Cells, 2005. **5**(1): p. 80-96.
202. Calise, F., Palombo, A., Vanoli, L., *Design and partial load exergy analysis of hybrid SOFC-GT power plant.* Journal of Power Sources, 2006. **158**(1): p. 225-44.
203. Zhang, X., Li, J., Li, G., Feng, Z., *Dynamic modeling of a hybrid system of the solid oxide fuel cell and recuperative gas turbine.* Journal of Power Sources, 2006. **163**(1 SPEC. ISS.): p. 523-531.
204. Stiller, C., *Design, operation and control modelling of SOFC/GT hybrid systems*, PhD thesis, Norwegian University of Science and Technology, 2006.
205. Thorud, B., *Dynamic modelling and characterisation of a solid oxide fuel cell integrated in a gas turbine cycle*, PhD thesis, Norwegian University of Science and Technology, 2005.
206. Zhu, Y., Cai, W., Wen, C., Li, Y., *Fuel ejector design and simulation model for anodic recirculation SOFC system.* Journal of Power Sources, 2007. **173**(1): p. 437-449.
207. Zhu, Y., Cai, W., Li, Y., Wen, C., *Anode gas recirculation behavior of a fuel ejector in hybrid solid oxide fuel cell systems: Performance evaluation in three operational modes.* Journal of Power Sources, 2008. **185**(2): p. 1122-1130.
208. Guckenheimer, J., *Nonlinear oscillations, dynamical systems, and bifurcations of vector fields*, ed. P. Holmes. 1983, New York: Springer. XVI, 459 s.
209. Kuznecov, J.A., *Elements of applied bifurcation theory*. 1995, New York: Springer. XV, 515 s.
210. Chen, Z., Elnashaie, S.S.E.H., *Bifurcation and its implications for a novel autothermal circulating fluidized bed membrane reformer for the efficient pure hydrogen production.* Chemical Engineering Science, 2005. **60**(15): p. 4287-4309.
211. Grotsch, M., Hanke-Rauschenbach, R., Mangold, M., *Bifurcation analysis of a two-phase PEMFC model.* Journal of Fuel Cell Science and Technology, 2008. **5**(2).
212. Krasnyk, M., Mangold, M., Kienle, A. *Numerical bifurcation analysis of periodic solutions of population balance models*. 2007. Salt Lake City, UT, United states: American Institute of Chemical Engineers.
213. Mangold, M., Kienle, A., Gilles, E. D., Mohl, K. D., *Nonlinear computation in DIVA - methods and applications.* Chemical Engineering Science, 2000. **55**(2): p. 441-454.
214. Mangold, M., Mohl, K. D., Grüner, S., Kienle, A., Gilles, E. D., *Nonlinear Analysis of gPROMS Models Using DIVA as via a CAPE ESO interface*, in *European Symposium on Computer Aided Process Engineering - 12*. 2002: The Hague, the Netherlands. p. 919-924.

215. Mangold, M., Krasnyk, M., Sundmacher, K., *Nonlinear analysis of current instabilities in high temperature fuel cells*. Chemical Engineering Science, 2004. **59**(22-23): p. 4869-77.
216. Sheng, M., Mangold, M., Kienle, A., *A strategy for the spatial temperature control of a molten carbonate fuel cell system*. Journal of Power Sources, 2006. **162**(2 SPEC. ISS.): p. 1213-1219.
217. Paulsen, O., *Rigid bonded glass ceramic seals for high temperature membrane reactors and solid oxide fuel cells*, PhD thesis, in *Department of materials science and engineering,* Norwegian University of Science and Technology, 2009.
218. Budd, M., *Barium lanthanum silicate glass-ceramics, US7,189,668B2*. 2007: US.
219. Blond, E., Richet, N., *Thermomechanical modelling of ion-conducting membrane for oxygen separation*. Journal of the European Ceramic Society, 2008. **28**(4): p. 793-801.

Paper I

Journal of Membrane Science 336 (2009) 50–60

Contents lists available at ScienceDirect

Journal of Membrane Science

journal homepage: www.elsevier.com/locate/memsci

Dynamic modelling of an oxygen mixed conducting membrane and model reduction for control

Konrad Eichhorn Colombo [a], Lars Imsland [b], Olav Bolland [a,*], Svein Hovland [c]

[a] Department of Energy and Process Engineering, Norwegian University of Science and Technology, Kolbjørn Hejes vei 1B, NO-7491 Trondheim, Norway
[b] SINTEF ICT, Applied Cybernetics, NO-7465 Trondheim, Norway
[c] Department of Engineering Cybernetics, Norwegian University of Science and Technology, O.S. Bragstads plass 2D, NO-7491 Trondheim, Norway

ARTICLE INFO

Article history:
Received 15 August 2008
Received in revised form 25 February 2009
Accepted 28 February 2009
Available online 14 March 2009

Keywords:
Dynamic modelling
Oxygen mixed conducting membrane
Monolith
Model reduction
Linear
Balanced residualisation
Air separation

ABSTRACT

In the first part of this paper we present a detailed model of an oxygen mixed conducting membrane (OMCM) monolith for air separation. In addition to the oxygen separation, the OMCM operates as a heat exchanger at elevated temperature and pressure. The model is based on energy and species conservation balances. It is shown that the oxygen permeation through perovskite-related materials is strongly dependent on the oxygen partial pressure difference across the membrane and on the temperature of the solid wall. The numerical results obtained from steady state as well as transient simulations agree well with the available data. In the second part, linear model reduction is applied to the OMCM model. The method for model reduction used here, balanced residualisation, reduces states while preserving steady-state behaviour. The comparison of two reduced-order models (19 states and 5 states, respectively) with the full-order model (>2000 states), reveals good agreement for frequencies lower than 1 Hz. The reduced models simulate faster, and can be used for controllability analysis and control design.

1. Introduction

In recent years the interest in efficient air separation has steadily increased. Existing technologies are, among others, cryogenic distillation and pressure swing adsorption. Another option is oxygen production by polymeric membranes. Whereas the former ones suffer from high capital and operation costs, polymeric membranes have a low separation factor for producing oxygen with purity not higher than 50% [1]. In contrast, air separation by means of perovskite-related oxygen mixed conducting membranes (OMCMs) is one of the most promising technologies combining high oxygen production and process simplicity [2,3,5]. In absence of leaks or cracks OMCMs exhibit 100% selectivity towards oxygen.

OMCMs can be incorporated in power cycles, where for example natural gas reacts with the separated oxygen in a nitrogen-free atmosphere[1] [6]. In the majority of research studies dealing with the design and operation of OMCMs in power cycles, lumped models have been applied in order to investigate the steady-state behaviour of both the OMCM and the whole power cycle [8,30].

In the present work, an oxygen mixed conducting membrane monolith model, based on the perovskite-related material $La_2NiO_{4+\delta}$ is studied, selected due to its good transport properties [3,5,9–13]. This compound belongs to the Ruddlesden–Popper series with the general composition $A_{n+1}B_nO_{3n+1}$, with A of group 1, 2, or 3 elements and B as a transition metal [3,5]. The crystal structure shows close proximity to the perovskite structure. Rocksalt-type AO sheets are inserted between blocks consisting of n ABO_3 perovskite-related layers [3,15,16]. $La_2NiO_{4+\delta}$ can accommodate considerable amounts of excess oxygen which is hosted in the form of oxygen interstitial defects in the La_2O_2 rock-salt layers. With increasing temperature this material undergoes a transition from semiconducting to pseudometallic behaviour. In this connection, the material loses its interstitial oxygen, and as a consequence thereof the concentration of electron holes decreases.

Monoliths for gas-phase applications have been extensively studied, in particular within the automobile industry [17]. The fabrication of OMCMs as monolith for power cycles is an interesting alternative to techniques such as the shell-and-tube configuration. Monoliths are characterised by low-pressure drop, high area-to-volume ratio, and ease of scale-up [14,18].

The transient monolith model is spatially distributed in one dimension with respect to energy and species conservation balances of gas and solid phase in the monolith. A two-dimensional model has been adopted for the insulation. Oxygen permeation of the OMCM incorporates bulk diffusion and surface reactions.

* Corresponding author.
E-mail addresses: konrad.eichhorn@ntnu.no (K. Eichhorn Colombo), olav.bolland@ntnu.no (O. Bolland).

[1] It is assumed that natural gas does not contain any impurities such as nitrogen and sulphur.

0376-7388/$ – see front matter © 2009 Elsevier B.V. All rights reserved.
doi:10.1016/j.memsci.2009.02.035

The initial transient process of oxygen permeation over perovskite-related membranes has been experimentally analysed by several authors [20–22]. As the oxygen-defect zone spreads towards the oxygen-rich surface, the bulk-controlled oxygen permeation gradually increases until a steady-state oxygen-defect gradient is established. Transition times between 3 and 100 h have been reported, depending on material and thickness of the membrane as well as oxygen permeation control by surface reactions. However, once the steady-state oxygen permeation is established at high temperatures, it remains stable during relatively fast process conditions [21,22]. Therefore, a steady-state solution for the oxygen permeation is assumed.

With increasing computing power, process modelling could meet a higher standard with respect to complexity and accuracy. However, when dealing with large processes, including several highly complex models, the computational effort to obtain numerical solutions is still too large for process control. Whereas for process engineers accurate process results of material and energy flows are usually of interest, control engineers have to cope with the inherent dynamics of all process units. Information about exact energy and material flows are of second-order importance. Nonetheless, simple lumping of complex process models for control may lead to large errors. In order to address both, process models which accurately predict the material and energy flows, and models simple enough for control applications, model reduction can be used.

In the literature there is a large variety of model reduction methods for simulation and control purposes. Model reduction for simulation attempts to retain process model states, i.e. system behaviour for a particular set of inputs. For control purposes model reduction should retain the input–output behaviour. Whereas model reduction for linear process models is well established, model reduction for non-linear models is still an on-going research topic. For an overview of model reduction methods, the interested reader is referred to Refs. [23,24].

Several new approaches emerged in the past three decades. In particular, the proper orthogonal decomposition[2] (POD) gained much attention for model reduction of large dynamical systems [25–27]. In POD, a singular value decomposition is applied in order to obtain an orthogonal basis for snapshots, where the most dominant singular vectors are retained. This method does not incorporate the state-to-output behaviour and does not always give satisfactory results for control purposes. In addition to POD, there appeared several contributions on system identification where the input–output behaviour is obtained by neural networks [28]. Neural networks, however, need to be trained for certain scenarios and give rather poor approximations when applying to operation regimes out of the training range. In addition, the system behaviour cannot be traced back to certain causes. Model reduction based on linearization and balancing still seems to be the most suitable model reduction method for control purposes. Several methods including a balanced realisation have been developed, such as balanced truncation, optimal Hankel norm approximation and balanced residualisation. Compared to the former two model reduction methods, balanced residualisation preserves the linearized system's behaviour in steady state. Merely scaling reduced-order models to recover steady-state behaviour may lead to large errors.

In this contribution, balanced residualisation is applied to the OMCM model. The input–output behaviour is retained in conjunction with good model approximations with respect to key process variables such as sweep gas temperature and oxygen mole fraction. Reduced-order models incorporating 19 and 5 states, respectively are compared to the full-order model. Whereas the model with 19 states contains 99% of the system's energy (measured in Hankel singular values), the model with 5 retains 95 of the system's energy.

2. Oxygen mixed conducting membrane model

The oxygen mixed conductive membrane model is based on conservation balances, spatially distributed with respect to the monolith length (z coordinate), shown in Fig. 1. The OMCM is assumed to be fabricated as a two-fluid monolith which results in a high area-to-volume ratio [29]. This in turn leads to high heat and mass transfer rates. The gas-phase is treated as an incompressible fluid. The two counter-current stream compositions differ in temperature, massflow and oxygen partial pressure. Oxygen permeation occurs from the high oxygen partial pressure air stream to the low oxygen partial pressure sweep gas. Heat transfer proceeds in the opposite direction. Each air stream is connected to four sweep gas streams and vice versa, resulting in a checkerboard pattern. The solid wall, separating the two gas streams, is composed of the OMCM layer and a porous support layer of similar material. On one hand this support should be sufficiently porous to retard oxygen permeation and on the other hand provide high mechanical strength in order to prevent fracture under varying process conditions. In addition, the porous support should have a similar thermal expansion coefficient to keep thermal stresses during load changes at a low level when there is no other possibility for the OMCM to relax the strains by either extension or bending [14,31–34]. The membrane layer and porous support are combined with respect to heat transfer for reason of model simplification. Oxygen residence times in the solid wall are not considered because of the fast exchange of oxygen through the membrane layer. Therefore, species conservation balances are only given for the gas phases. In order to keep the modelling effort to a reasonable level, a repeating element is defined, which represents the entire number of gas channels and solid walls in the monolith. This repeating element,

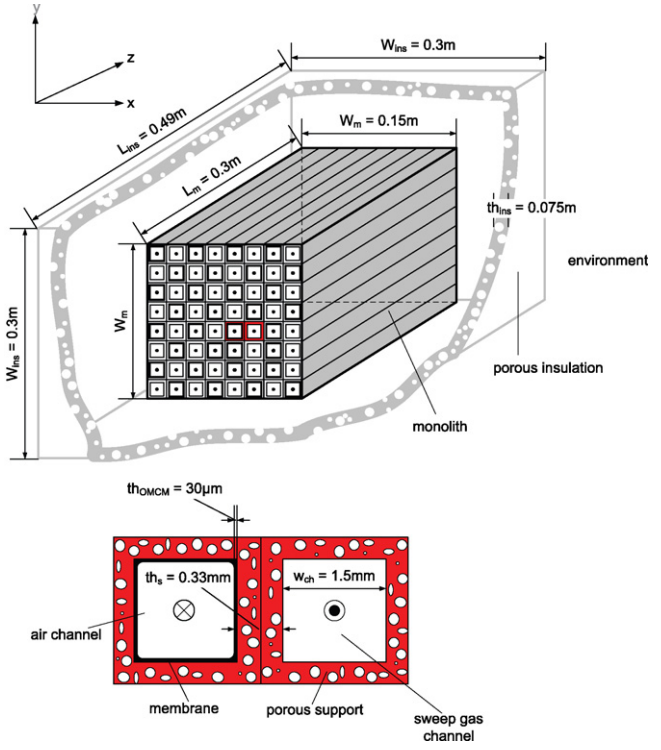

Fig. 1. Oxygen mixed conducting membrane: manifold (above), repeating element (below).

[2] POD is also known as the method of empirical orthogonal eigenfunctions, and Karhunen–Loève expansion.

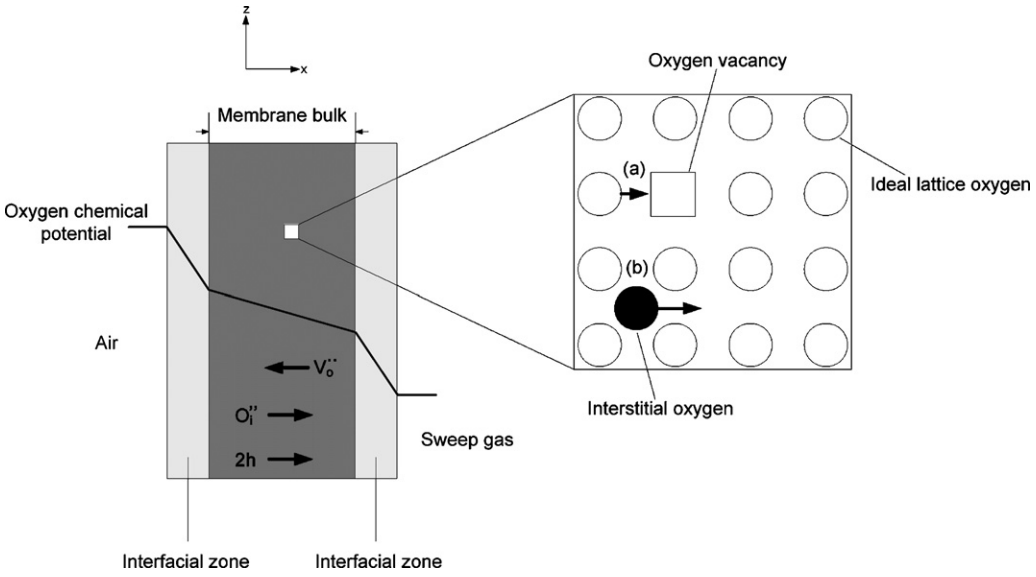

Fig. 2. Oxygen permeation through the oxygen mixed conducting membrane and lattice diffusion mechanism (a) via vacancy and (b) via interstitial positions.

which is shown on the bottom of Fig. 1, is assumed to be uniform in axial direction. Monolith boundary effects are not taken into account because of the large number of gas channels (>6000). Entrance effects on flow dynamics have been neglected. The oxygen permeation is controlled by bulk diffusion as well as surface reactions [5,12]. Modification of the Wagner equation for bulk diffusion and concentration balances makes allowance for both flux contributions. It is assumed that surface exchange and bulk diffusion of oxygen exhibit the same dependency with respect to the oxygen partial pressure gradient. This is a valid approximation for the simulation purposes interesting in this work. The monolith outer layer is in direct contact with a high-performance insulation case in order to reduce heat losses. The two-dimensional insulation model includes heat transfer by conduction, radiation and free convection.

2.1. Oxygen permeation

Oxygen permeation through a nonporous ceramic membrane is controlled by bulk diffusion and surface exchange kinetics. Surface exchange reactions may involve many sub-steps, including adsorption from the gas phase, charge transfer reactions between the adsorbed species and the bulk including the reverse reactions [3,14,35,36]. Reducing the membrane thickness increases the oxygen permeation as long as bulk diffusion prevails, but eventually the surface exchange reactions become rate-limiting [5]. A membrane exposed to an oxygen partial pressure gradient can be visualised by dividing it into three zones: an interfacial zone on the high oxygen partial pressure (air) side, a central bulk zone, and an interfacial zone on the low oxygen partial pressure (sweep gas) side. These zones with their oxygen partial pressure drop are shown in Fig. 2. The oxygen ion transport through the $La_2NiO_{4+\delta}$ bulk proceeds through the combination of interstitial oxygen ions migration in its rock-salt layers and lattice oxygen ions migration through oxygen vacancies in its perovskite layers, formed according to [14,22,36,37]:

$$O_O^x + 2h \rightleftharpoons V_O^{\cdot\cdot} + \frac{1}{2}O_2 \quad (1)$$

$$\frac{1}{2}O_2 \rightleftharpoons O_i'' + 2h \quad (2)$$

Oxygen flux can be described by an approximate equation [37], neglecting any influence of the porous membrane support:

$$J_{O_2} = -k_{sf}^J \frac{c_0 D_0}{4 th_m n}[p_{O_2,sweep}^n - p_{O_2,air}^n] \quad (3)$$

where k_{sf}^J is a parameter incorporating surface reactions, c_0 the oxygen concentration, D_0 the oxygen self-diffusion coefficient, th_m the membrane thickness, n represents an additional fitting parameter used for partial pressure dependency, and p_{O_2} the oxygen partial pressure.

2.2. Conservation balances

In energy and species conservation balances of the monolith, cross-sectional effects in the x- and y-coordinate, as shown in Fig. 1, are neglected. The fluids are described by plug-flow, i.e. the velocity over the gas channel cross section can be approximated by a constant value. Energy balances for the gas phases include heat transport by convection, conduction as well as heat transferred by oxygen molecule exchange. Pressure effects are neglected. The monolith outer wall is in direct contact with the insulation inner layer. Therefore, these two temperatures are set equal along the monolith length (z coordinate). A two-dimensional conduction model has been incorporated for the 'thick' insulation layer. The ambient temperature is assumed to be constant. Heat losses from the insulation outer layer to the environment by free convection as well as radiation are included. The species conservation balances incorporate convection and oxygen diffusion through the OMCM. Diffusion along the axial monolith length is neglected because of large Peclet numbers (>200). Initial conditions for all conservation balances are given by the steady state assumption.

2.2.1. Energy conservation

The energy balance for the air is given by

$$\rho_a c_{pg,a}\left(\frac{\partial T_a}{\partial t} - v_a\frac{\partial T_a}{\partial z}\right) = \frac{\partial}{\partial z}\left(\lambda_a\frac{\partial T_a}{\partial z}\right) + \alpha h_{f,a}(T_s - T_a) - 4J_{O_2}\frac{\partial h_{O_2,a}}{\partial z} \quad (4)$$

The energy balance for the sweep gas reads:

$$\rho_w c_{pg,w}\left(\frac{\partial T_w}{\partial t}+v_w\frac{\partial T_w}{\partial z}\right)=\frac{\partial}{\partial z}\left(\lambda_w\frac{\partial T_w}{\partial z}\right)+\alpha h_{f,w}(T_w-T_s)+4J_{O_2}\frac{\partial h_{O_2,w}}{\partial z} \quad (5)$$

The following Dirichlet boundary condition are applied at inlet:

$$T_g|_{inlet}=T_g^0 \quad (6)$$

and Neumann boundary condition at outlet:

$$\frac{\partial T_g}{\partial z}|_{outlet}=0 \quad (7)$$

The solid wall energy balance is given by

$$\rho_s c_{p,s}\frac{\partial T_s}{\partial t}=\lambda_s\frac{\partial^2 T_w}{\partial z^2}+\alpha h_{f,w}(T_w-T_s)+\alpha h_{f,a}(T_a-T_s)+J_{O_2}\left(\frac{\partial h_{O_2,a}}{\partial z}-\frac{\partial h_{O_2,s}}{\partial z}\right) \quad (8)$$

Please note that the permeation factor 4 for the oxygen permeation term does not occur in the energy balance for the solid wall. Each sweep gas channel receives four times the oxygen due to the checkerboard pattern. Each solid wall, however, receives only a single contribution of the oxygen permeation.

The solid wall ends are assumed to be adiabatic. It follows that

$$\frac{\partial T_s}{\partial z}|_{z=0}=0 \quad (9)$$

$$\frac{\partial T_s}{\partial z}|_{z=L_m}=0 \quad (10)$$

The OMCM is embedded in a high-performance insulation in order to reduce heat losses. The insulation thickness has been chosen so that the outer surface temperature is kept well below 100 °C [38]. The insulation thermal conductivity is based on the lowest value currently commercially available [39]. However, Apfel et al. [40] reported commercially available isolation materials with a thermal conductivity of 0.02 W/(mK), and Chen and Evans reported values of 0.001 W/(mK) [41]. Heat losses could then be further reduced. Compared to mobile applications (such as SOFC in vehicles), power cycles are usually not restricted by space. This results in a trade-off with respect to cost between insulation thickness and material applied:

The energy balance for the insulation reads:

$$\rho_{ins}c_{p,ins}\frac{\partial T_{ins}}{\partial t}=\lambda_{ins}\frac{\partial^2 T_{ins}}{\partial x^2}+\lambda_{ins}\frac{\partial^2 T_{ins}}{\partial z^2} \quad (11)$$

The insulation inner layer temperature equals the monolith solid temperature, expressed by

$$T_s|_z=T_{ins}|_{x=0,z} \quad (12)$$

At the insulation outer layer heat is released to the environment by a combination of free convection and radiation, it follows thus

$$-\lambda_{ins}\frac{\partial T_{ins}}{\partial z}|_{x=th_{ins},z}=(h_{conv}(T_{ins}-T_{amb})+\varepsilon_{ins}\sigma(T_{ins}^4-T_{amb}^4))|_{x=th_{ins},z} \quad (13)$$

In order to circumvent complex computation of the insulation, the ends in vertical direction are assumed to be adiabatic, resulting in

$$\frac{\partial T_{ins}}{\partial z}|_{x,z=0}=0 \quad (14)$$

$$\frac{\partial T_s}{\partial z}|_{x,z=L_m}=0 \quad (15)$$

The total heat emitted by free convection and radiation is calculated by integration over the heat flux along the length of the monolith, according to

$$\dot{Q}=\frac{A_{ext}}{L_{ins}}\int_0^{L_{ins}}\dot{q}\,dz \quad (16)$$

In the energy conservation balances ρ represents the density, c_p is the heat capacity, T the temperature, v the fluid velocity, λ the thermal conductivity, α the area-to-volume ratio of the monolith, h_f the heat transfer coefficient, J_{O_2} the oxygen flux through the membrane, h_{O_2} the enthalpy of oxygen, ε_{ins} the insulation emissivity, σ the Stefan–Boltzmann constant, A_{ext} the external radiant surface of the insulation outer layer, L_{ins} the length of the insulation, and $\dot{q}$ is the heat flux by free convection and radiation. The index *a* denotes air, whereas *w* stands for the sweep gas. The index *s* indicates the solid wall (membrane layer and porous support), *ins* the insulation, *conv* free convection, and *amb* ambient conditions.

2.2.2. Species conservation

The species conservation balance is presented for oxygen. Assuming absence of leakages or cracks in the OMCM layer, there is no permeation of other components but oxygen[3]. Axial diffusion is neglected because of the large monolith length relative to the channel width.

The species conservation balance for air is given by

$$\frac{\partial C_{O_2,a}}{\partial t}-v_{g,a}\frac{\partial C_{O_2,a}}{\partial z}=-4k_{sf}^C\frac{J_{O_2}}{w_{ch}} \quad (17)$$

and for the sweep gas:

$$\frac{\partial C_{O_2,w}}{\partial t}+v_{g,w}\frac{\partial C_{O_2,w}}{\partial z}=4k_{sf}^C\frac{J_{O_2}}{w_{ch}} \quad (18)$$

with the Dirichlet boundary condition at the channel inlet:

$$C_{g,O_2,k}|_{inlet}=C_{g,O_2,k}^0 \quad (19)$$

where C denotes the species concentration, k_{sf}^C a parameter accounting for surface reactions, J_{O_2} the oxygen flux and w_{ch} the width of one single monolith channel.

2.2.3. Geometry

The total number of channels in the monolith is calculated by

$$n_{ch}=|\frac{W-th_s}{w_{ch}+th_s}|^2 \quad (20)$$

where W denotes the monolith width th_s the solid wall thickness (membrane and porous support layer), and w_{ch} the channel width, obtained by

$$th_s=0.22w_{ch} \quad (21)$$

The proportionality factor between solid wall thickness and channel width can be considered as a trade-off between oxygen permeation and mechanical stability.

The area to volume ratio of the monolith with checkerboard layout is calculated by means of

$$\alpha=\frac{2w_{ch}}{(w_{ch}+th_s)^2} \quad (22)$$

[3] As for heat transfer, effects caused by the porous membrane support, such as diffusion, are neglected.

2.2.4. Flow velocity

The flow velocity in the monolith channels is based on the following continuity condition:

$$v_g = \frac{\dot{n}_{tot} V}{(n_{ch}/2) w_{ch}^2} \tag{23}$$

where $\dot{n}_{tot}$ is the total molar flowrate in the channel, V the vapour volume, and n_{ch} the total number of channels in the monolith.

2.2.5. Heat transfer coefficient

The convective heat transfer coefficient h_f between bulk flow and walls in square channels is known analytically for fully developed laminar flow for a uniform heat flux as [7]

$$Nu = \frac{h_f w_{ch}}{\lambda_{g,k}} = 3.091 \tag{24}$$

2.2.6. Pressure drop

Neglecting gravitational effects the pressure drop is calculated by [42]:

$$f = \frac{1}{4}\left(\frac{w_{ch}}{L_m}\right)\left(\frac{\Delta P}{(1/2)\rho v^2}\right) \tag{25}$$

with the friction factor [7]:

$$f\,Re = 56.91 \tag{26}$$

where f is the friction factor, ΔP the pressure drop along the OMCM, and Re the Reynolds number.

2.3. Numerical model implementation

The OMCM model is implemented in gPROMS, which is an equation oriented modelling tool. Physical gas properties are called by the property data package Multiflash in conjunction with a Soave–Redlich–Kwong equation of state [43].

The full OMCM model consists of 1523 algebraic and 623 dynamic state variables. A number of 30 modes in axial direction and 5 nodes in vertical direction for the insulation energy balance are found to be sufficient, as an increased number of nodes does not lead to improvements in numerical solution accuracy. The energy and species conservation balances of the sweep gas are discretised using a backward finite difference scheme, whereas for the reverse air fluid a forward discretisation scheme is applied for numerical stability. Central finite difference is used for the energy balance of the solid wall and insulation layer. The approximation for partial derivatives is of second order. A general rule for calculation time cannot be defined. The standard solver DASOLV applied here, varies time increments, depending on occurring discontinuities and current changes in process variables. However, with increasing model complexity (transient), changes in process constraints, and integration time period, time for solving the system also increases. For instance, the transient simulation of the OMCM model shown in Fig. 7 takes approximately 30 s with a total CPU time of 16.5 s. All other simulations require considerably less computation time. The parameters used in the mathematical OMCM model description are listed in Table 1. The model reduction code has been implemented in Matlab [44].

2.4. Operation regime

The OMCM is an oxygen separation device that operates at elevated temperature and pressure. The gas-phase temperatures should be high enough to heat the OMCM above 700 °C [37] in order to achieve desired oxygen permeation fluxes and to reduce the dimensions of the OMCM. Besides, elevated temperatures are necessary from a thermo-mechanical stability point of view [32].

Table 1
Monolith and insulation parameters used in the simulations.

Item	Value/expression	Units
$C_{p,ins}$	1000 [39]	J kg^{-1} k^{-1}
$C_{p,s}$	$1050 + 0.1T_s$ [45]	J kg^{-1} k^{-1}
h_{conv}	10 [46]	J s^{-1} m^{-2} s^{-1} K^{-1}
L_m	0.3	m
T_{amb}	308	K
th_{ins}	0.075	m
th_{OMCM}	30 [29]	μm
th_S	0.33	mm
w_{ch}	1.5	mm
ε_{ins}	0.3 [39]	–
λ_{ins}	0.03 [39]	J s^{-1} m^{-1} K^{-1}
λ_s	3 [45]	J s^{-1} m^{-1} K^{-1}
ρ_{ins}	320 [39]	kg m^{-3}
ρ_s	2400 [45]	kg m^{-3}

Table 2
Base case monolith parameters used for simulation.

Item	Value	Units
Sweep gas stream conditions at inlet		
Temperature	1350	K
Pressure	17	bar
Mass flowrate	0.075	kg s^{-1}
Water mole fraction	0.99	–
Oxygen mole fraction	0.01	–
Air stream conditions at inlet		
Temperature	1150	K
Pressure	17	bar
Mass flowrate	0.125	kg s^{-1}
Water mole fraction	0.79	–
Oxygen mole fraction	0.21	–

Pressure differences between the two gas phases should be kept low for reason of mechanical stability. The air mass flow is somewhat higher compared to the hotter sweep gas to optimise heat transfer. An oxygen mole fraction of 1% is assumed to be present in the sweep gas with the balance being steam. Using the OMCM in a natural gas-fired power plant as air separation device, the sweep gas may be a mixture mainly consisting of steam and/or carbon dioxide. These chemical components may react with the membrane which ultimately results in degradation [2]. Consequently, concentrations of water and carbon dioxide have to be minimised, in conjunction with the oxygen partial pressure and operation temperature. In this work, effects of different sweep gas compositions have not been studied. The values for the OMCM performance base case are given in Table 2.

3. Model reduction

Balanced model reduction is based on a certain system transformation that balances the input and output 'energies' as defined by the controllability and observability gramians. This transformation orders the system states, starting with the state that affects the input–output characteristic the most (contains the most input/output 'energy'). Moreover, the transformation provides a measure of these energies, the Hankel singular values. Balanced model reduction can then be performed by removing the transformed states with the smallest Hankel singular values (weakest input–output influence). Simply using the remaining reduced system is referred to as 'balanced truncation', while correcting the reduced system such that the steady state remains correct, is referred to as 'balanced residualisation'. The minimum requirement for balanced model reduction is that the system matrix A is Hurwitz, i.e. all eigenvalues are in the open left-half plane. Model reduction by balanced residualisation leads to a stable reduced-order model.

3.1. Linear system theory

A linear time invariant system is represented by the following state space formula [47]:

$$\frac{d}{dt}x(t) = Ax(t) + Bu(t) \tag{27}$$

$$y(t) = Cx(t) + Du(t) \tag{28}$$

where $x(t)$ is a vector containing the system states, $u(t)$ the input variable vector, and $y(t)$ the output variable vector. A, B, C and D are constant matrices.

The coupling between system inputs and states as well as system states and outputs, is represented by the system's controllability and observability gramian, respectively. These matrices are defined by [47]:

$$L_C := \int_0^\infty e^{At} BB^T e^{A^T t} dt \tag{29}$$

$$L_O := \int_0^\infty e^{At} C^T C e^{A^T t} dt \tag{30}$$

which are the unique positive definite solutions of the following two matrix Lyapunov equations:

$$AL_C + L_C A^T + BB^T = 0 \tag{31}$$

$$A^T L_O + L_O A + C^T C = 0 \tag{32}$$

The system matrix A is assumed to be Hurwitz.

The Hankel singular values measure the contribution to the input–output system behaviour from each state in state coordinates that have equal observability and controllability gramians, and therefore provide information about which parts of the system can be retained or removed. Hankel singular values are defined as the square root of the controllability gramian times the observability gramian. It follows thus [48]:

$$\sigma_i = \sqrt{\lambda_i(L_C L_O)} \tag{33}$$

3.2. Balancing

It can be shown that there is always a balanced realisation of the system's transfer function so that the following equality is satisfied [47]:

$$\hat{L}_C = \hat{L}_O = diag(\sigma_1, \sigma_2, \ldots, \sigma_n) > 0 \tag{34}$$

The transformed gramians are [47]:

$$\hat{L}_C = TL_C T^T \tag{35}$$

$$\hat{L}_O = (T^{-1})^T L_O T^{-1} \tag{36}$$

where T is a transformation matrix and the Hankel singular values σ exhibit the following property [47]:

$$\sigma_1 \geq \sigma_2 \geq \ldots \geq \sigma_n \tag{37}$$

In balanced form, the system is given by [47]:

$$\frac{d}{dt}\hat{x} = TAT^{-1}\hat{x} + TBu = \hat{A}\hat{x} + \hat{B}u \tag{38}$$

$$y = CT^{-1}\hat{x} + Du = \hat{C}\hat{x} + \hat{D}u \tag{39}$$

with

$$\hat{D} = D \tag{40}$$

It is important to emphasise that despite modifications of the system gramians, the original transfer function is preserved.

3.3. Residualisation

Let the states of a balanced system, corresponding to Hankel singular values larger than some limit, be collected in x_1, and the rest in x_2, and write the system as

$$\frac{d}{dt}\begin{pmatrix}\hat{x}_1\\ \hat{x}_2\end{pmatrix} = \begin{pmatrix}\hat{A}_{11} & \hat{A}_{12}\\ \hat{A}_{21} & \hat{A}_{22}\end{pmatrix}\begin{pmatrix}\hat{x}_1\\ \hat{x}_2\end{pmatrix} + (\hat{B}_1\hat{B}_2)\begin{pmatrix}u_1\\ u_2\end{pmatrix} \tag{41}$$

$$\begin{pmatrix}\hat{y}_1\\ \hat{y}_2\end{pmatrix} = (\hat{C}_1\hat{C}_2)\begin{pmatrix}\hat{x}_1\\ \hat{x}_2\end{pmatrix} + (\hat{D}_1\hat{D}_2)\begin{pmatrix}u_1\\ u_2\end{pmatrix} \tag{42}$$

We want to remove the states in x_2. This can be achieved by just removing the x_2-state (called balanced truncation), but this affects the system's steady state. Instead we can residualise the system:

$$A_{red} = \hat{A}_{11} - \hat{A}_{12}\hat{A}_{22}^{-1}\hat{A}_{21} \tag{43}$$

$$B_{red} = \hat{B}_1 - \hat{A}_{12}\hat{A}_{22}^{-1}\hat{B}_2 \tag{44}$$

$$C_{red} = \hat{C}_1 - \hat{C}_2\hat{A}_{22}^{-1}\hat{A}_{21} \tag{45}$$

$$D_{red} = -\hat{C}_2\hat{A}_{22}^{-1}\hat{B}_2 \tag{46}$$

This gives the reduced system the same steady-state gain from input to output as the original system.

4. Results

In the first part, steady state as well as dynamic results of the full-order OMCM model are presented with an emphasis on the oxygen permeation. In what follows, the eigenvalues of the linearized model at steady state are shown. In the third part, two reduced-order models, including 99 and 95% of the system's "energy" (in terms of Hankel singular values) are compared to the full-order model.

4.1. Full-order oxygen mixed conducting membrane model

4.1.1. Steady-state solutions

The initial case values for simulation can be found in Table 2. A total number of 6690 gas channels has been calculated, obtained by Eq. (20). The area-to-volume ratio is 896, based on Eq. (22). Due to small channel size, the flow is fully developed laminar with an average Reynolds number of 305 and 514 for the sweep gas and air stream, respectively. The corresponding pressure drops in the gas channels are 0.017 and 0.025 bar, respectively. Average heat transfer coefficients of 169.8 and 162.8 W/(m^2-K) are obtained for the sweep gas and air fluid, respectively. Flow velocities for the sweep gas and air at the inlet are 2.35 and 3.25 m/s, respectively. The insulation prevents too large heat losses to the environment. An average heat flux of 358.2 W/m^2 has been calculated.

Fig. 3 shows the oxygen flux through the OMCM in axial direction with variation of the gas-phase temperatures, and the corresponding oxygen partial pressure differences are shown in Fig. 4. Both temperatures are set constant (resulting in constant solid wall temperature) to study the effect of solid wall temperature only. All other model specifications are as in Table 2. The material-specific parameters D_0 and n in Eq. (3) increase with increasing temperature, whereas c_0 decreases. The net effect of these three parameters with variations in temperature is positive, i.e. the oxygen transport is enhanced for higher temperatures. An additional contribution for raised oxygen transport at elevated temperatures is the appearance of the parameter n as exponent for the partial pressure of oxygen. The general non-linear behaviour of the oxygen transport can be seen from Eq. (3). It can also be seen from Fig. 3 that oxygen transport mainly occurs at the sweep gas inlet, the location of the maximum partial pressure gradient of oxygen after which the

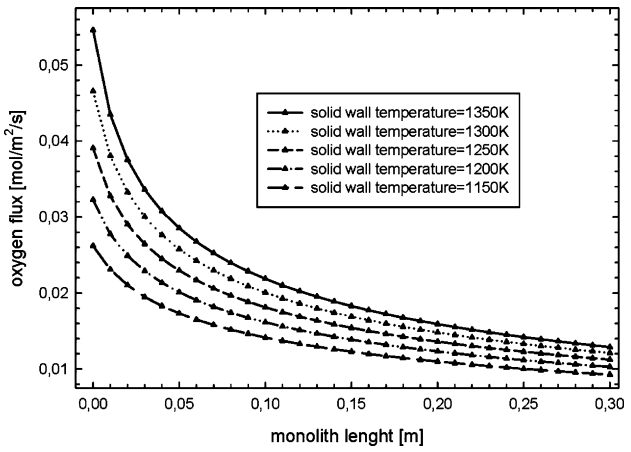

Fig. 3. Oxygen flux through the OMCM with varying gas-phase temperatures.

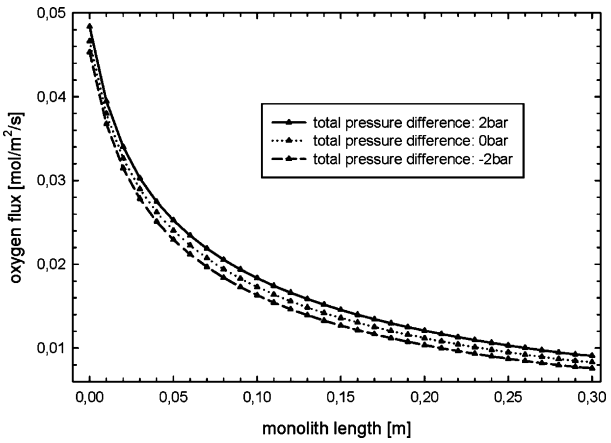

Fig. 6. Oxygen flux in axial direction for total pressure differences of 2 bar, 0 bar, and −2 bar.

profile of the oxygen transport becomes more and more flat. This means that for a larger gain in oxygen on the sweep gas side, considerably longer monoliths must be applied. One possible solution might be to use a reducing atmosphere on the sweep gas side that keeps the oxygen partial pressure low and the driving force high, respectively [22].

In Fig. 5 the oxygen flux in axial direction is shown for varying oxygen partial pressure differences. The oxygen partial pressure difference, starting at 20%, is decreased to 18.5, 16 and finally to 11%. All further process parameters of the two gas streams are as shown in Table 2. Eq. (3) shows a large dependency of the oxygen partial pressure difference on the amount of permeating oxygen. Whereas for large oxygen partial pressure differences the oxygen flux shows a steep profile it becomes more and more flat for small differences in oxygen partial pressure. The pressure difference between air and sweep gas across the solid wall of the OMCM should be rather small to minimise mechanical stresses. In Fig. 6, a pressure difference of +2, 0, and 2 bars is applied leading to different oxygen permeation rates. This can be explained on the basis of Dalton's law, where partial pressures of gas mixture components are calculated by the product of total pressure and mole fraction.

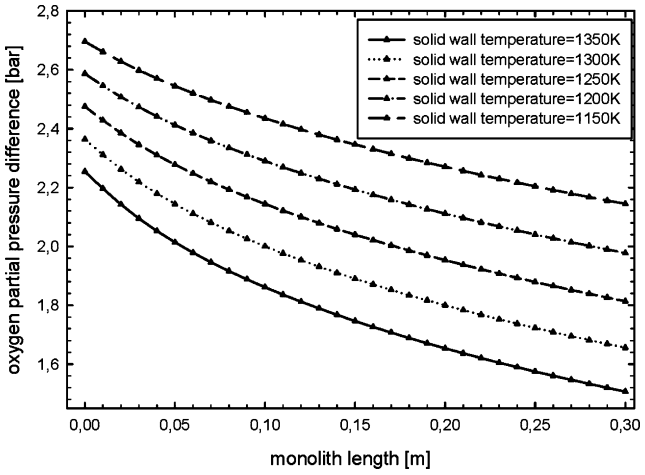

Fig. 4. Oxygen partial pressure difference with varying gas-phase temperatures.

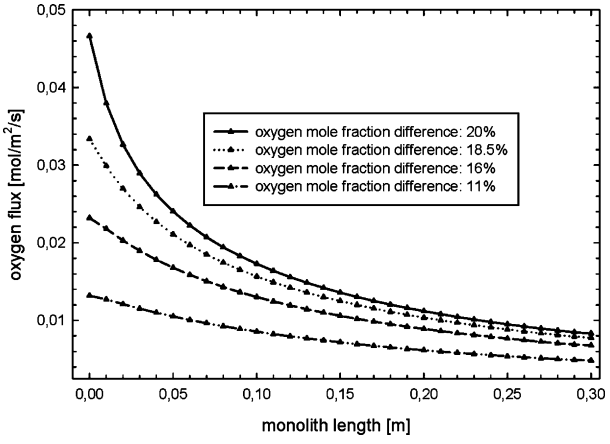

Fig. 5. Oxygen flux in axial direction with varying oxygen partial pressure differences.

4.1.2. *Transient solutions*

Fig. 7 presents heating of the solid wall at the air inlet. The thermal response of the monolithic OMCM is very fast, which is due to the thin solid walls. Starting at a solid wall temperature of 308 K, steady state is reached after approximately 300 s. All other operating conditions are as shown in Table 2. Fig. 9 shows the transient response of the oxygen permeation along the axial direction of the OMCM, starting at 308 K. Higher oxygen transport can be obtained at elevated temperatures with a strongly non-linear behaviour in axial direction. It should be noted that Fig. 9 does represent only the thermal response. Activation of oxygen transport through the membrane takes generally several hours [21,22] until a steady state is reached. Further, degradation of the OMCM by, e.g. gaseous species

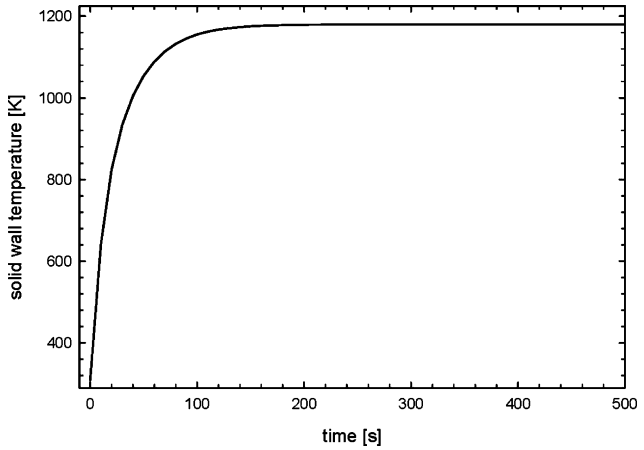

Fig. 7. Transient behaviour of solid phase temperature from 308 K to steady-state temperature of 1180 K at $L = 0.3$ m.

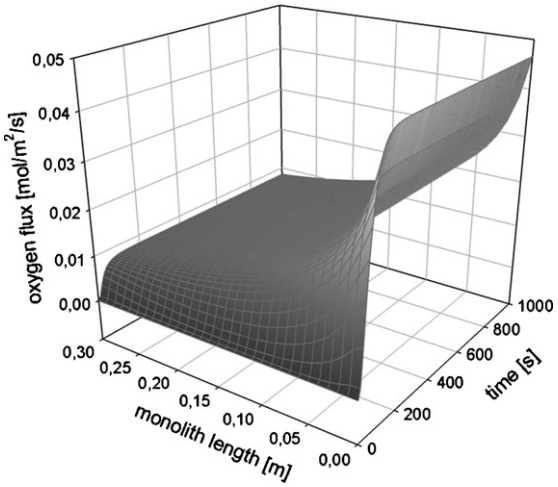

Fig. 8. Transient behaviour of oxygen permeation in axial direction for 1000 s, starting at 308 K.

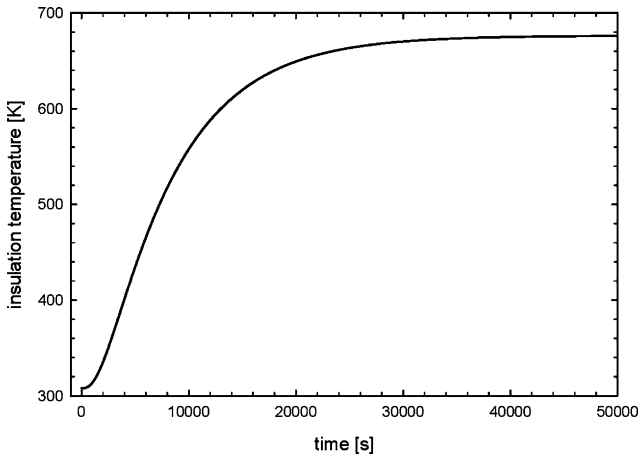

Fig. 9. Transient behaviour of insulation temperature at $th = 0.0375$ m and $L = 0.3$ m with for 50000 s.

in the feed and/or sweep gas may also affect the transport of oxygen. It should be noted that the heating profiles, shown in Figs. 7 and 9, represent a theoretical maximum of the OMCM's thermal response. Large temperature and oxygen partial pressure gradients across the OMCM may lead to failure and drastically reduce the system durability. In practice, operating conditions need to be carefully controlled, in particular during start-up and shut-down [49]. Fig. 8 shows the transient response in the insulation at $th = 0.0375$ m, starting at 308 K. All other operating conditions are as shown in Table 2. The apparent dead time in the beginning can be explained by the low insulation thermal conductivity. The thermal response in the insulation layer is very slow, leading to transients of several hours until a steady state is reached. This can be explained by the low thermal conductivity of the applied material. In addition to reduced heat losses, reduced start-up times after a short stop can be expected for the integrated OMCM.

4.2. Eigenanalysis

Fig. 10 shows the eigenvalues of the linearized OMCM model. All eigenvalues are in the right-half plane (the real part of the eigenvalues are negative), which means the model is stable. It should be emphasised that the location of some of the eigenvalues depends strongly on the applied discretisation method. One eigenvalue is located very close to the imaginary axis representing a characteristic slow dynamics mode. The large range of the real part of the eigenvalues indicates that there is room for model reduction if specific frequency ranges are more interesting than others. For instance, for control system design the frequency range above the closed loop system bandwidth is not very important.

4.3. Reduced-order oxygen mixed conducting membrane models

The oxygen mole fraction at the sweep gas outlet is one of the key quantities in the OMCM. As discussed earlier the oxygen permeation through the OMCM is a non-linear function of oxygen partial pressure difference in the two gas phases as well as the solid phase temperature. Incorporated into a process the transient response of the OMCM will strongly affect process units such as combustion located downstream this heat- and mass-transfer unit. Therefore, results for the reduced-order models are here limited to the sweep gas oxygen mole fraction at the outlet. The transient responses in the time domain are obtained with the parameters in Table 2, except for those the models are excited with.

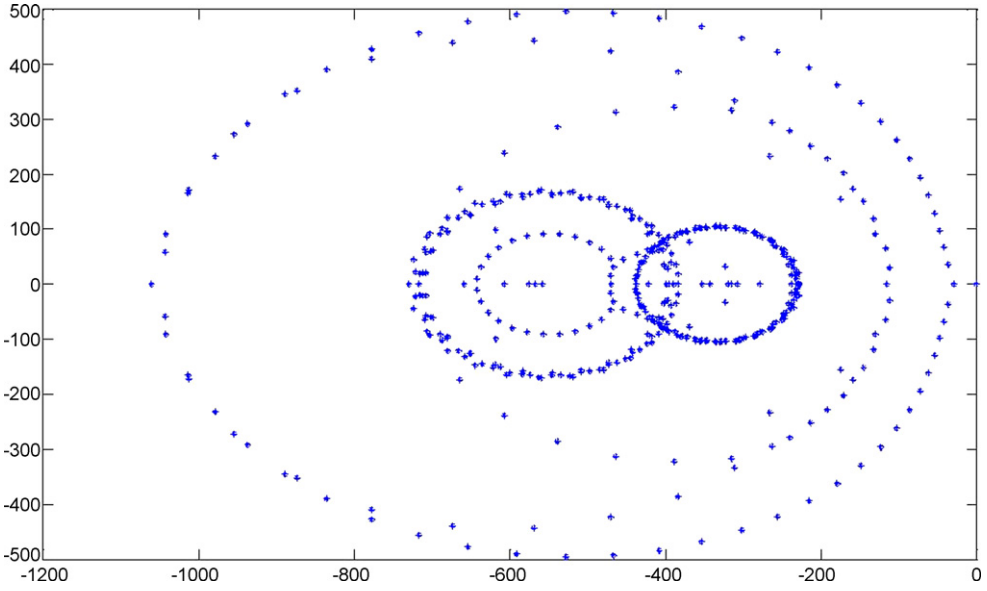

Fig. 10. Eigenvalues of the linearized OMCM model.

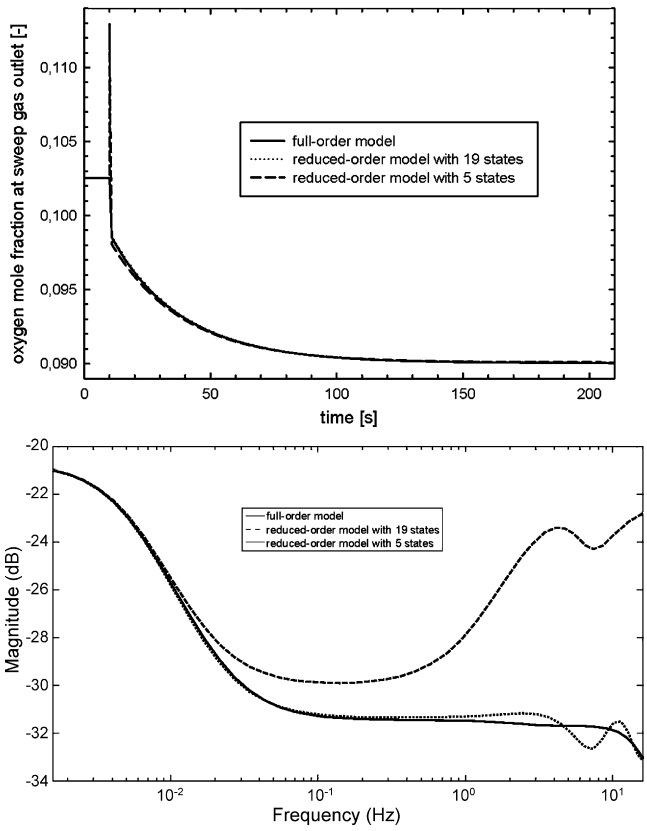

Fig. 11. Transient response of the oxygen mole fraction at the sweep gas outlet for the full-order model and two reduced-order models with 19 and 5 states. After 10 s the sweep gas inlet temperature is reduced by 10% (−135 K) (above). Frequency response of the oxygen mole fraction at the sweep gas outlet for the full-order model and two reduced-order models with 19 and 5 states when excited with a sinusoidal input signal of the sweep gas inlet temperature (below).

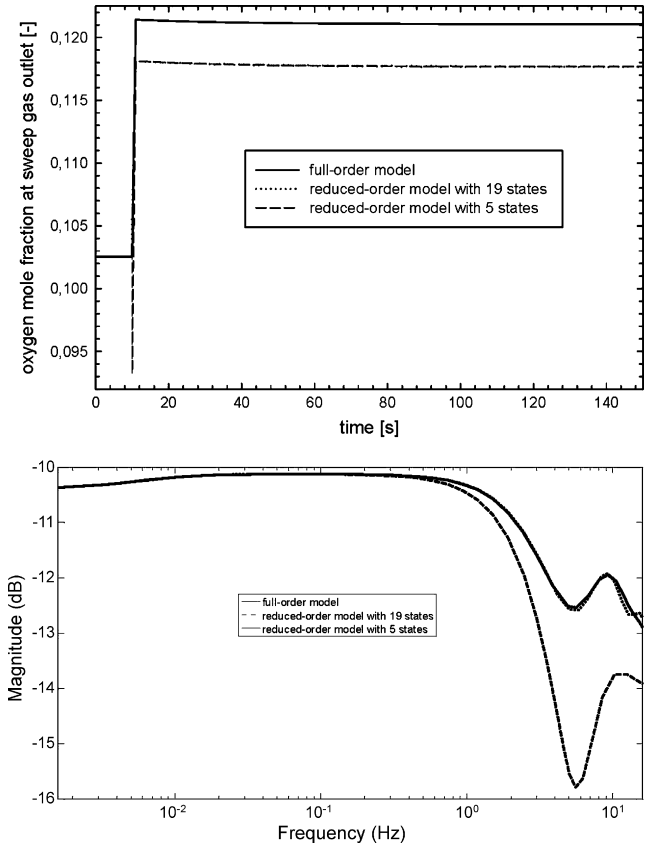

Fig. 12. Transient response of the oxygen mole fraction at the sweep gas outlet for the full-order model and two reduced-order models with 19 and 5 states. After 10 s the oxygen mole fraction at the sweep gas inlet is increased by 500% (+5% points in the oxygen mole fraction) (above). Frequency response of the oxygen mole fraction at the sweep gas outlet for the full-order model and two reduced-order models with 19 and 5 states when excited with a sinusoidal input signal of the sweep gas inlet oxygen mole fraction (below).

The upper part of Fig. 11 shows the transient response of the oxygen mole fraction at the sweep gas outlet for the full-order model and two reduced-order models including 19 and 5 states, respectively. After 10 s simulation a negative step change of 135 K of the sweep gas inlet temperature is applied to the models. The reduced-order model with 5 states exhibit a large inverse response directly after the model has been excited, whereas the transient response of the reduced-order model with 19 states is very close to that of the full-order model. The lower part of Fig. 11 illustrates the frequency response for the same input and output as for the figure above. The frequency response at a given frequency can be interpreted as the ratio of the output and input amplitude when the input is a sinusoidal signal at that frequency. The reduced-order model incorporating 19 states show very similar response to the linearized full-order model at frequencies up to 10 Hz. The reduced-order model with 5 states starts deviating at around 0.02 Hz, and shows qualitatively wrong behaviour for frequencies higher than 1 Hz. Consequently, one should be careful when using the reduced-order model including only 5 states for developing fast control structures. However, for control of power cycles including OMCMs, it is likely that one need not consider load changes (and other disturbances) with frequencies higher than 1 Hz, as such fast changes in operating conditions could be detrimental.

Fig. 12 shows the same variables as in Fig. 11, but now the oxygen mole fraction at the sweep gas inlet is increased by 500% (+5% points in the oxygen mole fraction) after 10 s. The transient response of the reduced-order model incorporating 19 states is very close to that of the full-order model. As for the case shown in Fig. 11, the reduced-order model with 5 states exhibit an inverse response immediately after the model has been excited with the input step function. The reduced-order model with 5 states uses the term $\hat{D}$ ("direct feedthrough") to approximate some of the faster dynamics in the full-order model, and this gives the (seemingly) inverse response in Figs 11 and 12 for this reduced-order model. However, as long as this inverse response is much faster than a desired closed-loop bandwidth, this model error will not affect control design. In the lower part of Fig. 12, the corresponding frequency response of the oxygen mole fraction at the sweep gas outlet is shown for the full-order model and two reduced-order models with 19 and 5 states. Both reduced-order models have similar response compared to the full-order model throughout the whole frequency domain shown here. The full-order and reduced-order models differ in required simulation time and the number of state variables. The CPU time ratio for full-order and reduced-order models can, for some cases, be larger than 100.

In general it can be stated that reduced models, which are generated by means of the linear model reduction technique applied here, will give a steady-state error in working points other than the one for which the linearization was obtained. This is shown in Fig. 12. This is due to model linearization rather than model reduction, as the reduced model retains the steady state of the linearized model. For control design, steady-state offsets in controlled variables can be removed by inclusion of integral action in the closed-loop controllers.

5. Conclusion

Based on energy and species conservation balances spatially distributed in one dimension, steady state and dynamic simulations

were performed in order to study the OMCM under variation of process conditions such as temperature, pressure and oxygen partial pressure differences. The oxygen permeation strongly depends on the oxygen partial pressure difference exposed to the OMCM. Furthermore, the oxygen transfer is an activated process and is also strongly depending on temperature. The monolithic geometry with a high number of gas channels results in highly efficient heat and mass transfer. Larger total pressure differences between sweep gas and air gives only small improvements in oxygen permeation. On the other hand, a small pressure difference leads to considerable longer lifetime of the OMCM and is therefore preferred.

Transient simulations reveal fast thermal response in the OMCM monolith. New operational conditions can therefore be adjusted in short time. The insulation, on the other hand, shows very slow thermal response because of the low thermal conductivity of the material. Steady state is reached after several hours. Heat losses are low and the OMCM can be maintained at high temperature after process shut-down.

All eigenvalues of the linearized OMCM model are in the right-half plane, which means the model is stable.

Model reduction by balanced residualisation was applied in order to reduce the model size with respect to the number of states. The frequency responses of the reduced-order models reveal good agreement to the linearized full-order model for frequencies lower than 1 Hz. Higher frequencies are of less importance when dealing with control of power cycles.

Model reduction of complex process units has the benefit of retaining the physical behaviour of key variables in conjunction with a small and fast model which can then be used for process control.

Often in process control, models are developed somewhat differently to those used in process engineering. These models attempt to capture the inherent dynamics between inputs and outputs, whereas steady-state values of variables such as temperature and concentration are of less importance. The approach taken herein, starting with a detailed model and then applying model reduction for control has the advantage that there is only one model to develop and maintain. The same model can be used for both, detailed analysis of, e.g. temperature and concentration distribution, and (after model reduction) for process control.

Acknowledgments

This publication forms a part of the BIGCO2 project, performed under the strategic Norwegian research program Climit. The authors acknowledge the partners: StatoilHydro, GE Global Research, Statkraft, Aker Clean Carbon, Shell, TOTAL, ConocoPhillips, ALSTOM, the Research Council of Norway (178004/I30 and 176059/I30) and Gassnova (182070) for their support. The first author acknowledges the discussions with his colleague Lars Olof Nord on gas turbine performance and thanks for his valuable comments on this paper.

Knut Ingvar Åsen, Jens Bragdø Smith, and John Arild Svendsen (StatoilHydro, Norway) are gratefully acknowledged for the discussions on several aspects of the oxygen mixed conducting membrane. The authors thank Vladislav V. Kharton (University of Aveiro, Portugal) for very useful feedback on the paper. Prof. Juergen Hahn (Texas A&M University, USA) is also acknowledged for the discussions on model reduction.

Nomenclature

Symbols

A_{ext}	external radiation surface (m^2)
C	molar concentration ($mol\,m^{-3}$)
c_p	heat capacity ($J\,mol^{-1}\,K^{-1}$) or ($J\,kg^{-1}\,K^{-1}$)
c_0	oxygen concentration ($mol\,m^{-3}$)
D_0	oxygen self-diffusion coefficient ($m^2\,s^{-1}$)
f	Fanning friction factor
h	electron holes
h_f	heat transfer coefficient
J_{O_2}	oxygen molar flux ($mol\,m^{-2}\,s^{-1}$)
k_{sf}	parameters for membrane surface reactions
L_m	monolith length (m)
n	temperature dependent parameter
n_{ch}	number of gas channels in the monolith
$\dot{n}_{tot}$	total mole flow ($mol\,s^{-1}$)
Nu	Nusselt number
O_2	oxygen molecule
O_i''	interstitial oxygen ion
O_O^x	lattice site oxygen
p	partial pressure
P	pressure (Pa)
$\dot{q}$	heat flux ($J\,s^{-1}\,m^{-2}$)
Q	heat ($J\,s^{-1}$)
R	universal gas constant ($J\,mol^{-1}\,K^{-1}$)
Re	Reynolds number
T	temperature (K)
t	time (s)
th	thickness (m)
V	volume ($m^3\,mol^{-1}$)
v_g	velocity ($m\,s^{-1}$)
$V_O^{\cdot\cdot}$	oxygen vacancy
w_{ch}	channel width (m)
W	monolith width (m)
x	radial direction (m)
z	axial direction (m)

Greek letters

α	area to volume ratio ($m^2\,m^{-3}$)
ε	emissivity
λ	thermal conductivity ($J\,s^{-1}\,m^{-1}\,K^{-1}$)
ρ	density ($kg\,m^{-3}$)
σ	Stefan–Boltzmann constant, Hankel singular values

Indexes

a	air
amb	ambient
C	concentration
c	controllability
$conv$	free convection
g	gas
n	counter for Hankel singular values
ins	insulation
J	oxygen flux
k	gas index (air or sweep gas)
m	monolith
o	observability
O_2	oxygen
r	reduced
s	solid wall
sf	surface reactions
w	sweep gas
T	transposed
tot	total
0	initial

References

[1] C. Hamel, A. Seidel-Morgenstern, T. Schiestel, S. Werth, H. Wang, C. Tablet, J. Caro, Experimental and modeling study of the O_2-enrichment by perovskite fibers, AIChE J. 52 (2006) 3118–3125.

[2] I. Kaus, K. Wiik, B. Krogh, M. Dahle, K.H. Hofstad, S. Aasland, Stability of $SrFeO_3$-based materials in H_2O/CO_2-containing atmospheres at high temperatures and pressures, J. Am. Ceram. Soc. 90 (2007) 2226–2230.

[3] M. Schroeder, M. Dragan, Oxygen transport in $La_{2-x}Sr_xNiO_{4+\delta}$: membrane permeation and defect chemical modelling, J. Mater. Sci. 42 (2007) 1972–1983.

[5] J.B. Smith, T. Norby, On the steady-state oxygen permeation through La[sub 2]NiO[sub 4+$_\delta$] membranes, J. Electrochem. Soc. 153 (2006) A233–A238.

[6] T. Griffin, S.G. Sundkvist, K. Åsen, T. Bruun, Advanced zero emissions gas turbine power plant, J. Eng. Gas Turbines Power 127 (2005) 81–85.

[7] F. Kreith, M.S. Bohn, Principles of Heat Transfer, vol. XVIII, 700, 6th revised ed., Brooks Cole, Pacific Grove, CA, 2000, 848 pp.

[8] E. Yantovski, J. Gorski, B. Smyth, J. ten Elshof, Zero-emission fuel-fired power plants with ion transport membrane, Energy 29 (2004) 2077–2088.

[9] A. Abrutis, A. Teiserskis, G. Garcia, V. Kubilius, Z. Saltyte, Z. Salciunas, V. Faucheux, A. Figueras, S. Rushworth, Preparation of dense, ultra-thin MIEC ceramic membranes by atmospheric spray-pyrolysis technique, J. Membr. Sci. 240 (2004) 113–122.

[10] X. Dong, Z. Wu, X. Chang, W. Jin, N. Xu, One-step synthesis and characterization of $La_2NiO_{4+[\delta]}$ mixed-conductive oxide for oxygen permeation, Ind. Eng. Chem. Res. 46 (21) (2007) 6910–6915.

[11] A. Julbe, D. Farrusseng, C. Guizard, Limitations and potentials of oxygen transport dense and porous ceramic membranes for oxidation reactions, Catal. Today 104 (2005) 102–113.

[12] E.V. Tsipis, E.N. Naumovich, A.L. Shaula, M.V. Patrakeev, J.C. Waerenborgh, V.V. Kharton, Oxygen nonstoichiometry and ionic transport in $La_2Ni(Fe)O_{4+[\delta]}$, Solid State Ionics 179 (2008) 57–60.

[13] D.C. Zhu, X.Y. Xu, S.J. Feng, W. Liu, C.S. Chen, La_2NiO_4 tubular membrane reactor for conversion of methane to syngas, Catal. Today 82 (2003) 151–156.

[14] J. Sunarso, S. Baumann, J.M. Serra, W.A. Meulenberg, S. Liu, Y.S. Lind, J.C. Diniz da Costa, Mixed ionic-electronic conducting (MIEC) ceramic-based membranes for oxygen separation, J. Membr. Sci. 320 (2008) 13–41.

[15] E.V. Tsipis, E.N. Naumovich, M.V. Patrakeev, J.C. Waerenborgh, Y.V. Pivak, P. Gaczyński, V.V. Kharton, Oxygen non-stoichiometry and defect thermodynamics in $La_2Ni_{0.9}Fe_{0.1}O_{4+[\delta]}$, J. Phys. Chem. Solids 68 (2007) 1443–1455.

[16] J. Wan, J. Goodenough, J. Zhu, $Nd_{2-x}La_xNiO_{4+[\delta]}$, a mixed ionic/electronic conductor with interstitial oxygen, as a cathode material, Solid State Ionics 178 (2007) 281–286.

[17] C. Depcik, D. Assanis, One-dimensional automotive catalyst modeling, Prog. Energy Combust. Sci. 31 (2005) 308–369.

[18] J. Chen, H. Yang, N. Wang, Z. Ring, T. Dabros, Mathematical modeling of monolith catalysts and reactors for gas phase reactions, Appl. Catal. A: Gen. 345 (2008) 1–11.

[20] J.E. ten Elshof, H.J.M. Bouwmeester, H. Verweij, Oxygen transport through $La_{1-x}Sr_xFeO_{3-[\delta]}$ membranes. I. Permeation in air/He gradients, Solid State Ionics 81 (1995) 97–109.

[21] S.J. Xu, W.J. Thomson, Stability of $La_{0.6}Sr_{0.4}Co_{0.2}Fe_{0.8}O_{3-[\delta]}$ Perovskite membranes in reducing and nonreducing environments, Ind. Eng. Chem. Res. 37 (4) (1998) 1290–1299.

[22] W. Zhang, J. Smit, M. van Sint, J.A.M. Annaland, Kuipers, Feasibility study of a novel membrane reactor for syngas production. Part 1. Experimental study of O_2 permeation through perovskite membranes under reducing and non-reducing atmospheres, J. Membr. Sci. 291 (2007) 19–32.

[23] A. Antoulas, An overview of approximation methods for large-scale dynamical systems, Annu. Rev. Control 29 (2005) 181–190.

[24] J. Hahn, T.F. Edgar, An improved method for nonlinear model reduction using balancing of empirical gramians, Comput. Chem. Eng. 26 (2002) 1379–1397.

[25] A. Chatterjee, An introduction to the proper orthogonal decomposition, Curr. Sci. 78 (2000) 808–817.

[26] M. Mangold, M. Sheng, Nonlinear model reduction of a two-dimensional MCFC model with internal reforming, Fuel Cells 4 (2004) 68–77.

[27] H.M. Park, D.H. Cho, Low dimensional modeling of flow reactors, Int. J. Heat Mass Transfer 39 (1996) 3311–3323.

[28] C. Sun, J. Hahn, Reduction of stable differential-algebraic equation systems via projections and system identification, J. Process Control 15 (2005) 639–650.

[29] S.G. Sundkvist, S. Julsrud, B. Vigeland, T. Naas, M. Budd, H. Leistner, D. Winkler, Development and testing of AZEP reactor components, Int. J. Greenhouse Gas Control 1 (2007) 180–187.

[30] H.M. Kvamsdal, K. Jordal, O. Bolland, A quantitative comparison of gas turbine cycles with CO_2 capture, Energy 32 (2007) 10–24.

[31] A. Atkinson, T.M.G.M. Ramos, Chemically-induced stresses in ceramic oxygen ion-conducting membranes, Solid State Ionics 129 (2000) 259–269.

[32] E. Blond, N. Richet, Thermomechanical modelling of ion-conducting membrane for oxygen separation, J. Eur. Ceram. Soc. 28 (2008) 793–801.

[33] P.V. Hendriksen, P.H. Larsen, M. Mogensen, F.W. Poulsen, K. Wiik, Prospects and problems of dense oxygen permeable membranes, Catal. Today 56 (2000) 283–295.

[34] A.F. Sammells, M.V. Mundschau (Eds.), Nonporous Inorganic Membranes for Chemical Processing, vol. XIV, Wiley-VCH, Weinheim, 2006, p. 277s.

[35] S. Lee, J.H. Yu, D.W. Seo, S.K. Woo, Thick-film type oxygen transport membrane: preparation, oxygen permeation and characterization, J. Electroceram. 17 (2006) 719–722.

[36] S.J. Xu, W.J. Thomson, Oxygen permeation rates through ion-conducting perovskite membranes, Chem. Eng. Sci. 54 (1999) 3839–3850.

[37] P.J. Gellings, H.J.M. Bouwmeester, The CRC Handbook of Solid State Electrochemistry, CRC Press, Boca Raton, FL, 1997, p. 630s.

[38] L. Petruzzi, S. Cocchi, F. Fineschi, A global thermo-electrochemical model for SOFC systems design and engineering, J. Power Sources 118 (2003) 96–107.

[39] T. Shimada, Y. Kato, Tanaka numerical analysis of thermal behavior of small solid oxide fuel cell systems, J. Fuel Cell Sci. Technol. 4 (2007) 299–307.

[40] H. Apfel, M. Rzepka, H. Tu, U. Stimming, Thermal start-up behaviour and thermal management of SOFC's, J. Power Sources 154 (2006) 370–378.

[41] Y. Chen, J.W. Evans, Cool-down time of solid oxide fuel cells intended for transpotation application, J. Power Sources 58 (1996) 87–91.

[42] R.B. Bird, W.E. Stewart, E.N. Lightfoot, Transport Phenomena, vol. XII, Wiley, New York, 2002, p. 895s.

[43] gPROMS (General Process Modelling and Simulation Tool), v.3.1.5, 2008, Process Systems Enterprise Ltd., London, http://www.psenterprise.com/.

[44] The MathWorks—MATLAB and Simulink for Technical Computing, R2008b, 2008, http://www.mathworks.com.

[45] S. Cimino, A. Di Benedetto, R. Pirone, G. Russo, Transient behaviour of perovskite-based monolithic reactors in the catalytic combustion of methane, Catal. Today 69 (2001) 95–103.

[46] P. Holtappels, H. Mehling, S. Roehlich, S.S. Liebermann, U. Stimming, SOFC system operating strategies for mobile applications, Fuel Cells 5 (2005) 499–508.

[47] G.E. Dullerud, A Course in Robust Control Theory: A Convex Approach, vol. XX, Springer, New York, 2000, p. 417s.

[48] S. Skogestad, Multivariable Feedback Control: Analysis and Design, vol. XIV, Wiley, Chichester, 2007, p. 574s.

[49] K. Eichhorn Colombo, O. Bolland, V.V. Kharton, C. Stiller, Design and Part-Load Performance of a Mixed Conducting Membrane-based Combined Power Plant, in preparation.

Paper II

Is not included due to copyright

Paper III

Is not included due to copyright

Paper IV

Is not included due to copyright